IMAGE PROCESSING BASED CONTAMINATION LEVEL MONITORING OF HIGH VOLTAGE INSULATOR

BY

LUQMAN SULYMAN FAEZ MARAABA

A Thesis Presented to the

DEANSHIP OF GRADUATE STUDIES

KING FAHD UNIVERSITY OF PETROLEUM & MINERALS

DHAHRAN, SAUDI ARABIA

In Partial Fulfillment of the

Requirements for the Degree of

MASTER OF SCIENCE

In

ELECTRICAL ENGINEERING

December 2013

KING FAHD UNIVERSITY OF PETROLEUM & MINERALS

DHAHRAN- 31261, SAUDI ARABIA

DEANSHIP OF GRADUATE STUDIES

This thesis, written by **Luqman Sulyman Faez Maraaba** under the direction his thesis advisor and approved by his thesis committee, has been presented and accepted by the Dean of Graduate Studies, in partial fulfillment of the requirements for the degree of **MASTER OF SCIENCE IN ELECTRICAL ENGINEERING.**

Thesis Committee

Prof. ZAKARIYA AL-HAMOUZ
(Advisor)

Dr. HUSSAIN N. AL-DUWAISH
(Co-Advisor)

Prof. SALAM ADEL ZUMMO
(Member)

Dr. WAIL A. MOUSA
(Member)

Dr. MUNIR A. AL-ABSI
(Member)

Dr. ALI AHMAD AL-SHAIKHI
Department Chairman

Prof. SALAM ADEL ZUMMO
Dean of Graduate Studies

15/1/14
Date

عمادة الدراسات العليا
DEANSHIP OF GRADUATE STUDIES

بسم الله الرحمن الرحيم

{قُلْ إِنَّ صَلاَتِي وَنُسُكِي وَمَحْيَايَ وَمَمَاتِي لِلَّهِ رَبِّ الْعَالَمِينَ}

This Thesis is dedicated to

The soul of my Mother (Fatima)

Dear Father (Sulyman)

Beloved sister Isra

Brothers Hammam and Mohammed

My uncle (Yousef)

My sister husband (Ahmad)

My sister son (Omar)

My Holy Homeland Palestine

ACKNOWLEDGMENTS

In the name of Allah, the most gracious, the most merciful all praise is to almighty Allah for having guided me all over my life. Acknowledgement is due to King Fahd University of Petroleum and Minerals for the great support to this work. My deep appreciation is reserved for thesis advisor **Prof. Zakariya Al-Hamouz** for his guidance, valuable time and attention he devoted throughout the course of this work. My numerous intrusions into his office were always met with a considerable response and care. Thanks are also due to my co-advisor **Dr. Hussain N. Al-Duwaish** and committee members **Prof. Salam Adel Zummo**, **Dr. Wail A. Mousa** and **Dr. Munir A. Al-Absi** for their interest, attention and suggestion. I wish also to thank all parties who have contributed to support me in this work, namely Center of engineering research director **Dr. Luai M. Al-Hadhrami** and department chairman **Dr. Ali Alshaikhi** and other faculty members for their supports. My great appreciations are also due to all members of my family and to friends who give me the self-confidence to face the challenge.

TABLE OF CONTENTS

LIST OF TABLES

LIST OF FIGURES

LIST OF ABBREVIATIONS

ESDD	:	Equivalent Salt Deposit Density
EPDM	:	Ethylene Propylene Diene Monomer
KFUPM	:	King Fahd University of Petroleum and Minerals
SiR	:	Silicon Rubber
NSDD	:	Non Soluble Deposit Density
RTV	:	Room Temperature Vulcanized
IEC	:	International Electro-Technical Commission
SEC	:	Saudi Electricity Company
LC	:	Leakage Current
ANN	:	Artificial Neural Network
PD	:	Partial Discharge
AE	:	Acoustic Estimation
TD	:	Temperature Distribution
UV	:	Ultra Violet
RFVT	:	Rapid Flashover Voltage Technique
FOV	:	Flashover Voltage

HSV	:	Hue, Saturation, and Value
RGB	:	Red, Green, and Blue
HSL	:	Hue, Saturation, and Lightness
CMYK	:	Cyan, Magenta, Yellow, and Black
CV	:	Chan-Vese model
SVD	:	Singular Value Decomposition
MFNN	:	Multi-layer Feed-Forward Neural Network
RBFNN	:	Radial Basis Function Neural Network
MSE	:	Mean Square Error

THESIS ABSTRACT

Full Name : Luqman Sulyman Faez Maraaba

Thesis Title : Image Processing Based Contamination Level Monitoring of High Voltage Insulators

Major Field : Electrical Engineering

Date of Degree : December 2013

Flashover of high voltage insulators used in transmission system and substations is treated as a major problem that can affect the transfer of large amount of electrical energy over long distances. Contamination in coastal, industrial, desert and agricultural areas under environmental conditions of fog, light rain and dew is the main cause of high voltage insulator flashovers. Flashover in most cases leads to lengthy service outage; hence it has a considerable impact on power system reliability. As such, several methods have been used in order to improve the performance of high voltage insulators under polluted conditions. Among these methods are creepage extender, Coating and regular washing of insulators. Washing of insulators is the most common suppressing method where power system utilities spend huge amount of money and time. Selection of the optimal time for insulator washing is still an issue that depends on the contamination level. At present, different methods have been developed to monitor and assess the surface contamination level of high voltage insulators. Leakage current, Acoustic estimation, Thermovision and ultraviolet methods are examples of these monitoring methods. In this thesis, contamination level monitoring tool for high voltage insulators has been developed. A digital camera has been used to capture pictures. Image processing has been used to extract needed features form the captured images to assess the contamination level that would lead to a flashover. Two types of features were considered. The first is “histogram based statistical

feature" such as mean, variance, skewness, kurtosis, energy and normalized histogram error. The second feature is "singular value decomposition theorem based linear algebraic feature" such as the singular values. Using statistical features / linear algebraic feature or a combination of both, a neural network has been successfully designed to correlate the insulator captured image and the contamination level. This contamination level monitoring tool will provide essential information for maintenance departments in the electric utility companies to properly schedule the expensive and extensive high-pressure water live line and substation insulator washing without the need of human intervention. This will result in huge savings in maintenance costs and improves the electrical system reliability.

ملخص الرسالة

الاسم الكامل: لقمان سليمان فايز مراعبة

عنوان الرسالة: مراقبة مستوى التلوث على عوازل الجهد العالي بالأعتماد على معالجة الصور الرقمية

التخصص: الهندسة الكهربائية

تاريخ الدرجة العلمية: كانون أول 2013

يعدّ فقدان عازلية العوازل ذات الفولتية العالية المستخدمة في خطوط نقل الطاقة و المحطات الكهربائية مشكلة أساسية من شأنها التأثير سلبا على كفاءة نقل كميات كبيرة من الطاقة الكهربائية لمسافات بعيدة. يعدّ التلوث في المناطق الساحلية و الصناعية و الصحراوية و الزراعية في ظروف بيئية من الضباب و المطر الخفيف و الندى السبب الرئيس لفقدان العوازل ذات الفولتية العالية عازليتها . يؤدي فقدان العازلية في معظم الحالات إلى انقطاع مطوّل للخدمة و بالتالي فقدان العازلية لها أثر معتبر و مهم على المقدرة على الاعتماد على نظام الطاقة. و على هذا النحو ، فإن العديد من الطرق تمّ استخدامها من أجل تحسين أداء العوازل ذات الفولتية العالية في ظروف التلوث تلك. من هذه الطرق : زيادة المسافة بين طرفي العازل ، و طلاء العوازل ، و غسل العوازل بانتظام. غسل العوازل هي الطريقة الأكثر شيوعا بحيث أن شركات خدمات نظام الطاقة تنفق الكثير من المال و الوقت حيث أن اختيار الوقت الأفضل لغسل العازل ما تزال قضية تعتمد على مستوى التلوث. تمّ تطوير طرق مختلفة لمراقبة و تقييم مستوى التلوث على سطح العوازل ذات الفولتية العالية حاليا . مقدار التيار المتسرب ، و تقدير الانبعاث الصوتي على سطح العازل ، و الرؤية الحرارية ، و الطرق الفوق بنفسجية هي أمثلة لطرق المراقبة هذه.

في هذه الأطروحة ، تمّ تطوير أداة لمراقبة مستوى تلوث العوازل ذات الفولتية العالية . تمّ استخدام كاميرا رقمية لالتقاط الصور. كما تمّت الاستعانة بتقنية معالجة الصور لاستخلاص السمات المطلوبة من الصور المُلتَقَطة حتى يتم تقييم مستوى التلوث الذي قد يؤدي إلى فقدان العازلية . تمّ اعتماد نوعين من السمات . أمّا النوع الأوّل فهو: الرسم البياني المبني على بعض المقاييس الإحصائية مثل المعدل و التباين و الحيود و الطاقة و غيرها . أمّا النوع الثاني فهو نظرية تجزئة القيمة المفردة المعتمدة على سمة الجبر الخطي مثل القيم المفردة . باستخدام المقاييس الإحصائية أو سمات الجبر الخطي أو الاثنين معا ، تمّ تصميم الشبكات الذكية الصناعية بنجاح لربط صورة العازل المُلتَقَطة مع مستوى التلوث. ستقدم أداة مراقبة مستوى التلوث هذه معلومات هامة لإدارات الصيانة في شركات خدمات الكهرباء من أجل جدولة مناسبة لخط الماء الحي ذي الضغط العالي جدا و

غسل عوازل محطات الكهرباء دون الحاجة للتدخل البشري . سيؤدي هذا إلى التوفير الكبير في تكاليف الصيانة و التحسين من القدرة على الاعتماد على الأنظمة الكهربائية.

CHAPTER ONE

INTRODUCTION

1.1 Background

Electric power is the backbone of development and economy of any country. Demand for electricity is increasing rapidly worldwide and consequently construction of power plants and overhead transmission lines has increased. Overhead transmission lines and substations insulators are one of the cheapest but the most vital part of a power system. Insulators only amount to a small percentage of a new line's and substations total capital cost, but majority of power outages can be attributed to their bad performance, which directly influence the reliability of any electric power system. They are considered the most significant single piece of hardware item, which can affect the overall performance of high voltage transmission lines and substations. The economic impact of failure of a single insulator in-service can be very high [1]. Insulators are designed to withstand both mechanical and electrical stresses under specified operating conditions and at the same time meeting the user's applicable economic criteria. When an insulator is polluted and wetted, its withstand and flashover voltages are reduced. Contaminant particles in the presence of moisture form conducting films on the insulator surface, allowing leakage current to pass. This current will heat the surface leading to formation of dry bands in areas of high current density. High voltages will build up across those bands and may cause partial discharges leading to insulator flashover [2, 3]. Insulator surface contamination and

subsequent flow of leakage current have caused operating problems for electric power utilities since electrical power has been in use. The effect of leakage current and insulator flashover is a major practical concern for continuity of electric power supply. Mitigating measures may have to be adopted in order to improve the performance of the power transmission system. The measures to be taken depend on the contamination severity of the region. These include choosing insulator designs that promote minimum deposit accumulations, choosing insulators with longer leakage paths or performing insulator washing etc [4, 5].

The climatic conditions and geography in Kingdom of Saudi Arabia's are unique, with vast areas of desert, surrounded to a large extent by sea. It can be characterized by high ambient temperatures, wide variations in relative humidity, significant temperature changes between day and night, fine airborne suspended dust particles, strong dust and sand-carrying winds, some misty and foggy days and mostly sunny days throughout the year. These conditions set the stage for the unique type pollution observed in the Middle East. Heavy wetting of deposits by morning and evening dews, moisture-laden winds, and/or light rain trigger insulator pollution flashover [6]. Hence, insulator performance in Saudi Arabia is determined by a number of parameters, some of which are variable and mostly unpredictable.

Given this brief background, this thesis proposes a MATLAB^{TM}-based efficient algorithm to develop a contamination level monitoring tool for high voltage insulator. The new algorithm is based on a combination of image processing principles and artificial neural networks

1.2 Thesis Motivation

As mentioned earlier, insulator performance in Saudi Arabia is determined by a number of parameters, some of which are variable and mostly unpredictable. As such, this thesis proposes a MATLAB^{TM}-based efficient algorithm to develop a tool for monitoring the contamination level for high voltage insulator. The motivation of developing such a tool can be summarized in the following points:

- Preventing catastrophic flashovers and reduces forced outage time by giving accurate information about the contamination level in advance without human intervention.
- Enabling efficient maintenance planning and reduce maintenance costs.
- Improving the overall reliability of the electrical system.
- Enabling efficient use of limited manpower and resources by establishing priorities for maintenance of insulators units.

1.3 Thesis Objectives

This thesis aims at proposing and developing a contamination level monitoring tool. Using image processing and neural networks, important features extracted from digital camera images of insulators are correlated to the contamination level and, hence, the possibility of flashovers can be detected. The developed tool will provide an early warning of possible insulators flashover due to contamination without the need for human intervention. The objectives of this thesis can be summarized as follows:

Objective 1: Exploring the industry practice in dealing with the contamination problem on high voltage insulators.

Objective 2: Collecting samples of contaminated insulators from the industrial partners.

Objective 3: Building image data set for the collected naturally contaminated insulators.

Objective 4: Analyzing of flashover voltage and equivalent salt deposit density (ESDD) levels of the collected naturally contaminated insulators at the labs of the research institute (RI) of KFUPM.

Objective 5: Extracting image features and correlating these features with the ESDD levels using image processing and neural network. Testing of the developed correlation has been carried out on new contaminated samples.

1.4 Thesis Organization

Besides the introduction, the thesis contains five chapters as follows: the second chapter presents a comprehensive literature review about high voltage insulators, their engineering aspects and actual problems associated with pollution, flashover phenomena and its mechanism, methods for improving the performance of high voltage insulators, and insulators contamination severity diagnostic techniques. The proposed algorithm of the contamination level monitoring tool using image processing and artificial neural network is presented in chapter three. Chapter four presents the high voltage laboratory testing, proposed algorithm results, validation, analysis and discussion of the monitoring algorithm. Finally, conclusions and suggestion for future work are pointed out in chapter five.

CHAPTER TWO

LITERATURE REVIEW

2.1 Overview

There has been a substantial growth in electricity demand due to more consumption of power in the industrial sector and other activities. A steady growth in transmission line voltages required for optimum and economic transfer of large amount of power over long distances. As the level of transmission voltage is increased, withstand ability of the high voltage insulator under polluted conditions has become one of the essential issues for researcher. In response to that much efforts, studies and research have been focused on how to improve the performance of the high voltage insulators in the adverse environmental conditions.

Flashover of contaminated insulators in polluted areas represents one of the most important factors that affect the operation of high voltage transmission lines and substations. These flashovers of insulators usually take place in wet weather conditions such as dew, fog, drizzle or light rain. Thus, the reliability of the transmission system mainly depends on the environmental and weather conditions which cause flashover on the polluted insulators leading to system outages.

2.2 Insulators

Insulators are considered as one of the most significant parts in power systems which can affect the overall performance of high voltage transmission lines and substations. Industrial loads such as steel mills and medical loads such as hospitals are examples of loads which need an uninterrupted supply of power. As such, any impairment in the performance of insulators will lead to a large loss of money.

In practice, transmission lines are utilizing two types of insulators which are ceramic (porcelain and glass) and polymeric (composite) insulators. Selection of the type of insulators to be used depending on many factors such as the nature of the region, industrial, dessert or costal. In the early days, ceramic insulators made from glass or porcelain material as shown in Figure 2.1, were considered as the basic insulators used in the design of high voltage transmission lines and substations. In the 1960s, polymeric insulators became more attractive to be used in harsh environmental areas as it has many benefits over ceramic insulators, Figure 2.2 [7]. In recent years, the use of composites insulators has increased rapidly especially ethylene propylene diene monomer (EPDM) and silicone rubber (SiR) [8].

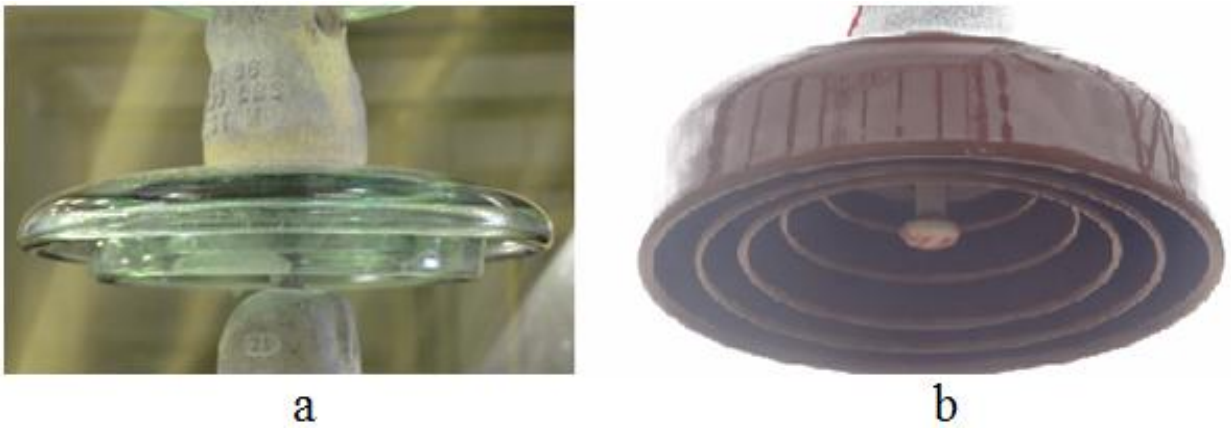

Figure 2.1 (a) Class insulator, (b) porcelain insulator (High Voltage Lab, Research Institute, KFUPM)

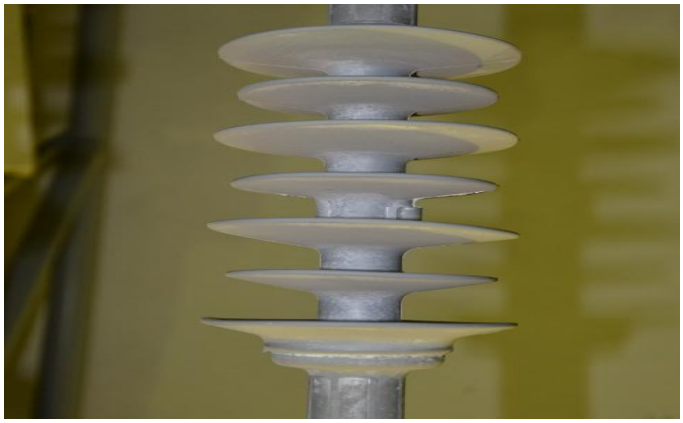

Figure 1.2 Polymer insulator (High Voltage Lab, Research Institute, KFUPM)

The electrical and mechanical behaviors of ceramic and composite insulators are different. Therefore, the materials that have been used in the manufacturing have different properties. Ceramic insulators are electrostatically strongly bonded together (between oxygen and silica) which results in increasing the melting point, mechanical strength and resistance to chemical compounds of the insulator. In contrast, the composite insulators are chemically weakly bonded, and hence, it decomposes when subject to high temperatures (hundreds of degrees centigrade). On the other hand, the surface energy of polymeric insulators (EPDM and silicone rubber) is low, causing it to prevent the formation of continuous film of water along the surface of insulators. Such material is called hydrophobic. Hydrophobic materials cause the formation of distinct droplets of water on the surface of insulator. This property gives the polymer insulator the ability to limit the formation of leakage current better than the ceramic insulators. On the contrary, ceramic insulators have high surface energy, which increases the probability of formation of continuous film of water on the surface of the insulator. In addition, this property makes insulator easily contaminated. Considering the above mentioned characteristics of ceramic and polymeric insulators, the later have much better flashover performance under contamination

conditions with respect to ceramic insulators [7]. Table 2.1 summarizes the comparison between polymeric and ceramic insulators.

Table 2.1 Comparison between polymeric and ceramic high voltage insulators [7]

Property	polymer	Ceramic
Cost	Cheaper	more expensive
Weight	Light weight	Heavy weight
Manufacturing time	Shorter	longer
Handling and installation	Easy	Need more efforts
Brittle characteristics	Non brittle	brittle
Impact resistance	High	low
Flexibility in product design	Greater	Less
Resistance to vandalism	high	low

2.3 Contamination Flashover

Flashover of insulator is a complicated phenomenon, with many factors playing role in motivating and enhancing the chance of flashover such as weather, insulator design, nature of region and operating conditions. In the literature, a lot of efforts have been put to model, predict and solve flashover problems. Technically speaking, flashover means that the insulation of the insulator breaks down. This is clearly demonstrated in Figure 2.3 [9], where an arc builds up on the surface of a string of class insulators as a result of insulation breakdown. Such flashovers

which result from high levels of contamination reduce the reliability of power systems and the flashover performance of insulators [10].

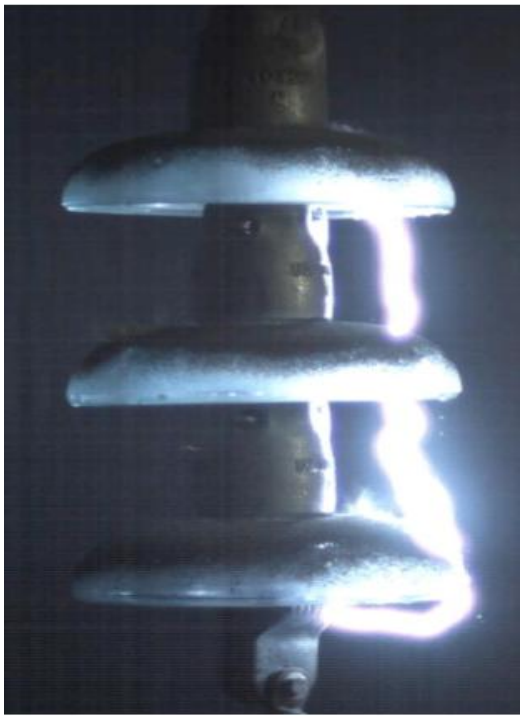

Figure 2.2 Flashover across a string of three glass 'fog-type' insulators [9].

2.4 Contamination Flashover Mechanism

2.4.1 Precipitation of Contaminants

High voltage insulators, ceramic or polymeric, will be significantly affected by the type of the environmental conditions. Different types of pollutants tend to deposit on the insulator surface. These pollutants are categorized into two types; namely, non-soluble and soluble. Insulators which exist beside industrial regions are exposed to non-soluble pollutants such as carbon, cement, dust and calcium chloride. On the other hand, insulators close to coastal areas are exposed to soluble pollutants, especially sodium chloride [11]. Figure 2.4 shows two porcelain

insulators samples, one naturally contaminated (Costal area contamination) and the other is clean. Table 2.2 shows the sources of insulator contamination [12].

Figure 2.3 (a) Naturally contaminated porcelain insulator, (b) Clean porcelain insulator: (KFUPM Dhahran station)

Table 2.2 Sources of insulator contamination [12]

Location	Source of pollutant
Coastal areas	Sea salt
Rural areas	Soil dust, fertilizers, etc.
Desert	Sand
Industrial	Fly-ash, industrial smokestacks
Highways	Road salt, smoke

2.4.2 Wetting of Contaminants

Contamination in coastal, industrial, desert and agricultural areas under the environmental conditions of fog, light rain and dew is the main cause of high voltage insulator flashovers. Thus, under dry conditions, the polluted surface of insulator does not conduct and pollution is of less important. As mentioned before, porcelain and glass insulators have high surface energy which increases water adhesion to the surface of insulator, and hence it becomes easily wet. Therefore, the drops of water spread on the surface due to energy exert from the surface. As a result, the probability of formation of continuous film of water on the surface of insulator is increased. The water on insulator surface wets the contamination layer, forcing the salts and any conducting material in the contaminants to dissolve to form a conducting layer [12].

2.4.3 Leakage Current and Dry-band Formation

The existence of a conducting layer on the surface of energized insulator allows a leakage current to flow through insulator surface. The density of the leakage current is based on insulator surface shape; and hence, the highest leakage current density lies around the pin of the insulator. The flow of an electric current in any conductor or object generates heat, which depends on the resistance of the object. So, leakage current that flows on the surface of the insulator generates heat, which in turn heats the conductive layer causing an increase in current and conductivity of the insulator surface. As the leakage current increases, the heat caused by current increases, leading to evaporation of the water at the area of high current density. Evaporation of water leads to generation of dry bands near insulator pin. Because of high resistance of the dry bands, the system voltage is impressed across them. If the dry bands cannot withstand the voltage, arcs occur across them. Moreover, glows and streamer discharges occur across dry bands. At the end,

partial streamer (partial flashover) are connected to each other forming large arc across the insulator, as shown in Figure 2.3 and, finally, complete flashover occurs [12] [13].

2.5 Equivalent salt deposit density (ESDD)

In order to determine the amount of pollutants on insulator surface, ESDD term is used to express soluble pollutants, with a unit of mg (sodium chloride)/unit surface area, whereas, non-soluble deposit density (NSDD) term is used to express non-soluble pollutants, with a unit of mg (Kaolin)\unit surface area [7].

The conductivity of a deposit contamination with unknown components can be reported clearly using the ESDD term. Often, the bottom surface of ceramic insulator is larger than the upper surface. The upper surface of insulator gets contaminated faster than the bottom surface with respect to time, since rain usually cleans the upper surface and removes most of the pollutants, whereas it does not for the bottom surface. Therefore, the ESDD level is always larger on the bottom surface [14]. Table 2.3 shows the international electrotechnical commission (IEC-60815) classification of contamination severity [15].

Table 2.3 IEC-60815 classification of contamination severity [15].

ESDD ($\boldsymbol{mg/cm^2}$)	**Pollution level**
0.03 to 0.06	Light
0.10 to 0.20	Medium
0.30 to 0.60	Heavy
> 0.60	Very Heavy

2.6 Methods for Improving Insulator Performance

As mentioned earlier, flashover of insulators is a complicated phenomenon in which many factors play role in motivating and enhancing the chance of its occurrence. Among these factors are weather, insulator design, nature of region and operating conditions. The following sub-sections describe different methods for improving the performance of insulators either by inhibiting the formation of a conductive layer or increasing the insulation of the insulator.

2.6.1 Coating of Insulator

Many methods are adopted by service providers in order to improve the performance of insulators exposed to contamination. Recently, adding hydrophobic material on the surface of insulators was introduced to improve the performance of Ceramic insulators. Room temperature vulcanized (RTV) silicon rubber and silicon grease are the two types of coating materials that have been used in insulator coating. Such materials provide a hydrophobic surface, which prevents the formation of conducting layer. As a result, it decreases the magnitude of leakage current flow on the surface and leads to a decrease in the chance of flashover [16]. Suwarno and Ario Basuki investigated the effect of RTV silicon rubber coating of ceramic insulator on the magnitude of leakage current. Two groups of suspension insulators (one group is coated with RTV silicon rubber and the other is not) were tested. Testing results revealed that coating of insulators decreased leakage current and reduced the chance of flashover and increased the hydrophobicity of insulator surface as listed in Table 2.4 [17].

Table 2.4 Leakage current magnitude of using insulator coating [17]

Voltage (kV)	Leakage Current (mA) Non-coated	Leakage Current (mA) RTV Coated
5	0.226	0.073
10	0.358	0.151
15	0.371	0.224
20	0.695	0.305
25	1.601	0.394
30	-	0.478
35	Flashover	0.580
40	-	0.705
45	-	0.811

Using grease silicon as a coating material, the pollutants on the surface of insulator encapsulate within the grease, but at the same time the hydrophobicity was not affected. Continuation of that process means that there is a saturation point, after which the performance of the grease decreased to be at a certain point worse than the uncoated insulator. According to that, using grease silicon as a coating material is not economical because every six months it has to be replaced. The life of the grease silicon is limited. Therefore, service providers spent money, time and extra man hours by using it. On the other hand, if the insulator is coated with the RTV silicon rubber, the pollutants will not encapsulate within the material but still separated (no encapsulation), so pollutants on surface of RTV silicon rubber coated insulator are still exposed

to rain, which cleans the pollutants. The other advantage of using the RTV silicon rubber is that its life time exceeds five years. The selection of the optimum time for replacing coating is still a topic for research [4]. In addition, coating is difficult to apply and is also difficult to remove when its life time is exceeded [18].

2.6.2 Optimization of Electric Field Distribution

Due to the shape of insulator and the formation of dry bands, the distribution of electric field along insulator surface is uneven; the value of electric field is highest near the end parts when compared with any other points on the insulator surface. As a result, the nonuniform distribution of electric field leads to partial discharge and even flashover. In addition, it causes aging of the insulating material. So improving the distribution of electric field along the insulator increases flashover voltage and reduces aging of insulation material.

Yang et al. [19] proposed a new approach for optimizing the distribution of electric field along composite insulators using finite element method [19]. They derived a three-dimensional model for the calculation of the electric field and the surface voltage distribution along the composite insulator. The simulated model consists of the main composite insulator, glass insulator units, transmission line and steel tower. The proposed method depends on the use of additional glass insulator units to improve the distribution of electric field. The main composite insulator is connected in series with a number of glass insulator units which are connected to the high voltage side of the composite insulator. The proposed model has been used to perform sets of calculation on a group of composite insulators connected with different number of glass insulator units at different voltage levels. They deduced from their studies that near the end of composite insulator the electric field was significantly reduced as the number of combined glass insulators

increases. In addition, based on their results they could recommend the number of glass insulator units that have to be used at any voltage levels. Table 2.5 shows the reduction of electric field strength along the composite insulator after the installation of different glass insulator units in series at 500 KV voltage level, with *n* is the number of glass insulator units connected with the composite insulator [19].

Table 2.5 Reduction of electric field strength along the composite insulator after the installation of different glass insulators [19]

n	**0**	**1**	**2**	**3**	**4**
% Voltage of composite insulator	100	73.62	63.76	57.91	53.26
Maximum electric field Strength (kV/mm）	2.0	1.01	0.65	0.536	0.39
Voltage of 20% distance in high voltage end %	63.5	51.75	45.44	41.61	38.36

The effect of using corona rings in improving the distribution of electric field for different types of insulators (glass and porcelain) has been investigated by Akbari et al. [20]. Where they proposed a three-dimensional model to improve the distribution of electric field along composite insulators based on finite element method. The simulated model consists of 230-kV disc insulators (glass and porcelain with different types and shapes), tower, transmission line and corona ring. They deduced from their investigation that the use of corona ring decreases the maximum electric field strength and improves the distribution of electric field along the insulator [20].

2.6.3 Creepage Extenders

The use of creepage extender is considered as a good solution for the contamination flashover problem. By increasing the creepage distance of insulator, the flashover voltage will be increased, leakage currents will be reduced, insulator shape will be improved and the strike distance will be increased. Creepage extender is made from flexible polymeric skirts or from a semi-rigid polymer depending on the type of insulator. Creepage extender can be applied to any type of insulators. This method is costly and is adopted when other methods are not sufficient. Figure 2.5 shows standard (IEC507) flashover test done on 66 KV post insulators with constant contamination level and different creepage distance (using creepage extender). The results show that when the creepage distance increases, the flashover voltage increases [18].

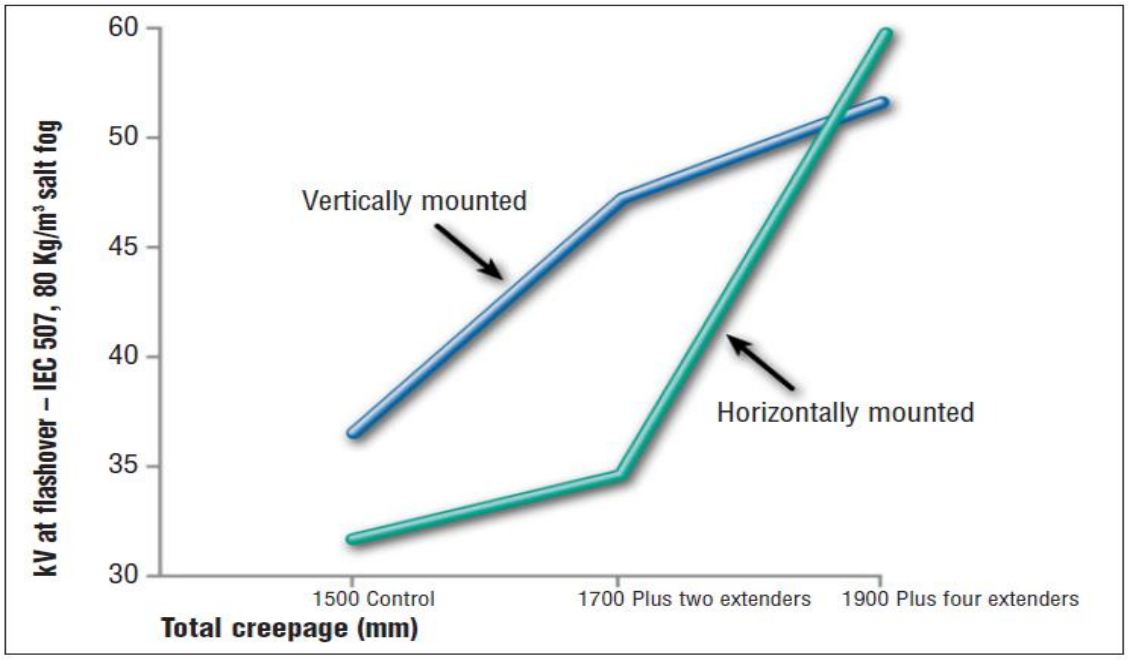

Figure 2.4 Flashover voltage versus number of extenders on 66 kV post insulator [17]

2.6.4 Washing of Insulator

Electrical utilities are forced to deal with the pollution problem by introducing expensive and extensive high-pressure water live-line insulator washing. Methods of insulator washing have been improved and developed to allow washing of insulator under energized conditions. This reduces the need for line outages in connection with insulator washing. The live-line insulator washing is accomplished by means of high pressure, high resistivity water jets and various live-line insulator-washing systems with a pressure of approximately 550 psi at the nozzle. The time interval between washings depends on the criticality of the line and the pollution severity [21]. Emergency washings are also required when special conditions result in sudden build up of contaminants on the insulators.

Adoption of live-line and substation insulators washing techniques and subsequent improvements in washing skills, wash equipment maintenance, right-of-way maintenance, and optimized wash schedules contributed significantly to enhancing the overall reliability of the power transmission system. It is a demonstrated fact that washing is a very effective but very expensive way to clean the insulators. In Saudi Electricity Company (SEC), the annual cost of washing transmission line insulators is about 15 million Saudi Riyals (about US $ 4 million) not counting the substation insulators wash cost. There are different methods of cleaning insulators. Selection of the appropriate methods depend on the type of contamination, number of insulators to be washed, the corresponding cost to select the suitable method. The two popular methods are summarized in Table 2.6. The major problem of using the washing technique is the selection of the optimum washing time. If the washing time is delayed the possibility of insulator failure will increase. On the other hand, if the washing is done earlier, then it may lead to fast build up of pollutants on insulator surface [4].

Table 2.6 Methods of washing insulators [4]

	Cleaning method	Deposit	Comments
Insulator washing	High pressure washing	Deposits with poor adhesion	Time of washing Live washing? Work hours Cost if power interruptions are required
Insulator cleaning	Dry cleaning	Cement Fertilizers	Time of cleaning Dry material deposits Cost Glaze damage and insulator shattering

2.7 Insulator Contamination Severity Diagnostic Techniques

Insulator contamination is normally measured in terms ESDD expressed in mg/cm^2 of salt (NaCl) of insulator surface area. In some coastal areas, contamination level of insulators has been found to build up ESDD values exceeding 0.1 mg/cm^2 within a time period of two months [6]. Therefore, this pollution level requires special attention to reduce its impact on the power system.

Monitoring and prediction of contamination level for high voltage insulators will provide essential information for maintenance departments in the electric utility companies to properly schedule the high-pressure water live-line and substation insulator washing. This will result in huge savings in maintenance costs, improve the electrical system reliability and aid in preventing catastrophic flashovers.

In [22], an expression that relates the ESDD and five metrological factors has been derived using artificial neural networks (ANN). The derived expression predicts the value of ESDD based on

the known metrological values, which are the rainfall, velocity of wind, humidity, pressure and temperature. Extensive series of experiments have been performed on several samples of glass insulator, which were used to examine the proposed expression. For each insulator, the value of ESDD has been measured in addition to the metrological factors. Sixty (60) sets of measured data have been collected from the field, 46 sets have been used to train the neural network system. Among the remaining 14 data sets, 4 have been selected randomly to test the expression. Measured values of the ESDD have been compared with the estimated ones; results show that the ANN is an effective tool in the derivation of that expression [22]. In another reported research work [23], a relation between the ESDD and other variable such as salinity, type of water, plate area and temperature have been derived using ANN. To train the ANN, a series of experiments have been done on several glass insulators to measure ESDD, conductivity, salinity, temperature and plate area. Result shows that the measured and tested ESDD values are almost the same with R^2 value 0.981 (R^2 ranges between 1 and 0. When the model fits the data well, the value of R^2 is close to unity). It has also been found that the main variable that affects the prediction of ESDD is the plate area.

2.7.1 Leakage Current Method

Many utilities, universities and independent laboratories use the magnitude of leakage current (LC) developed on the insulator surface due to contamination as an indicator of the insulation pollution severity, surface degradation or the condition of the insulator and its performance. LC is responsible for dry-band arcing and associated problems of flashover and/or material degradation. As the wetting of the insulator surface progresses, the surface resistance is influenced by the drying effect of the leakage current. The voltage distribution becomes non-linear due to the thermal effects of the leakage current on the contaminant and “dry banding”

results. As this situation progresses, the dry bands eventually bridge a portion or the entire insulator and cause flashover.

Therefore, the magnitude of LC is an important indication of the insulation condition and pollution severity. For each design of insulator there exists a maximum value of LC, above which the probability of flashover increases rapidly. Over the past 25 years, a large amount of information from online LC measurements has been collected in Sweden. Online LC monitoring systems have been installed at Annenberg, Bohus-Malmon and Ludvika field stations. Similar facilities have also been established in Australia, France, Japan, South Africa, UK and USA. Vlastos and his co-workers have presented the Swedish study results in numerous publications. A good correlation between the LC intensity and weather conditions, especially the humidity level, has been reported. This refers to the evaluation of the pollution severity from LC measurements [24].

The shape and frequency components of the LC waveform are a good indicators of the contamination level severity. Tomotaka Suda [25] studied the relationship between the pollution level and the waveform of LC on 120KV string of suspension insulator. Through several field and artificial tests, it was deduced from his experiments and measurements that the LC waveform became symmetrical as the partial discharge (PD) and local arc increase. He also found that the magnitude of the odd order frequency component of LC waveform was increased. So, the pollution levels were categorized into six levels according to thresholds values in the LC waveform (peaks magnitude) and the prominent odd order harmonic component of LC waveform. As a result, there were no thresholds in the magnitude of the prominent harmonic component of LC waveform. Therefore, Tomotaka results were not conclusive and further research work required [25].

Online contamination level monitoring system has been established in four states in Brazil. Six units for acquisition and sending data have been installed on 230 and 500 KV transmission lines; with each unit containing LC, temperature, and humidity transducer, as well as data processer in addition to satellite link for sending data to the utility station database computer. Measurements showed strength correlation between the contamination levels obtained by the monitoring system. Since the satellite communication service covers wider areas compared to other communication systems, it is feasible to be used in data transmission [26]. However, under conditions where the relative humidity was less than 90%, it appears that the LC would not be a good indicator of the contamination level [27, 28]. Very low leakage currents not exceeding 10 mA, were recorded even with heavy contamination levels on porcelain and composite insulators at different locations near the coast. This indicated that the LC parameter varies significantly with relative humidity. In another study, aging cycles modeled for a 500-kV line with lower contamination levels have shown significant degradation of certain insulator units closer to the live-end even though negligible LCs were measured [24, 29]. Furthermore, LC measurements can be significantly affected by the presence of other electromagnetic waves in the site. Also, installing LC apparatus requires certain arrangement and reconstructing of insulator [30].

2.7.2 Acoustic Estimation (AE) Method

It is well-known that precipitation of contaminants on the insulator surface causes partial discharges (PD). Practically, the severity of PD activity increases as the level of contamination increases. Occurrence of PD will generate acoustic noise and this noise can be acquired and correlated to the contamination level in order to predict the pollution severity. C.Pen et al. [31] proposed a system to monitor the contamination severity of ceramic insulators by using the acoustic emission caused by PD. Set of artificial pollution test have been conducted to correlate

the PD noise (acquired signal) and contamination level. The proposed AE system consists of an acoustic sensor and an acquisition system. It was concluded from the experiments on the AE system that the system yeilds good indication about the contamination level [31]. In [32], a system has been built to acquire the ultrasonic signal resulting from the PD on the insulator surface in order to predict the level of pollution severity. The acquired signal has been analyzed and classified using artificial neural networks (ANN) tool. A set of artificial pollution tests have been preformed, in order to collect data for training and testing the ANN. The contamination levels have been classified into six groups based on the features extracted from the acquired signals. Each group was identified by a code as shown in Table 2.7. The results showed that sounds emission is a useful tool for early detection of the contamination level of insulators [32]. However, this method can be influenced by the background noise such as wind and corona [6].

Table 2.7 Category of contaminatin levels and their codes [32]

Class	Pollution Level	Codification
A	non-polluted atmosphere	1 0 0 0 0 0
B	clean atmosphere	0 1 0 0 0 0
C	very light contamination	0 0 1 0 0 0
D	light contamination	0 0 0 1 0 0
E	heavy contamination	0 0 0 0 1 0
F	very heavy contamination	0 0 0 0 0 1

2.7.3 Thermovision Method and Infrared

The flow of LC through the insulator surface generates heat which depends on the density of LC. Temperature distribution (TD) on the insulator surface depends on the density of LC. Therefore, TD can help in motoring of the insulator contamination level as the difference in TD increases with the increase of the contamination level. Infrared camera can be used to detect the TD by taking thermovision images; features can be extracted from these images and correlated to the level of contamination. This method is appropriate for all insulator types. However, sun, humidity, wind and temperature can affect the performance of this method [33, 34].

2.7.4 Ultraviolet (UV) Method

UV imaging is a technique that can detect UV signals with wavelengths varying between 240-280 nm. Before a complete flashover occurred, long-time of pre-discharge occurs on polluted insulator surface. Partial discharge (PD) is related strongly to the pollution level. PD generates electromagnetic waves, sound, heat and light. UV method is considered as an effective way to detect PD. Fangcheng et al. in [35], investigated the use of UV imaging method in the prediction of contamination level of ceramic insulators through the detection of discharges on the insulator surface. Several artificial pollution tests were conducted and image processing was used to process the UV images in order to extract the PD from the background. Fuzzy logic has been used to correlate the extracted features from the images with the pollution levels [35]. On the other hand, it is worth mentioning that UV method is significantly affected by environment [34].

2.7.5 Digital Image Processing Method

Image processing has played an important role in providing valuable analysis to various applications including medicine, seismology, geology, face recognition, finger-print recognition, and many other pattern recognition applications [36, 37, 38]. Once digital images are acquired, pre-processing will be done, followed by an application of suitable edge detection techniques and segmentation. Segmented parts can be used for further analysis such as estimation of unique features. Once the features are extracted, there exist many classification methods such as statistical, algorithm- based, neural networks, among others, to provide the user with the necessary information for an accurate recognition [39].

Two different groups of researchers, Xin et al. [40]and Xia et al. [41] investigated the use of a digital camera to determine the dirty-area ratio of insulators using digital image processing. They used watershed algorithm to segment the insulator image in order to exclude the background from the image, then processed the segmented image to determine the dirty-area region using the hue, saturation and intensity color model (HSI). Finally, they found out that the ratio of the dirty area with respect to the insulator total area may help in determining the contamination severity.

2.8 Conclusion

Based on a preliminary literature and industrial surveys, there exists no tool that can predict contamination level on high voltage insulators using image processing and artificial neural network algorithms. As such, this thesis aims at developing and testing a tool for monitoring contamination level of high voltage insulators based on image processing and artificial neural networks. Using this tool, important features extracted from camera images of insulators will be correlated to the ESDD level and, hence, the possibility of flashovers can be detected. The

developed tool will provide an early warning of possible insulators flashover due to contamination without the need for human intervention. The contamination level monitoring tool, which is developed in this thesis can be easily integrated to the predictive maintenance system of any electricity utility company. This will help electric utilities and industrial plants to run their facilities at high efficiency and reduce maintenance costs. It is believed that the developed tool will encourage the local industry to utilize this technology which will result in huge savings, improving productivity, and reducing unnecessary outages.

CHATPTER THREE

PROPSED MONITORING ALGORITHM

3.1 Overview of the Proposed Algorithm

As mentioned earlier, the aim of this thesis is to develop a contamination level monitoring tool, which provides early warning of possible flashovers. The flowchart shown in Figure 3.1 is a complete step-by-step description of the work that has been done which can be summarized as follows:

Step 1: Collecting samples of naturally contaminated insulators from SEC and Saudi Aramco as well as Dhahran Electrical Insulator Research Station at KFUPM.

Step 2: High resolution camera is used to build an image data bank for the collected naturally contaminated insulators.

Step 3: Using the labs of the RI at KFUPM, flashover voltages and ESDD levels of the collected naturally contaminated insulators were estimated.

Step 4 & 5: Image processing techniques and artificial neural network were employed to develop the correlation between the selected image features and ESDD levels.

Step 6: Testing of the developed correlation were carried out on new contaminated samples.

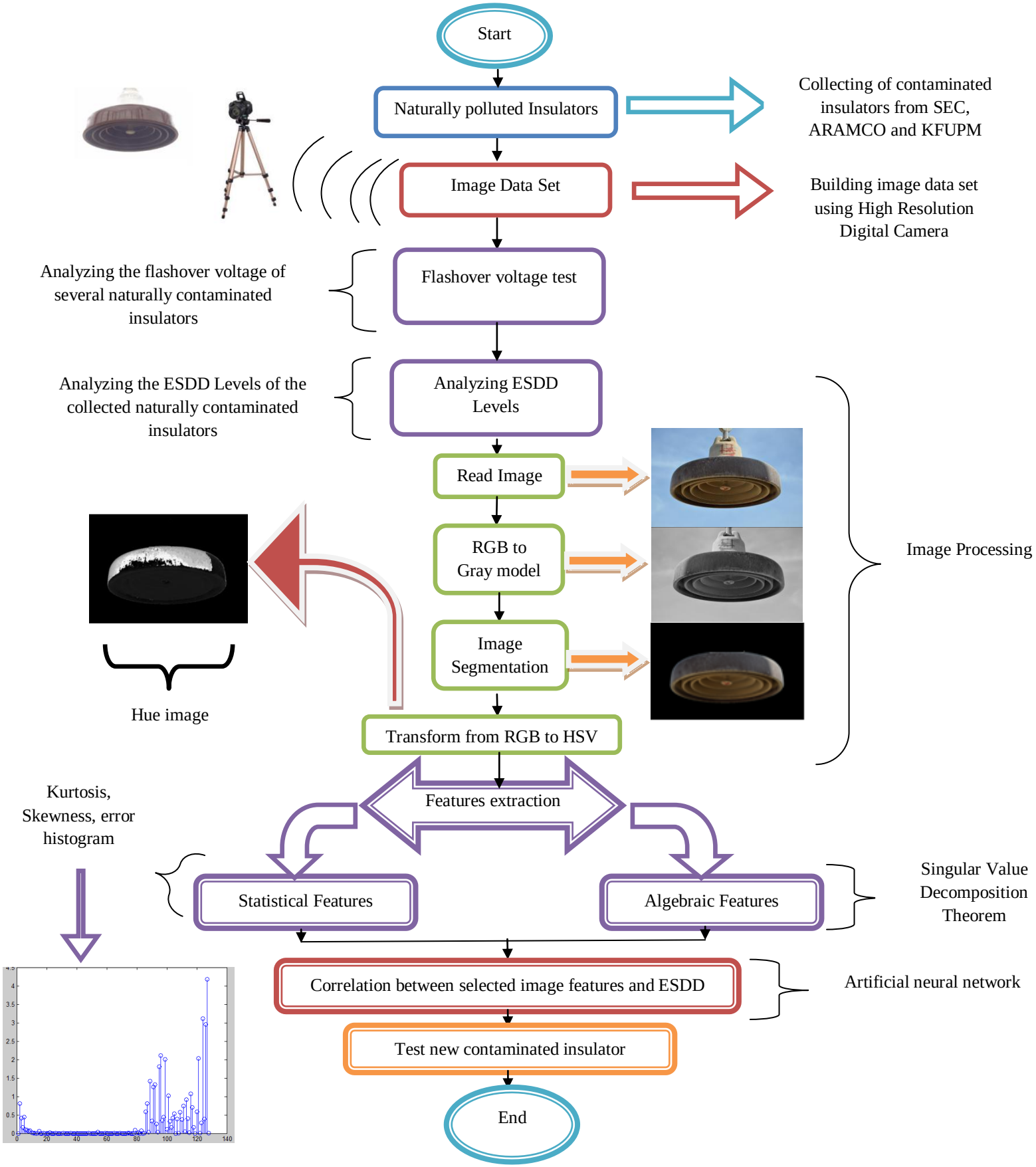

Figure 3.1 Flow Chart of the proposed monitoring algorithm

3.2 Collecting Insulators samples

Samples of naturally contaminated insulators were collected from Saudi Electricity Company (SEC) and Dhahran Electrical Insulator Research Station at KFUPM. The types of the collected insulators are super fog porcelain high voltage insulators. These insulators are of different pollution levels. All of the collected insulators have been stored in Dhahran Electrical Insulator Research Station which shown in Figure 3.2.

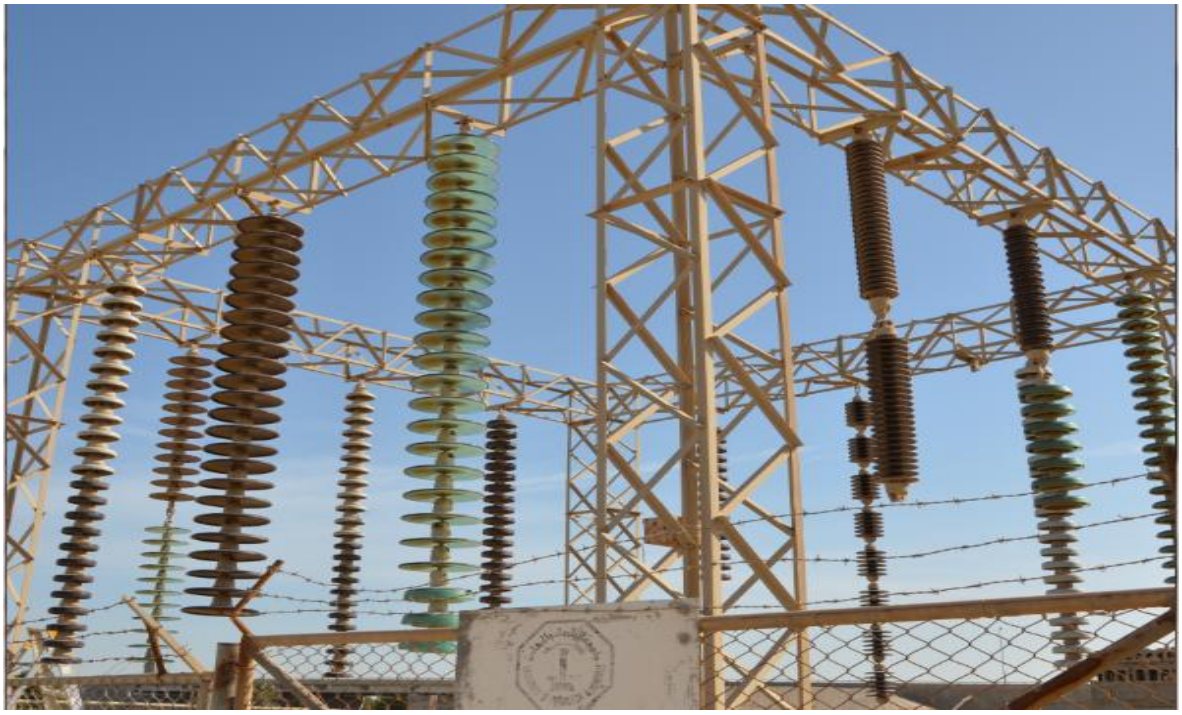

Figure 3.2 Dhahran Electrical Insulator Research Station in KFUPM

3.3 Preparing Image Data Set

A digital camera (Nikon D7000) is used to capture images for insulators. In order to emulate the natural field of insulators, the images of insulators have been taken at Dhahran Electrical Insulator Research Station.

3.4 Flashover Voltage Test

Flashover tests on several collected sample of insulators have been conducted. The testing procedure that has been used in the experiment is a revised version of the conventional clean-fog method [42, 43]. This test procedure is called the rapid flashover voltage technique (RFVT). Using this method, the duration of the test can be reduced considerably. A brief description of the procedure is given below. Figure 3.3 shows the testing setup.

- The insulator is placed in the fog chamber, and energized with a voltage estimated about 20% or more above the expected mean flashover value.
- Steam fog is injected into the fog chamber at a rate of 0.074Kg/h/m3.
- If no flashover occurs within 25 minute, the voltage increased by 5% every minute until flashover.
- After flashover, the insulator is re-energized at a voltage 3 step below the preceding flashover value (one step being 4% of the test flashover value).
- The voltage is increased by one step every 3 minutes until flashover.
- This sequence is repeated, with flashover voltage (FOV) values decreasing to a minimum and then gradually rising until they are considerably above the minimum.
- The performance criterion is the minimum FOV value, which can be defined depending on the wetting time. If it is short, the lowest flashover voltage (V_{min}) is used, and if the wetting time is long enough, the minimum of the means of five consecutive FOV values ($V_{5\ min}$) is used. The flowchart shown in Figure 3.4 is a complete step by step description of the Rapid Flashover Voltage Test.

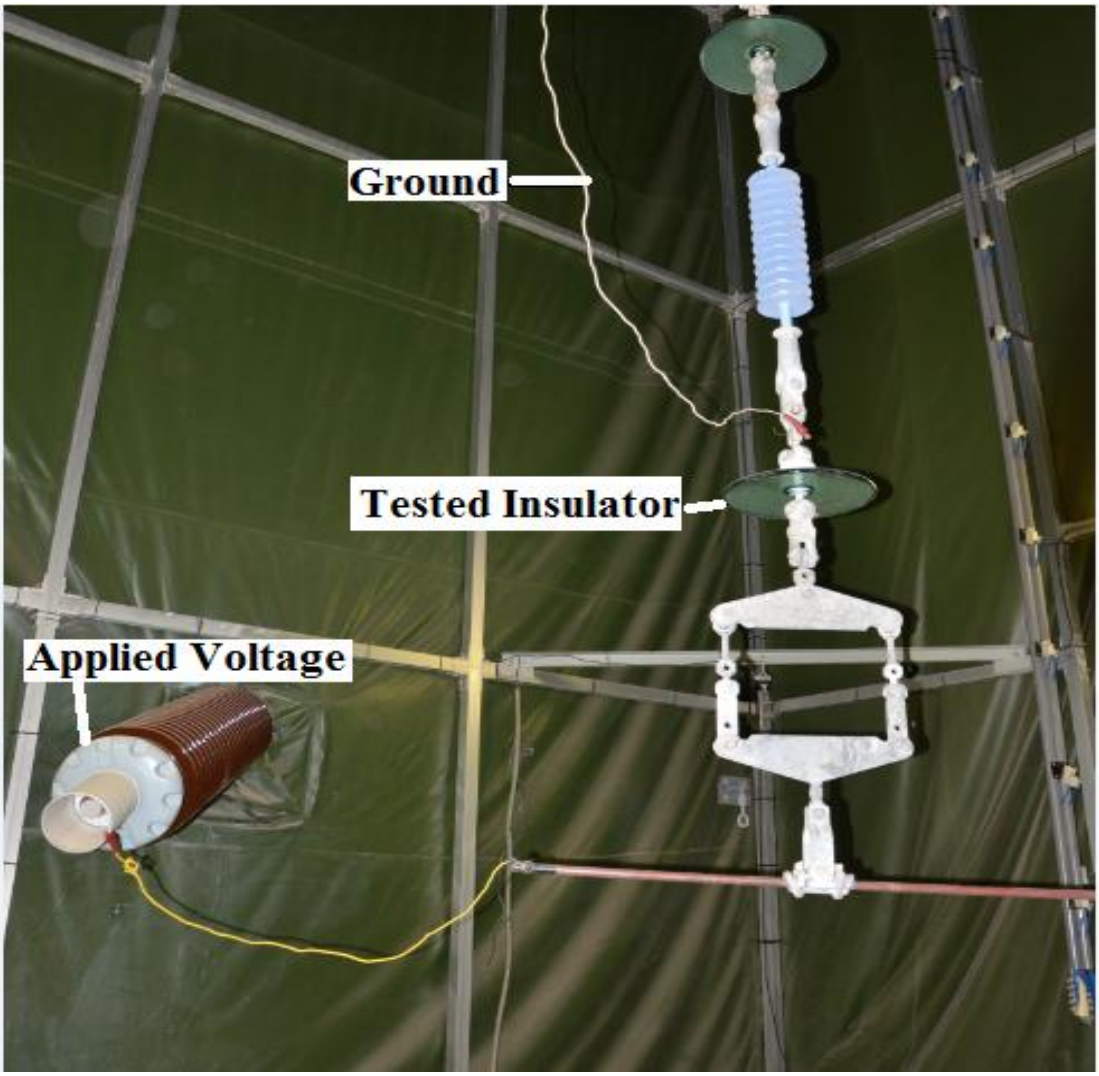

Figure 3.3 Flashover testing setup

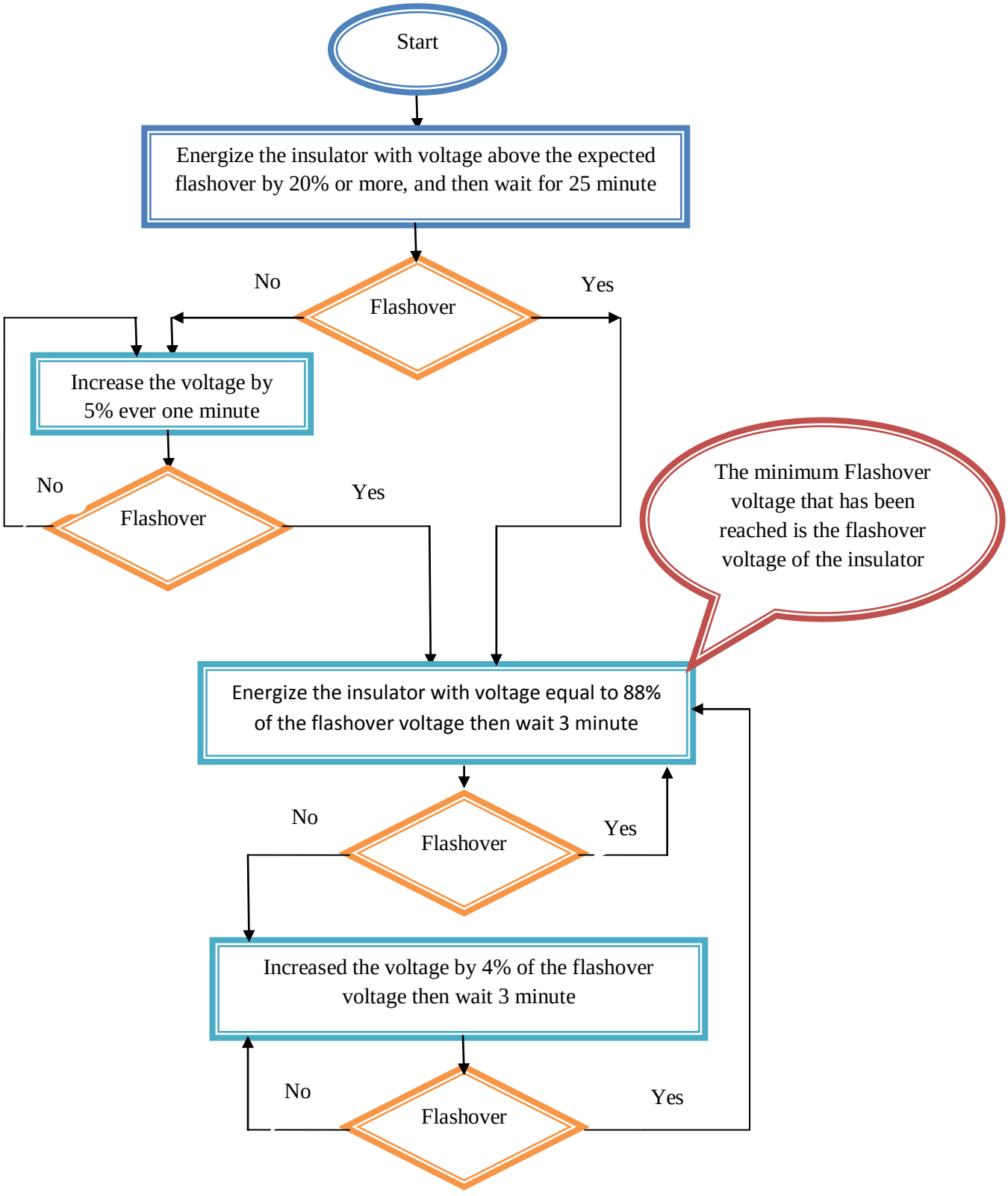

Figure 3.4 Rapid flashover test algorithm

3.5 Measuring ESDD Levels

The International Electro technical Commission (IEC) adopted a standard method to find the ESDD value in case of glass or porcelain insulators [44]. The ESDD is obtained by measuring the conductivity of the solution containing the pollution removed from insulator surface and calculating the equivalent amount of NaCl having the same conductivity.

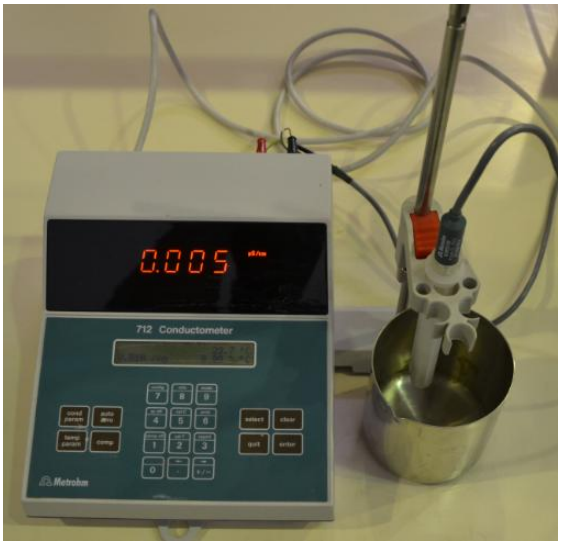

Figure 3.5 Conductivity meter (High-Voltage Lab, Research Institute, KFUPM)

The conductivity and temperature of the polluted solution is measured by the conductivity meter shown in Figure 3.5. If the solution temperature is not $20^{\circ}C$, conductivity values shall be corrected using the following formula:

$$\sigma_{20} = \sigma_{\theta}[1 - b(\theta - 20)] \qquad (3.1)$$

Where

σ_{20} is the volume conductivity at 20 ℃ (in S/m), σ_{θ} is the volume conductivity at a temperature of θ ℃ (in S/m), θ is the solution temperature (℃) and b is the factor depending on temperature θ, as given in Table 3.1.

Table 3.1 Values of the factor *b*

θ (C°)	***b***
5	0.03156
10	0.02817
20	0.02277
30	0.01905

The temperature of the salt solution shall be between $5^{\circ}C \; and \; 30^{\circ}C$, since no experience is available to validate tests performed outside this range of solution temperatures. For other values of the temperature θ, within the range $5^{\circ}C \; and \; 30^{\circ}C$ which are not stated in Table 3.1, the corresponding b factor is obtained by interpolation [44]. The calculation of the ESDD value of each surface (top and bottom) of the insulator is achieved separately using the same formulas as in [44]. The salinity, Sa in (kg/cm^3) and the ESDD are calculated as follows

$$Sa = (5.7 * \sigma_{20})^{1.03} \tag{3.2}$$

$$ESDD = \frac{Sa*Vol}{A} \tag{3.3}$$

Where V is the volume of distill water (in cm^3) and A is the area of the insulator surface (top or bottom) (in cm^2). The total ESDD value (ESDD_{total}) of the insulator is calculated as follows

$$ESDD_{total} = \frac{ESDD_{top} \; x \, A_{top} + ESDD_{bottom} x \; A_{bottom}}{A_{total}} \tag{3.4}$$

$$A_{total} = A_{bottom} + A_{top} \quad (3.5)$$

Where $ESDD_{top}$ is the ESDD value of the top surface of insulator (mg/cm^2), $A_{top}$is the area of the top surface of insulator (in cm^2), $ESDD_{bottom}$ is the ESDD value of the bottom surface of insulator (mg/cm^2), A_{bottom} is the area of the bottom surface of insulator (in cm^2) and A_{total} is the total surface area of insulator (in cm^2)

3.6 Image Processing

Image processing is a multi-disciplinary field, where different areas of science contribute to it, such as computer science, mathematics, electrical engineering, physics and computer engineering. In addition, it overlaps with other research areas like artificial intelligence, machine learning, human vision and pattern recognition. This mix of intersecting fields and cross-disciplinary research forces the image processing research to grow rapidly. Moreover, technology developments in computer processers and mass storage devices have helped in its growth also. Areas were analog imaging is used are now changing to use digital systems, for their flexibility. Medicine, seismology, film, photography, video production, security monitoring, geology, face recognition, finger-print recognition, and many other engineering applications produce a huge volume of digital image data every day. Extracting important and representative information from digital images is considered as the primarily concern of image processing. Such extraction has been conducted using computer, with little or no man intervention [45, 46].

Image processing operations are divided into three levels. Low level (primitives operation): are those techniques which handle raw image data, where both input and output are images, contrast enhancement and noise reduction being good examples. In the middle level, attributes are

extracted from images by utilizing the obtained result from the low level operations, such as edges, contour and regions. At the highest level, analysis and interpretation of the contents of the image using the information gained from the lower levels, such as handwriting recognition and pattern recognition [45].

In this thesis, different image processing techniques and algorithms have been used in order to extract representative features from the processed images. The background and insulator cap of the captured images have been excluded using some segmentation algorithms. Segmentation of the images requires transforming the image from red, green, blue (RGB) color space into gray-scale model. After that, the images are transformed back to RGB color space model using the matrix manipulation method. Contaminants on insulator surfaces affect the color of the insulator. Accordingly, the insulator image is transformed from RGB to HSV (hue, saturation, value) space model. Hue (color) image of insulators is more representative to the contamination on insulator surface and hence it has been used in extracting features.

3.6.1 Digital Image

A digital image is a discrete two-dimensional function $f(x, y)$ that represents an image produced by an optical device. This representation is achieved using finite number of picture elements (pixels); each pixel has one or more numerical value. Accordingly, it can be assumed that the digital image is a rectangular matrix; with X columns and Y rows, each entry of the matrix is the pixel numerical value. XxY represents the resolution of the image [46]. The numerical value of each pixel depends on the type of digital image. Color images are made up of colored pixels, where three values (e.g., representing the amount of red (R), green (G), and blue (B)) are usually

required for each pixel. In black-and-white images, a single value representing the light intensity (usually in a [0, 255] range) is required.

Gray-scale (black and white image) and colored images are the important types of a digital image. A gray-scale image is composed of pixels which have different levels of gray in which each pixel is represented by one scalar value, and this value is the measure of light intensity, which vary from black at the weakest intensity (minimum brightness) to white at the strongest (maximum brightness). Figure 3.6 shows a grayscale high voltage insulator string image. On the other hand, color image is composed of colored pixels; each pixel is a vector of color components. Red, green and blue which are the primary colors; hence we can obtain any color by mixing these colors by certain amounts. Other common color spaces are cyan, magenta, yellow, black (CMYK) and hue, saturation, value (HSV). In addition to the previous two types of digital images, there is another type called the binary image where the image is made up of pixels that are represented by a single bit. Accordingly, a single bit has one of two values (two colors), usually, black or white [47].

Figure 3.6 Grayscale image of high voltage insulator string

3.6.2 Color Space Models

Color models use the fact that colors can be described by combinations of three basic colors, called primary colors. Thus, a color space (color system) is a mathematical representation of a set of colors, where any color can be created and specified. Each color model has a specified coordinate system and subspace within the system where any color is represented by single point as shown later. Different applications require different color spaces. For example, computer graphics use RGB color space while in color printing CMYK model is used [48]. Moreover, HSV and hue, saturation and lightness (HSL) color models are used in processing, programming and end user manipulation. All of the colors system can be derived from the RGB model.

3.6.2.1 RGB Model

Red, green and blue (RGB) color model is the most common option for computer graphics because color monitors used red, green and blue to create any desired color. This model depends on Cartesian coordinate in representing any color within the system.

RGB model can be converted to grayscale where the pixel is represented by one value instead of three values as in RGB. Conversion algorithms are based on forming a weighted sum of the R, G, and B components to calculate grayscale values. There are a lot of approaches for finding the values of the weights. Equations (3.6) and (3.7) show the weighted sum of the R, G, and B components to calculate grayscale values in two different approaches [49] and [50], respectively.

$$\text{Gray value} = 0.2989 * \text{R} + 0.5870 * \text{G} + 0.1140 * \text{B} \tag{3.6}$$

$$\text{Gray value} = 0.333 * \text{R} + 0.5 * \text{G} + 0.1666 * \text{B} \tag{3.7}$$

3.6.2.2 HSV Model

HSV (hue, saturation, value) model was fabricated to be more perceptual and intuitive in handling colors, and it is designed to emulate the way humans interpret and perceive colors. The hue (hue component of the image) is the pure color of light. In physics, each color has its particular wavelength; the dominant wavelength at which most of the energy is concentrated is the hue. For example, all green colors have the same hue value even if they are pastel, intense, dark, or light. The saturation is a measure of the color purity; colors which are saturated are pure hue. If the color is mixed with white, the saturation will decrease. The value (brightness) of a color is a measure of how dark or light it is. The color of zero brightness is black color regardless of how much it is hue or saturated. HSV model uses the cylindrical coordinates in representing any color within the system as shown in Figure 3.7 [45].

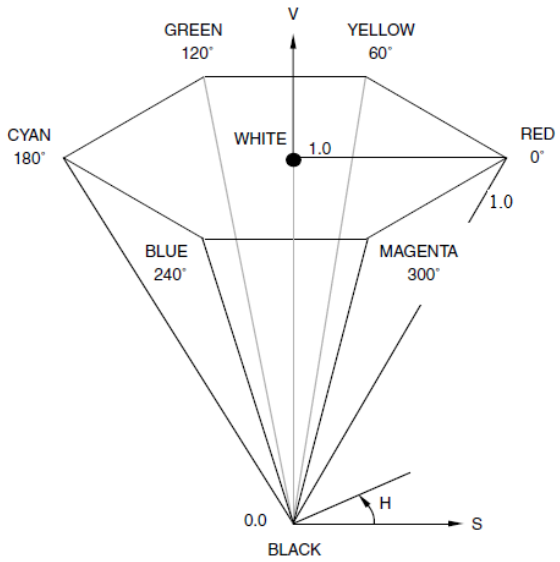

Figure 3.7 HSV color model as a hexagonal cone [44]

The structure of HSV model in Figure 3.7 shows that any color within the system can be specified by its hue (the value of the angle from the red position), its saturation (how far from the

V-axis), and its brightness (how far up from the black point) [47]. The HSV model can be obtained from the RGB model [48]. Equations (3.8)-(3.16) show the step by step conversion process. The R, G, B values are divided by 255 to change the range from 0...255 to 0...1(normalization of RGB model)

$$\grave{R} = \frac{R}{255} \tag{3.8}$$

$$\grave{G} = \frac{G}{255} \tag{3.9}$$

$$\grave{B} = \frac{B}{255} \tag{3.10}$$

$$C_{max} = \max(\acute{R}, \acute{G}, \acute{B}) \tag{3.11}$$

$$C_{min} = \min(\acute{R}, \acute{G}, \acute{B}) \tag{3.12}$$

$$\Delta = C_{max} - C_{min} \tag{3.13}$$

Hue calculation;

$$H = \begin{cases} 60^{\circ} * \left(\frac{\grave{G}-\grave{B}}{\Delta} \ mod\ 6\right) & , \quad C_{max} = \acute{R} \\ 60^{\circ} * \left(\frac{\acute{B}-\acute{R}}{\Delta} + 2\right) & , \quad C_{max} = \grave{G} \\ 60^{\circ} * \left(\frac{\acute{R}-\grave{G}}{\Delta} + 4\right) & , \quad C_{max} = \acute{B} \end{cases} \tag{3.14}$$

Saturation calculation

$$S = \begin{cases} 0 & , \ \Delta = 0 \\ \frac{\Delta}{C_{max}} & , \ \Delta > 0 \end{cases} \tag{3.15}$$

The hue is undefined when S=0.

Value (brightness) calculation

$$V = C_{max} \tag{3.16}$$

Figure 3.8 shows an example of transforming an RGB image to HSV image using MATLAB^{TM}, where hue, saturation and brightness component are displayed separately. In addition to the previous mentioned advantage of HSV model that this model emulates the way humans interpret and perceive colors, it also allows the independent control of hue, saturation, and brightness. Therefore, it has the ability to separate the brightness from the other two components (hue and saturation).

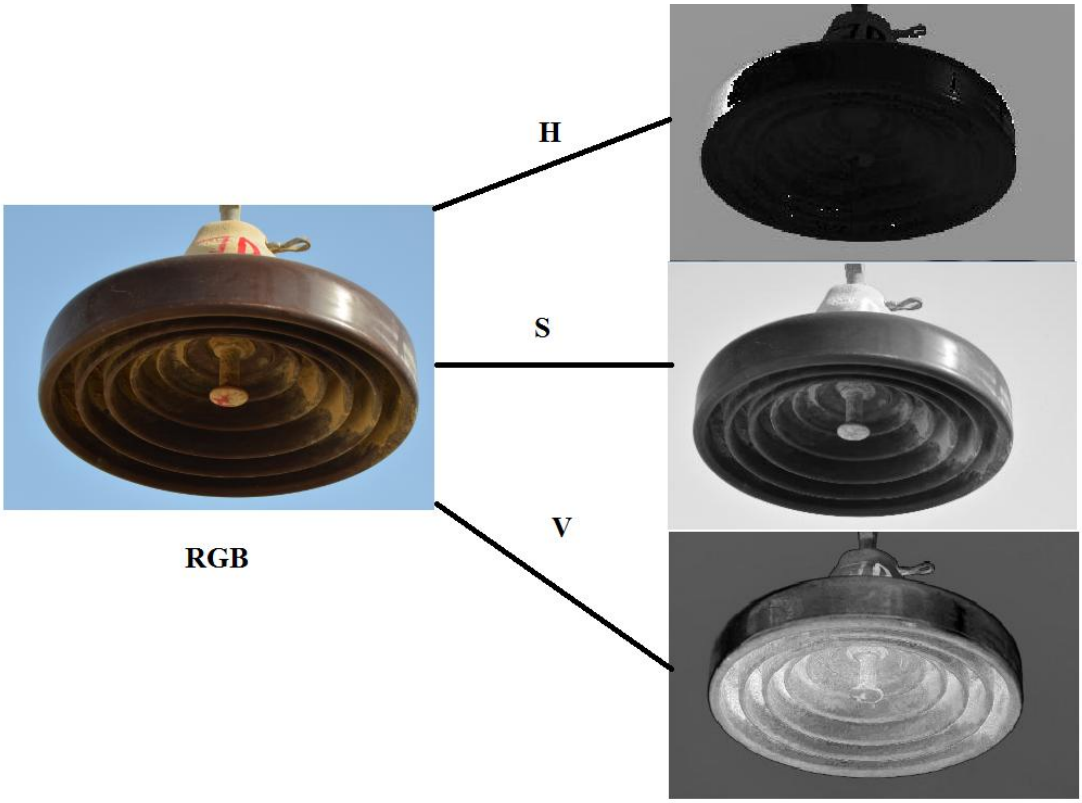

Figure 3.8 RGB to HSV image components

3.6.3 Image Segmentation

Segmentation of image is considered as one of the most important pre-processing tasks in image processing. It is used in many applications that depend on computer vision such as hand written recognition, locating objects in images, medical imaging, machine vision, face and finger print recognition and many other applications. Therefore, image segmentation is the bridge that links low-level image processing with image interpretation and analysis. Image segmentation is defined as the process of dividing an image into non-overlapping meaningful regions (separating the objects from the background in an image) which have similar attributes. Discontinuity and similarity of pixel value are considered as the basic properties that most of segmentation algorithms depend on. In addition to these basic attributes, texture, image edges, color, motion and intensity are useful properties for segmentation [51].

Non-uniform lighting, over-lapping among objects, shadows, poor contrast between objects and background in images, in addition to non-trivial images made the segmentation problem very hard. The precision of image segmentation step would have large influence on the performance of the subsequent steps of image processing. There are a lot of factors that play role in the existence of different image segmentation algorithms in spite they have the same goal. Among these factors are image type (e.g., gray, color, binary), type of attributes (e.g., color, texture, intensity) and selection of mathematical approach (e.g., image statistic, graph theory). Accordingly, the existing segmentation algorithms have been categorized into four types; namely, region-based segmentation [52], intensity-based methods [52], edge-base segmentation and matching [45].

The following two subsections demonstrate the two techniques of segmentation (Edge based segmentation, Chan-Vese model) which have been employed in this piece of work.

3.6.3.1 Edge-Based Segmentation Methods

Edge-based segmentation means partitioning an image based on the edge in that image. The edge is defined as the boundaries between two regions in an image having different attributes according to some property such as intensity (gray level), texture or color. Therefore edge based segmentation requires some edge detection techniques before segmentation. Using this method, the boundaries that represent objects in an image are detected, thus these boundaries can be used to specify and identify these objects [53].

Edge detection is a fundamental tool for image segmentation. It utilizes the benefit from the difference of gray tone in an image to detect the edges. Therefore, the aim of edge detection techniques is to detect the boundaries of objects of interest based on discontinuities in intensity levels. In this thesis, we focus on finding the edges in grayscale images, which are related to abrupt change in the intensity function across a portion of the image. Figure 3.9 shows two types of edges; one is an ideal edge (sharp transition) and the other is a ramp edge (gradual transition between dark and bright region).

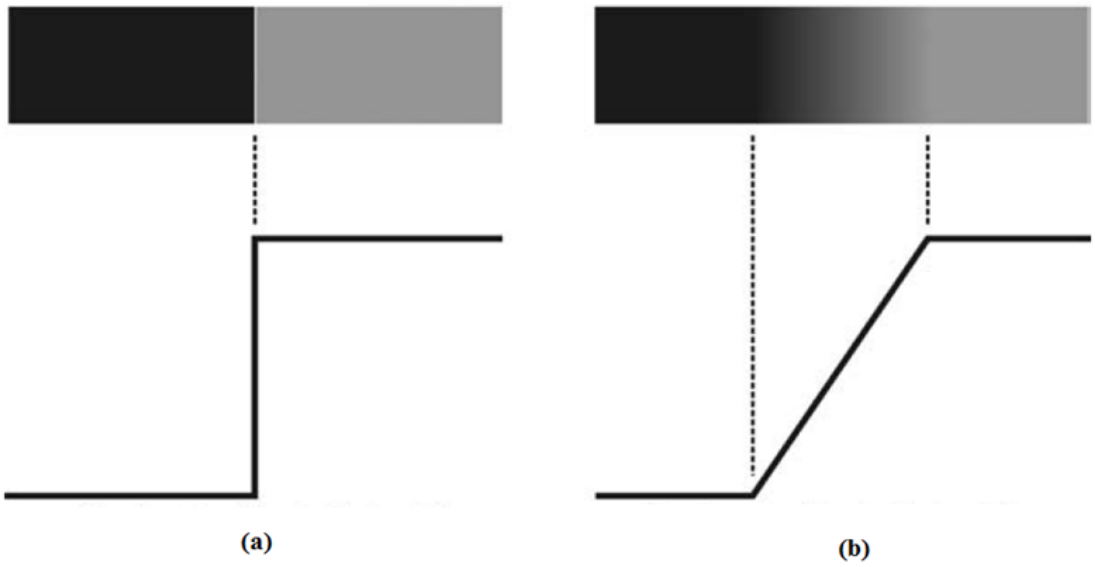

Figure 3.9 (a) Ideal edge of a digital image (b) Ramp ideal edge of a digital image [44]

Edge detection methods are usually grouped into two different categories: gradient and laplacian. These two categories depend on the calculation of the first or second order derivatives of the intensity function to detect the edges in an image, respectively. In Gradient methods, the magnitude of the first derivative (looking for maximum and minimum) is used to detect the existence of an edge in the image. While laplacian methods detect the edges by looking for the zero crossing in the second derivative of the intensity function. Moreover, the sign of the second order derivate can help in determining whether a pixel lie on the bright side or dark side of the edge. In computer vision, edge detection is conventionally executed by convolving the grayscale image with some form of linear filter (operator) which usually approximates the first or second derivative. Sobel, Canny, Prewitt and Roberts's operators are examples of edge detection operator. However, many factors have great impact on the performance of the edge detection technique such as contrast between objects and background, position and size of objects, shadows, uneven illumination and noise [45, 54]. Edge detection process consists of four main steps [45].

1- Noise reduction.

2- Edge point detection (edge enhancement): done by using edge detection operator.

3- Thresholding: keeps only edge points and eliminates false edge points.

4- Edge localization: compute location and orientation of edges.

In this thesis, Sobel edge detection operator is used. Technically, this operator is used to detect the edges (sharp intensity variations) in grayscale images based on performing a 2D spatial gradient calculation; hence, the areas of high gradient values are related to edges. Thus, it is a discrete differentiation operator measuring the approximation of the gradient of the image intensity function [55].

The gradient of a function $f(x,y)$, which is equivalent to the first order derivative can be calculated as follows [55]:

The gradient of f at coordinate (x,y) is defined as the two dimensional column vector

$$\nabla f = grad(f) = \begin{bmatrix} g_x \\ g_y \end{bmatrix} = \begin{bmatrix} \frac{\partial f}{\partial x} \\ \frac{\partial f}{\partial y} \end{bmatrix} \tag{3.17}$$

$$g_x(x,y) = \frac{\partial f}{\partial x} \cong f(x+1,y) - f(x,y) \tag{3.18}$$

$$g_y(x,y) = \frac{\partial f}{\partial y} \cong f(x,y+1) - f(x,y) \tag{3.19}$$

where $g_x$and g_y are the gradient in the x-direction and y-direction respectively. The magnitude of the gradient vector, denoted as $|g|$

$$g = mag(\nabla f) = \sqrt{g_x^2 \quad + \quad g_y^2} \tag{3.20}$$

which can be approximated by

$$|g| = |g_x| + |g_y| \tag{3.21}$$

In sobel operator, the calculation of the gradient at each point in a grayscale image is done using two convolution masks (kernels) h_x and h_y with 3x3 size. These masks are convolved with the image, one of them approximate the gradient in the x-direction $G_x(x,y)$, the other approximate the gradient in y-direction $G_y(x,y)$ as in equations (3.22) and (3.23)

$$h_x = \begin{bmatrix} -1 & 0 & 1 \\ -2 & 0 & 2 \\ -1 & 0 & 1 \end{bmatrix}, \quad h_y = \begin{bmatrix} -1 & -2 & -1 \\ 0 & 0 & 0 \\ 1 & 2 & 1 \end{bmatrix}$$

$$G_x(x,y) = h_x * f(x,y) \tag{3.22}$$

$$G_y(x,y) = h_y * f(x,y) \tag{3.23}$$

The convolution in the *x*-direction is done by sliding h_x over the image, starting from left (the beginning of a row) then shifted to the right by one pixel each step until the mask reach the end of a row, then starts at the beginning of the next row where at each shifting step, $G_x(x, y)$ is calculated. Similarly, convolution in the *y*-direction is done by sliding h_y over the image, starting from up (the beginning of a column) then shifted down by one pixel each step until the mask reach the end of a column where at each shifting step, $G_y(x, y)$ is calculated. Looking at the convolution sobel masks, it can be found that the sum of coefficients (entries) equals to zero. This means that when it is applied to a perfectly homogenous area (constant intensity values) of an image, the result will be zero (black color). Figure 3.10 illustrates the operation of Sobel pseudo convolution mask when it is applied to an input image. The sobel pseudo mask performs the following operation to calculate the point $B22$ of the image [54]:

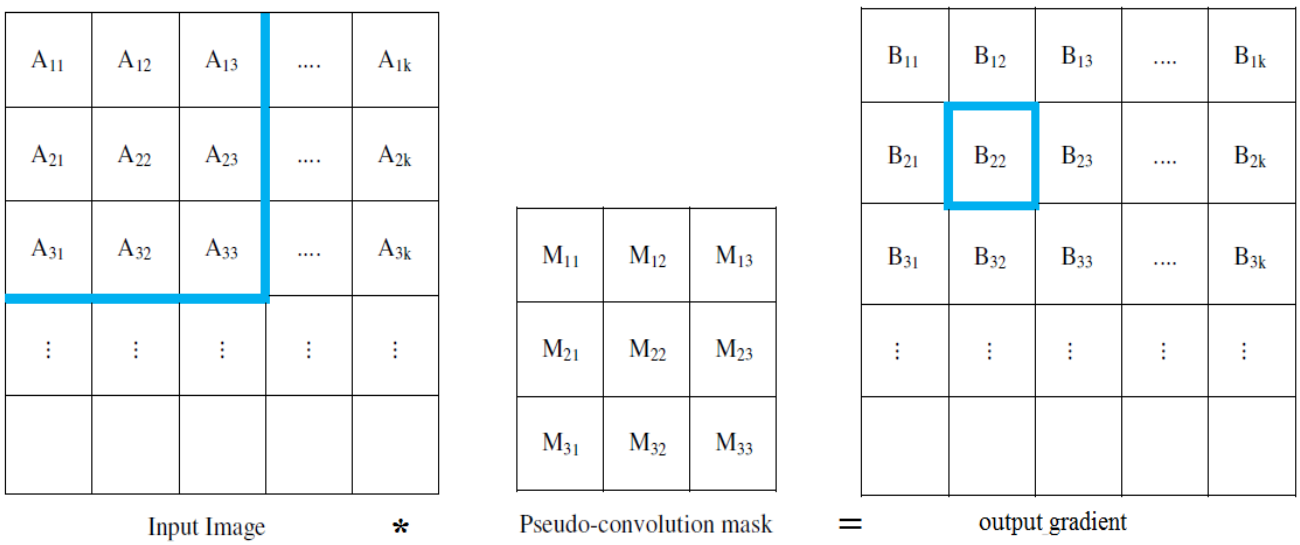

Figure 3.10 Sobel Pseudo Convolution Mask Applied to an Image [54].

$$B_{22} = (A_{11}xM_{11}) + (A_{12}xM_{12}) + (A_{13}xM_{13}) + (A_{21}xM_{21}) + (A_{22}xM_{22}) + (A_{23}xM_{23}) + (A_{31}xM_{31}) + (A_{32}xM_{32}) + (A_{33}xM_{33}) \quad (3.24)$$

Accordingly, the gradient components $G_x(x,y)$ and $G_y(x,y)$ are produced separately which can then be combined together to calculate the absolute magnitude of the gradient and the direction of the gradient at each point [56].

The approximate magnitude and angle (θ) of the gradient are calculated as follow:

$$|G| = |G_x| + |G_y| \tag{3.25}$$

$$\theta = arctan\left(\frac{G_y}{G_x}\right) \tag{3.26}$$

where θ: measured with respect to the x-direction.

3.6.3.2 Active Contour Models for segmentation

The fundamental idea in active contour models is to evolve a curve, subject to constraints which are mainly from image data in order to detect objects in that image. Such a model starts with a contour selected around the object to be detected in the image. This contour which defines an initial segmentation evolves, according to some evolution equation, in such a way that it stops on the boundaries of the desired object as shown in Figure 3.11. There are various ways to define the evolution equation; for instance, the contour might move with a velocity that depends on the image gradient at a given point or based on global region information in the image [57].

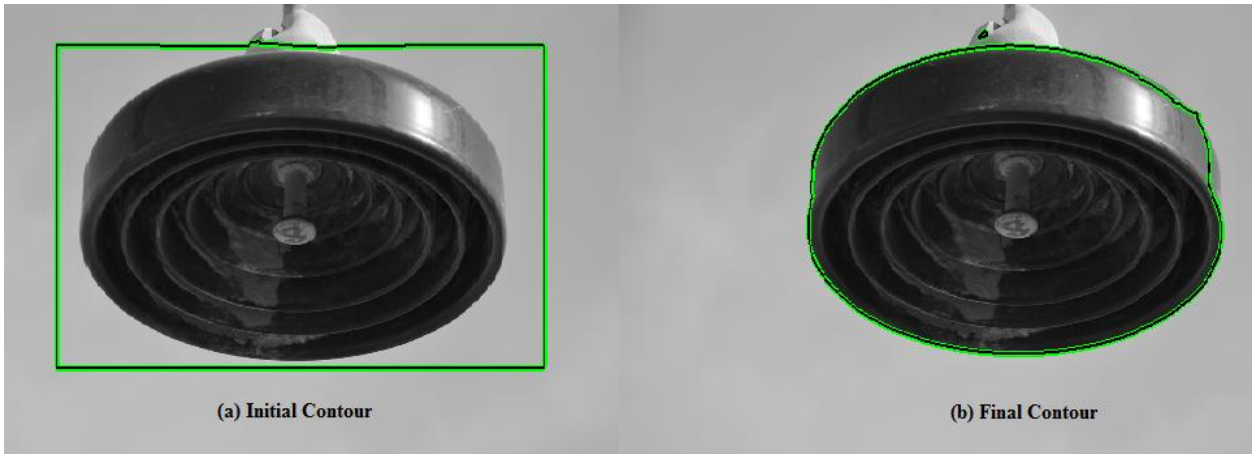

Figure 3.11 Active contour segmentation principle

Edge based and region based models are two types of active contour models [58]. The edge based model usually depends on the image gradient information to build some stopping function in order to evolve the contour to stop at the desired object boundary. Therefore, this model can detect only objects with edges defined by gradient. In practice, this model is suffering from critical boundary leakage for images with discrete gradient (weak boundary) and noise. Active contour model or snake model proposed by Kass et al. [59] is an example of edge based models. On the other hand, region based active contour model usually utilizes the global region information to evolve the curve. In this way, this model can detect contours both with and without gradient, i.e. objects with very smooth boundaries or even with discontinuous boundaries. Chan and Vese model [60] is an example of the region based contour models.

3.6.3.2.1 Chan-Vese Model

Mumford-Shah model is considered as a general image segmentation model [61]. By using Mumford-Shah model the image can be partitioned into sub-regions. Inside each of the separated region, the original image is approximated by a smooth function. Therefore, based on this model an image is modeled as a piecewise-smooth function. Consider an image I with a domain Ω, let U be the image's model, and let C be the boundaries that are associated with the model. Therefore, the Mumford-Shah energy functional F [U, C] is defined [60]:

$$F(U,C) = \int_{\Omega}(I-U)^2\ dx\,dy + \mu\int_{\Omega-C}|\nabla U|^2\,dx\,dy\ + v|C| \qquad (3.27)$$

where $\mu, v > 0$ are two fixed parameter. The Mumford-Shah energy functional F [U, C] is composed of three terms which measure the degree of match between the input image and its model. The first term is a measure of the distance between the model and the input image, the second term measures the lack of smoothness of the model within the sub-regions, while the

third term measures the length of the boundaries of the sub-regions [61]. The optimal segmentation of the image can be computed by minimizing the Mumford-shah functional $F(U,C)$ with respect to U and C. However, in practice it is difficult to minimize $F(U,C)$ because the set C of lower dimension is unknown and the problem is non convex [62]. Some simplified models of the Mumford-shah functional have been proposed such as Chan-Vese (CV) model. Using the level set function, Chan-Vese model successfully solve the minimization problem. This model uses the global image statistical information inside and outside the evolving contour rather than the gradient on the boundaries. In addition, using this model the curve can be driven by evolving the level set function instead of directly evolving the curve. In practice, the evolution of the contour is driven by a time dependent partial differential equation. Taking the above mentioned point into consideration, Chan–Vese model is an alternative solution to the Mumford–Shah problem which solves the minimum of $F(U,C)$ by minimizing the following energy functional:

$$F(c_1,c_2,C) = \mu * length(C) + v * area(inside\ C) + \lambda_1 \int_{\text{inside(C)}} |I - c_1|^2\ dx\,dy + \lambda_2 \int_{\text{outside(C)}} |I - c_2|^2\ dx\,dy \quad (3.28)$$

where I is an input grayscale image, μ, v, λ_1 and λ_2 are positive fixed constants, c_1 and c_2 are the average intensity levels of image I inside and outside of the contour respectively. To solve the minimization problem, the level set method was used [63] which is considered as a powerful tool for performing contour evolution. In the contour segmentation model the level set function is defined as $\emptyset(x,y,t)$, where (x,y) is the coordinates in the image plane and t is an artificial "time". At any given time, the level set function simultaneously defines an edge contour and a segmentation of the image. In the level set method, an evolving curve C is represented by the zero level set, $C = \{(x,y) \in \Omega : \emptyset\,(x,y) = 0\}$. $\emptyset$ was chosen to be positive inside C (

$inside(C) = \{(x,y) \in \Omega : \emptyset(x,y) > 0\})$ and negative outside C $(outside(C) = \{(x,y) \in \Omega : \emptyset(x,y) < 0\})$. Therefore, the energy functional can be reformulated in term of the level function as follow [64].

$$F(c_1, c_2, \emptyset) = \mu * length(\emptyset = 0) + v * area(\emptyset \geq 0) + \lambda_1 \int_{\emptyset \geq 0} |I - c_1|^2 \, dx\, dy + \lambda_2 \int_{\emptyset < 0} |I - c_2|^2 \, dx\, dy \quad (3.29)$$

To express the terms of $F(c_1, c_2, \emptyset)$ using the Heaviside function H and the Dirac delta function, the energy function $F(c_1, c_2, \emptyset)$ can be written as:

$$F(c_1, c_2, \emptyset) = \mu \int_\Omega \delta(\emptyset)|\nabla\emptyset| \, dx\, dy + \int_\Omega H(\emptyset) \, dx\, dy + \lambda_1 \int_\Omega |I - c_1|^2 \, H(\emptyset)\, dx\, dy + \lambda_2 \int_\Omega |I - c_2|^2 (1 - H(\emptyset)) \, dx\, dy \quad (3.30)$$

This minimization problem can be solved by taking the Euler–Lagrange equations and updating the level set function $\emptyset(x,y)$ by the gradient descent method. The derived evolution equation for the level set function $\emptyset(x,y)$ is [64]:

$$\frac{\partial \emptyset}{\partial t} = \delta(\emptyset)\left[\mu \, div\left(\frac{\nabla\emptyset}{|\nabla\emptyset|}\right) - \lambda_1 (I - c_1)^2 + \lambda_2 (I - c_2)^2\right] \quad (3.31)$$

c1 and c2 can be, respectively, updated at each iteration by:

$$c_1(\emptyset) = \frac{\int_\Omega I \, H(\emptyset)\, dx\, dy}{\int_\Omega H(\emptyset)\, dx\, dy} \quad (the\ average\ of\ I\ in\ \{\emptyset \geq 0\}) \quad (3.32)$$

$$c_2(\emptyset) = \frac{\int_\Omega I\,(1 - H(\emptyset))\, dx\, dy}{\int_\Omega (1 - H(\emptyset))\, dx\, dy} \quad (the\ average\ of\ I\ in\ \{\emptyset < 0\}) \quad (3.33)$$

However, Chan-Vese model may become time consuming algorithm (solving partial differential equation several times); in addition this model usually depends on the placement of the initial curve.

3.7 Feature Extraction

Image feature is considered as a distinguishing primitive attribute or characteristic of an image. Image features are classified into two types, natural and artificial features. A natural feature is the feature which is specified by the visual appearance of the image, while artificial feature is obtained by doing particular modifications and manipulation of an image. Histogram based statistical features, spatial frequency spectra and linear algebraic features are examples of artificial features.

Image features are of major importance in identification and analysis of regions in an image (image interpretation). In this section, several types of image features such as histogram based statistical feature and linear algebraic features have been described.

3.7.1 Histogram-Based Statistical Features

The histogram of the hue image is a graphical representation of the frequency occurrence of each hue value in the image. The data structure that stores the frequency values is a one dimensional array of numerical values, whose individual entries store the number or percentage of image pixels that are related to each possible hue value in the image [45]. Let $k = 0, 1, \dots\dots\dots, L-1$, where L is number of hue levels in the image. Therefore, the normalized histogram can be determined as follow:

$$p(r_k) = \frac{n_k}{n} \tag{3.34}$$

where $p(r_k)$ is the percentage (probability) of the number of pixels which belongs to level *k*, while n is the total number of pixels in the image and n_k is the number of pixels at level *k*. The histogram is usually represented using a bar chart with one bar per hue level. The amplitude of

each bar represents the number or percentage of pixels that are related to each level. Figure 3.12 shows an insulator image and its hue histogram with 250 levels.

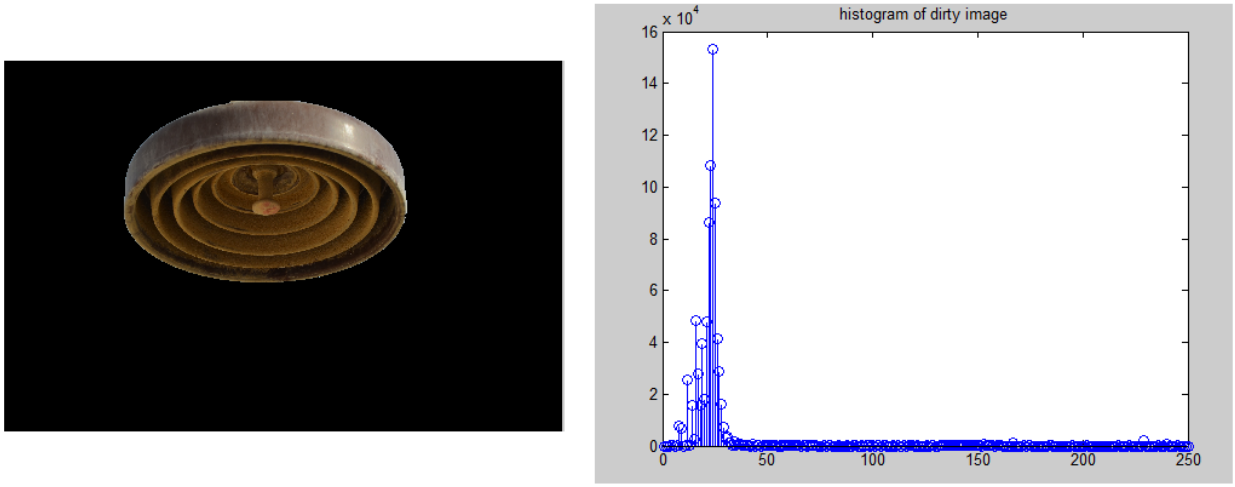

Figure 3.12 Image and its hue histogram with 250 levels

Many numerical statistical features can be extracted from histogram of an image, which describe an image or its objects [51]. The simplest histogram feature is the mean (m) which provides a measure of the overall hue (color) of the image. It is given by

$$m = \sum_{j=0}^{L-1} r_j \, p(r_j) \tag{3.35}$$

where r_j is the j^{th} hue level (number of level in histogram is L) and $p(r_j)$ is the probability of occurrence of j^{th} level. Variance is another statistical feature which indicates how far the pixels values spread out from the mean. If the value of the variance is high, this mean that pixels values are very spread out from the mean and from each other. On the other hand, if the variance is small then it indicates that the pixels values are close to the mean and to each other. The variance of an image is given by

$$variance = \sigma^2 \tag{3.36}$$

$$\sigma = \sqrt{\sum_{j=0}^{L-1} (r_j - m)^2 \, p(r_j)} \tag{3.37}$$

Where σ is the standard deviation. Skewness is one of the important histogram based descriptors which is a measure of its symmetry about the mean value. Skewness can be positive or negative. Positive skew mean that the histogram tail spread to the right (right-skewed), while negative skew indicates that the histogram tail spread to the left (left-skewed). Skewness is defined as:

$$skew = \frac{1}{\sigma^3} \sum_{j=0}^{L-1} (r_j - m)^3 \, p(r_j) \tag{3.38}$$

The kurtosis descriptor provides a measure of the width of the peak (peakedness) and the weight of the tail in histogram. Small kurtosis value indicates that the histogram has a more rounded peak and shorter, thinner tail; while high kurtosis value indicates that the histogram has a sharper peak and longer, thicker tail. Kurtosis can be calculated as:

$$kurtosis = \frac{1}{\sigma^4} \sum_{j=0}^{L-1} (r_j - m)^4 \, p(r_j) - 3 \tag{3.39}$$

The energy feature provides another measure about how pixels values are distributed along the hue levels range. If the entire pixels of the image have the same values then the energy of the image is maximum (energy=1), therefore image with many hue levels will have smaller energy than the ones with few hue levels. The energy feature can be measured as:

$$energy = \sum_{j=0}^{L-1} [\, p(r_j)]^2 \tag{3.40}$$

The normalized histogram error between two images (have the same view but one of the image has some noise) provides a good measure about the difference between the two images. Hence a high value of the normalized error means the difference between the two images is high (the

image which have noise are highly polluted) and vise versa. The normalized histogram error can be calculated as follow

$$Normalized\ histogram\ error = \sum_{j=0}^{L-1}[\,p_1(r_j) - p_2(r_j)]^2 \tag{3.41}$$

3.7.2 SVD-Based Linear Algebraic Features

Singular value decomposition (SVD) theorem is said to be one of the important mathematical tools in linear algebra which can be applied to a matrix in order to factorize it into the multiplication of three matrices. One is a diagonal matrix D and the other two are unitary matrices (orthogonal matrix with length one) U and V. Therefore, singular value decomposition theorem can be applied to an image in order to extract some useful features by factorizing the image into three matrices each one of them has certain properties [65, 66]. Let $\boldsymbol{A}$ be a rectangular matrix, then the SVD of matrix $\boldsymbol{A}$ is

$$\boldsymbol{A = USV^T} \tag{3.42}$$

Where $\boldsymbol{A}$ is a mxn rectangular matrix, $\boldsymbol{U}$ and $\boldsymbol{V}$ are mxm and nxn orthogonal matrices respectively. $\boldsymbol{S}$ is a mxn diagonal matrix, where the entries at the diagonal are called the singular values of $\boldsymbol{A}$. These singular values arise at the diagonal in descending order $\sigma_1 \geq \sigma_2 \geq \sigma_3 \geq \cdots \geq \sigma_n \geq 0$. Therefore, decomposing $\boldsymbol{A}$ using SVD can be written in matrix form as follow

$$\begin{bmatrix} a_{11} & \cdots & a_{1n} \\ \vdots & \ddots & \vdots \\ a_{m1} & \cdots & a_{mn} \end{bmatrix} = [u_1\,, u_2, \ldots, u_m] \begin{bmatrix} \sigma_1 & 0 & \cdots & 0 \\ 0 & \sigma_2 & 0 & 0 \\ \vdots & 0 & \ddots & 0 \\ 0 & \cdots & 0 & \sigma_n \end{bmatrix} \begin{bmatrix} {v_1}^T \\ {v_2}^T \\ \vdots \\ {v_n}^T \end{bmatrix} \tag{3.43}$$

The singular values of the matrix $\boldsymbol{A}$ are unique and can be calculated by taking the square root of the Eigen value of $\boldsymbol{AA^T}$ and $\boldsymbol{A^TA}$, while $\boldsymbol{U}$ and $\boldsymbol{V}$ are not unique matrices and they are calculated

as an Eigen vector of $\boldsymbol{AA^T}$ and $\boldsymbol{A^TA}$ respectively. Moreover the rank of the matrix $\boldsymbol{A}$ is equal to the number of nonzero singular values.

3.8 Artificial Neural Network

With the advancement in Neural Network theory, a wide range of neural networks are available today. Notable neural networks used for classification and regression include the Multi-layer Feed-forward Neural Network (MFNN), the Radial Basis Function Neural Network (RBFNN), Support Vector Machines (SVM), etc. In general, a MFNN consists of an input layer, several hidden layers, and an output layer. The MFNN is one of the most commonly used neural networks with many applications in engineering and other fields, and hence, MFNN is the neural network utilized in this thesis [67]. Each layer consists of several numbers of nodes (neuron). Figure 3.13 shows a single node where each node includes a summer and an activation function g.

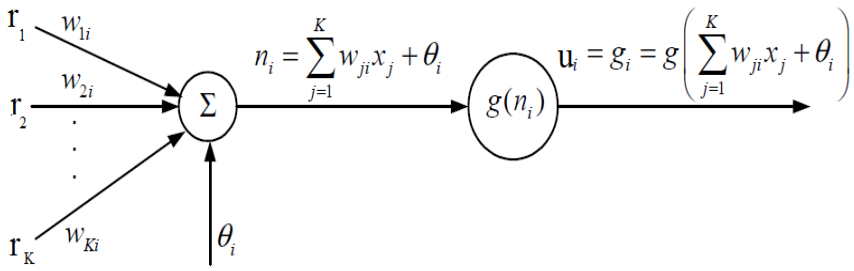

Figure 3.13 Single node (Neuron)

The inputs, r_k ($k = 1,2, \ldots\ldots, K$) to the neuron are multiplied by weights w_{Ki} and summed up together with the constant bias term θ_i. The resulting n_i is the input to the activation function g .

There are several types of activation function used in neural network such as hyperbolic tangent (tanh) function, this function is defined as :

$$\tanh(\mathrm{x}) = \frac{1-\mathrm{e}^{-\mathrm{x}}}{1+\mathrm{e}^{-\mathrm{x}}} \tag{3.44}$$

The output of neuron *i* (node *i*) becomes:

$$u_i = g_i = g\left(\sum_{j=1}^{K} w_{ji} r_j + \theta_i\right) \tag{3.45}$$

Connecting several nodes in parallel and series, a MFNN network is formed. A typical Multi-layer feed-forward neural network is shown in Figure 3.14.

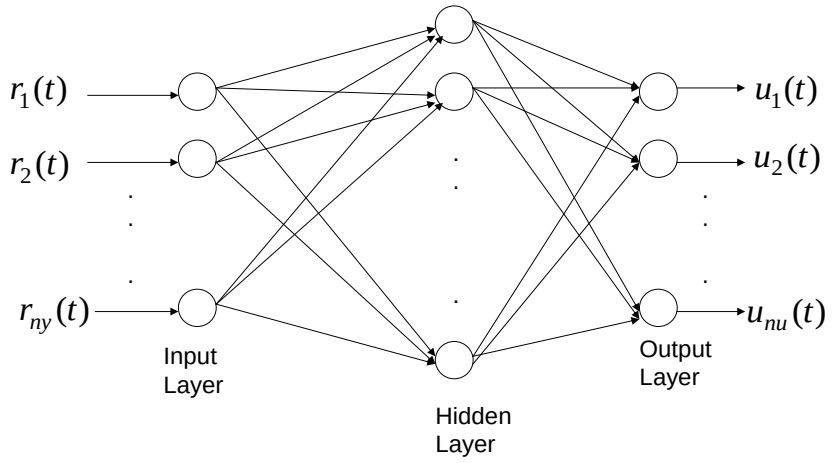

Figure 3.14 Typical multi-layer feed-forward neural network

The input to the i^{th} hidden unit is given by:

$$net_i^h(t) = w_i^h\, r(t) + \theta_i^h \tag{3.46}$$

where *r(t)* is the input, w_i^h are the weights on the connection from the input unit and θ_i^h are the weights on the connection from the bias unit. The "*h*" super script refers to the hidden layer. The output of the *i*th hidden unit is:

$$g_i(t) = f_i^h\,(net_i^h(t)) \tag{3.47}$$

where f_i^h is the activation function. The equations for the output node are

$$net^{\circ}(t) = \sum_{i=1}^{l} w_i^{\circ} g_i(t) + \theta^{\circ} \tag{3.48}$$

$$u(t) = f^{\circ}(net^{\circ}(t)) \tag{3.49}$$

where the " ° " superscript denotes the output, L is the number of neurons in the hidden layer, w_i° are the weights on the connections from the i^{th} hidden node to the output, θ° is the weight on the connection from the bias to the output, and f° is the activation function of the output node. The activation functions for the MFNN are normally chosen as tangent sigmoid and linear functions for the hidden layer and the output layer respectively [68, 69]. For mulit-input multi-output networks, the input vector to the MFNN is given by $R(t) = [r_1(t) \ldots r_{ny}(t)]^T$. The input to the j^{th} hidden unit is

$$net_j^h(t) = \sum_{i=1}^{ny} w_{ji}^h r_i(t) + \theta_j^h \tag{3.50}$$

Where w_{ji}^h are the weights of the hidden layer and θ_j^h is the bias term. The output of the j^{th} hidden neuron is

$$g_j(t) = f_j^h(net_j^h(t)) \tag{3.51}$$

Where f_j^h is the activation function. The equations for the output nodes with linear activation functions are

$$u_k(t) = \sum_{j=1}^{L} w_{kj}^{\circ} g_j(t) + \theta_k^{\circ} \tag{3.52}$$

where L is the number of neurons in the hidden layer, $u_k(t)$ denotes the k^{th} output unit where k *from (* 1, *...,nu.)*

The neural network is trained using the back-propagation algorithm, which seeks to find optimum weights biases of the neural network along the negative gradient of a cost function. The cost function is described by:

$$J = \sum_{i=1}^{n} [\, u(i) - u_r(i) \,] \tag{3.53}$$

where u and u_r denote the actual and desired outputs, respectively.

CHAPTER FOUR

RESULTS AND DISSCUSION

4.1 Insulators Collected Samples

As a result of the continued efforts to collect insulator samples from ARAMCO, SEC and SABIC as well as KFUPM Dhahran Electrical Insulator Research Station, only samples from SEC and KFUPM Dhahran Electrical Insulator Research Station were secured.

A total of 51 samples of super-fog porcelain insulators were collected; 11 samples from SEC and the others are from KFUPM Dhahran Electrical Insulator Research Station. Figure 4.1 shows three samples of a super-fog insulator with different levels of pollution. All of the samples were manufactured by NJK Insulator LTD Company (Japan), with a mechanical strength (89KN), Creepage distance (640 mm), top porcelain surface area (1315 cm^2) and bottom porcelain surface area (2810 cm^2).

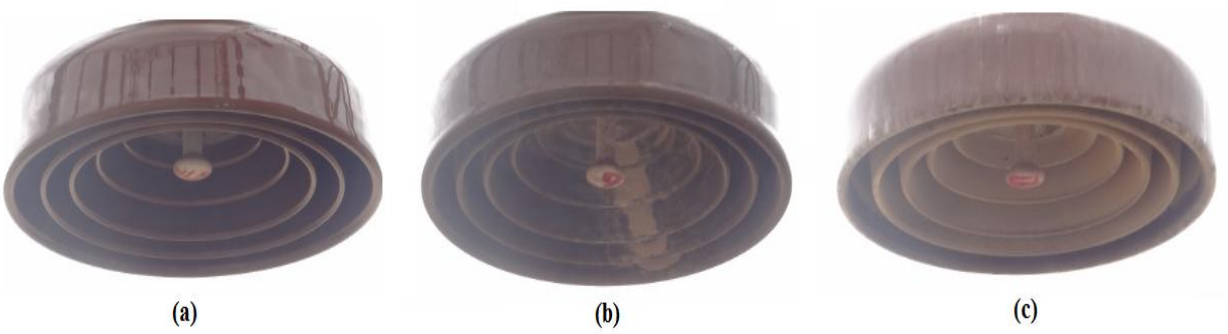

Figure 4.1 (a) KFUPM clean insulator (b) SEC contaminated insulator (c) KFUPM contaminated insulator

Table 4.1 gives detailed information about the collected insulator samples such as, the sample code number, location and the period of operation.

Table 4.1 Details of the collected insulatos samples

#	Insulator code	Location	Period of operation (year)	#	Insulator code	Location	Period of operation (year)
1	5DE	DAMMAM BSP - GHAZLAN POWER PLANT	30	27	6G	KFUPM STATION	0.6
2	8A	QATIF BSP - RAS TANURA	15	28	7G	KFUPM STATION	0.6
3	11BE	KFUPM STATION	35	29	8G	KFUPM STATION	0.6
4	12B	KFUPM STATION	35	30	9G	KFUPM STATION	0.6
5	14B	KFUPM STATION	35	31	10G	KFUPM STATION	0.6
6	13BT	KFUPM STATION	35	32	1H	KFUPM STATION	0.6
7	5AT	QATIF BSP - RAS TANURA	15	33	2H	KFUPM STATION	0.6
8	9AE	QATIF BSP - RAS TANURA	15	34	3H	KFUPM STATION	0.6
9	6AE	QATIF BSP - RAS TANURA	15	35	4H	KFUPM STATION	0.6
10	6DT	DAMMAM BSP - GHAZLAN POWER PLANT	30	36	5H	KFUPM STATION	0.6
11	1F	KFUPM STATION	0.16	37	6H	KFUPM STATION	0.6
12	2F	KFUPM STATION	0.16	38	7H	KFUPM STATION	0.6
13	3F	KFUPM STATION	0.16	39	C1	KFUPM STATION	0 (new)
14	4F	KFUPM STATION	0.16	40	C2	KFUPM STATION	0 (new)
15	Clean	KFUPM STATION	0 (new)	41	C3	KFUPM STATION	0 (new)
16	10BE	KFUPM STATION	35	42	C4	KFUPM STATION	0 (new)
17	7A	QATIF BSP - RAS TANURA	15	43	C5	KFUPM STATION	0 (new)
18	3DE	DAMMAM BSP - GHAZLAN POWER PLANT	30	44	C6	KFUPM STATION	0 (new)
19	2D	DAMMAM BSP - GHAZLAN POWER PLANT	30	45	C7	KFUPM STATION	0 (new)
20	4D	DAMMAM BSP - GHAZLAN POWER PLANT	30	46	C8	KFUPM STATION	0 (new)
21	1D	DAMMAM BSP - GHAZLAN POWER PLANT	30	47	C9	KFUPM STATION	0 (new)
22	1G	KFUPM STATION	0.6	48	C10	KFUPM STATION	0 (new)
23	2G	KFUPM STATION	0.6	49	C11	KFUPM STATION	0 (new)
24	3G	KFUPM STATION	0.6	50	C12	KFUPM STATION	0 (new)
25	4G	KFUPM STATION	0.6	51	C13	KFUPM STATION	0 (new)
26	5G	KFUPM STATION	0.6				

4.2 Image Data Bank

Building of image data sets was not a trivial step. A lot of factors such as the type and position of the camera, and picture capturing time have a significant effect on building representative image data sets for insulators.

The images of insulators were taken at KFUPM Dhahran Electrical Insulator Research Station; this location was selected because it shares similar environmental conditions (may be worse conditions) with many transmission lines and substations in the Kingdom. Specified position for hanging insulators samples was chosen. A digital camera (Nikon D7000, 16.9 mega pixels) was used to capture images for the collected insulators. Two stands were used to fix the camera in two different positions, one of them was fixed to the ground using concrete and the other was portable. Figure 4.2 shows the fixed stand and the position of hanging insulators.

At morning (around 7:00 am), four pictures were taken with and without flash for each high voltage insulator sample. Two of them were taken using the fixed stand and the other using the portable one. Also, other four pictures were taken at afternoon (around 4:00 pm). The distance between the insulator hanging position and each one of the stands was different, a round 2.5 m for the fixed stand and 3.5 the portable one. As such, the ratio of the insulator surface area (between top and bottom surface) which has been seen from the two stand positions are different as shown in Figure 4.3. Taking into consideration different images taken at different times and positions for each collected sample, analysis has been made to select the most appropriate combination of these factors. Different insulators images with different pollutin levels are shown in appendix A.1.

Figure 4.2 The fixed stand and the hanging position of insulators sample

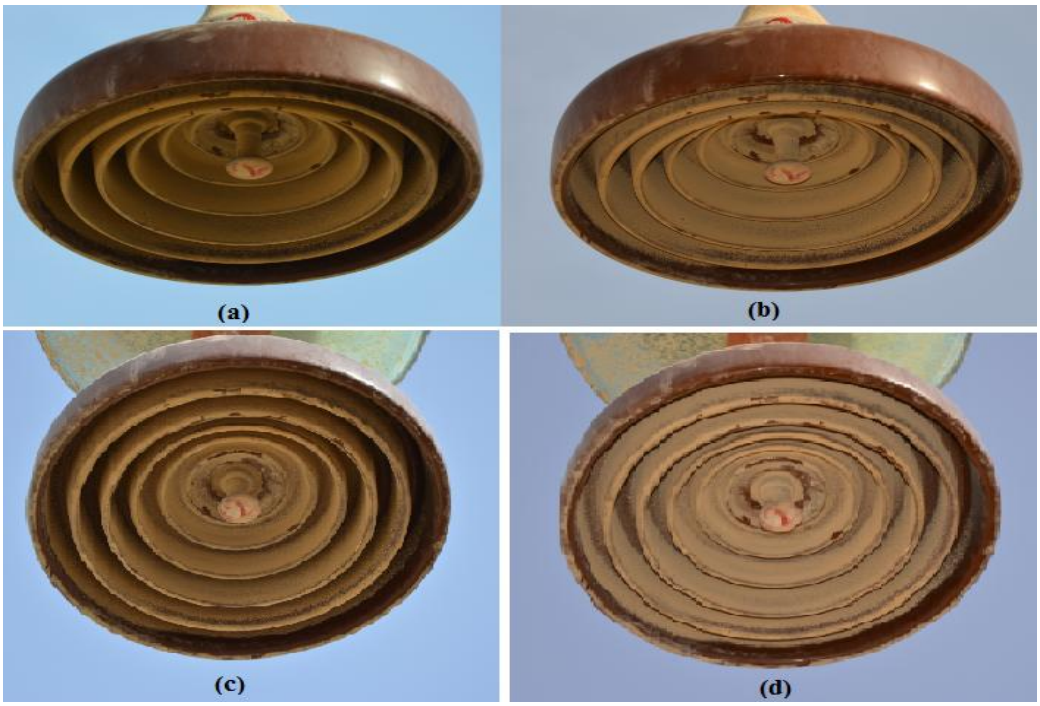

Figure 4.3 Four pictures of insulator sample taken at moring, (a) and (b) were taken with fixed stand with and without flash, respectively, (c) and (d) were taken with portable stand with and without flash respectively

4.3 Flashover voltage test

In order to study the effect and relation of pollution level and distribution of contamination on insulator flashover voltage (FOV), six representative insulator samples were chosen to be tested to measure the flashover voltage (50% flashover voltage ($U_{50\%}$)). The procedure used to conduct the test is based on "Rapid Flashover Voltage Technique" which has been described in section 3.4 and which has been adopted by the high voltage lab of the research institute at KFUPM.

The insulators which had been tested are chosen to be from different operating areas; two are from KFUPM station (14B and 12B), and two are from Qatif BSP – Ras tanura (5AT and 6AE) area and the last two are from Dammam BSP – Ghazlan Power plant (2D and 6DT). Applying this procedure, Figure 4.4 shows the relation between the flashover (kV) and time (minute) of insulator number 12B. It can be seen that the flashover voltage ($U_{50\%}$) is the lowest point (minimum flashover voltage) is in the graph of the Figure which corresponds to 33.6 kV.

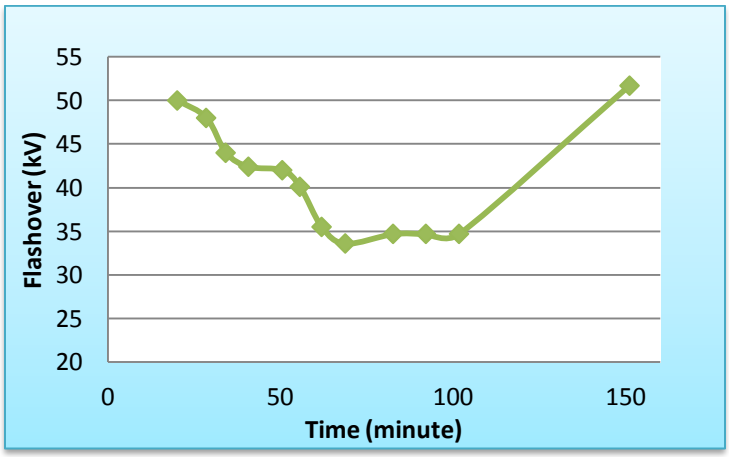

Figure 4.4 Relation between flashover and time of insulator 12B

The flashover voltages ($U_{50\%}$) for the six tested insulator samples are listed in Table 4.2. Results details for flashover tests are given in Appendix A.2.

Table 4.2 Flashover voltage for the tested insulators

Insulator code	Flashover voltage ($U_{50\%}$) (kV)
12B	33.6
14B	33.8
2D	44.5
6DT	48.5
5AT	43.3
6AE	43

4.4 Analyzing ESDD Levels of Collected Insulators

The International Electro technical Commission (IEC) adopted a standard method to find the ESDD value in case of porcelain insulators, which has been described in chapter 3, section 3.5. Based on that method, the ESDD levels of the 51 collected insulator samples were estimated at the high voltage laboratory at the RI-KFUPM.

For completeness, estimation of the ESDD of one sample (12B) was done as follows: Two beakers were filled by 1200 ml of distilled water (each with 600 ml). Two absorbent cotton pieces were immersed in the distilled water and then used to wipe off the contaminants from the top and bottom surfaces of insulator (each surface has it is own cotton piece). Wiping of the

contaminants was repeated until the two surfaces of the insulator are clean. After that, the conductivity and temperature of the water containing the contaminants were measured. For the top surface of insulator the conductivity and temperature were $2088\,\mu S/cm$ and $25.6\,℃$, respectively while for the bottom surface the values were $3465\mu S/cm$ and $25.2\,℃$, respectively.

The ESDD value of each surface (top and bottom) is calculated as in the following steps [44]:

Step 1: Calculate the factor b for the top and bottom surface by interpolation as follow:

$$b_{top} = 0.02277 + \frac{(\theta_{top} - 20)(0.01905 - 0.02277)}{(30-20)} = 0.02277 + \frac{(25.6 - 20)(0.01905 - 0.02277)}{(30-20)} = .02068 \quad (1.4)$$

$$b_{bottom} = .02277 + \frac{(\theta_{bottom} - 20)(.01905 - .02277)}{(30-20)} = .02277 + \frac{(25.2 - 20)(0.01905 - 0.02277)}{(30-20)} = .02083 \quad (2.4)$$

Step 2: Correct the conductivity values to be at 20 ℃ as follows:

$$\sigma_{20_{\text{top}}} = \sigma_{\theta_{\text{top}}}\left[1 - 0.020686\left(\theta_{top} - 20\right)\right] = 2088[1 - 0.020686(25.6 - 20)]$$

$$= 0.18461\ \mu\text{S/cm} \quad (3.4)$$

$$\sigma_{20_{\text{bottom}}} = \sigma_{\theta_{\text{bottom}}}[1 - .020686(\theta_{bottom} - 20)] = 3465[1 - .020686(25.2 - 20)]$$

$$= 0.30851\ \mu\text{S/cm} \quad (4.4)$$

Step 3: Realizing that the distilled water that was used has a conductivity of 2.7 $\mu S/cm$ at a temperature of $22℃$, it's corrected conductivity at $20℃$ has been calculated to be

0.000258106 $\mu S/cm$. Therefore, the conductivities of the top and bottom surfaces were modified by subtracting the conductivity of distilled water.

$$\sigma_{20_{\text{top\_m}}} = \sigma_{20_{\text{top}}} - \sigma_{20_{\text{distilled water}}} = 0.18461 - 0.000258106 = 0.18435\ \mu\text{S/cm} \quad (4.5)$$

$$\sigma_{20_{\text{bottom\_m}}} = \sigma_{20_{\text{bottom}}} - \sigma_{20_{\text{distilled water}}} = .30851 - .000258106 = .30825\mu\text{S/cm} \quad (4.6)$$

Step 4: The salinity of both solutions is calculated as:

$$\text{Sa}_{\text{top}} = (5.7 * \sigma_{20_{\text{top}_{\text{m}}}})^{1.03} = (5.7 * 0.18435\ )^{1.03} = 1.052358\ \text{kg/cm}^3 \quad (4.7)$$

$$\text{Sa}_{\text{bottom}} = (5.7 * \sigma_{20_{\text{bottom}_{\text{m}}}})^{1.03} = (5.7 * 0.30825\ )^{1.03} = 1.78698\ \text{kg/cm}^3 \quad (4.8)$$

Step 5: The ESDD values of both top and bottom surfaces are

$$\text{ESDD}_{\text{top}} = \frac{\text{Sa}_{\text{top}} * \text{Vol}}{\text{A}_{\text{top}}} = \frac{1.052358 * 600}{1315} = 0.48017\text{mg/cm}^2 \quad (4.9)$$

$$\text{ESDD}_{\text{bottom}} = \frac{\text{Sa}_{\text{bottom}} * \text{Vol}}{\text{A}_{\text{bottom}}} = \frac{1.78698 * 600}{2810} = .38156\ \text{mg/cm}^2 \quad (4.10)$$

Step 6: The total ESDD value (ESDD_{total}) of insulator is calculated

$$\text{ESDD}_{\text{total}} = \frac{\text{ESDD}_{\text{top}}\ \text{x}\ \text{A}_{\text{top}} + \text{ESDD}_{\text{bottom}} \text{x}\ \text{A}_{\text{bottom}}}{\text{A}_{\text{total}}} \quad (4.11)$$

$$\text{A}_{\text{total}} = 1315 + \ 2810 = 4125\ \text{cm}^{\ 2} \quad (4.12)$$

$$\text{ESDD}_{\text{total}} = \frac{0.48017\ \ \text{x}\ 1315 + .38156\ \text{x}\ 2810}{4125} = 0.413\ \text{mg/cm}^2 \quad (4.13)$$

This procedure has been repeated for all samples and the results are given in Table 4.3. As can be seen, the estimated ESDD values ranges from 0.0001 to more than 0.4mg/cm^2. Therefore, the

levels of contamination were classified into four ranges: light pollution level ($ESDD < 0.1$), medium pollution level($0.1 \leq ESDD < 0.2$), heavy pollution level ($0.2 \leq ESDD < 0.3$) and very heavy pollution level($0.3 \leq ESDD$).

Table 4.3 Collected insulators ESDD values

Insulator code	ESDD (mg/cm^2)	Contamination (Pollution) Level	Insulator code	ESDD (mg/cm^2)	Contamination (Pollution) Level
5DE	0.2737574	Heavy	**6G**	0.1658598	Medium
8A	0.2002777	Heavy	**7G**	0.1083919	Medium
11BE	0.4083126	Very Heavy	**8G**	0.0907294	Light
12B	0.4133858	Very Heavy	**9G**	0.0881737	Light
14B	0.4162485	Very Heavy	**10G**	0.0357207	Light
13BT	0.4468404	Very Heavy	**1H**	0.0279298	Light
5AT	0.2107419	Heavy	**2H**	0.1554117	Medium
9AE	0.1817315	Medium	**3H**	0.0313867	Light
6AE	0.1700989	Medium	**4H**	0.1399967	Medium
6DT	0.3023930	Very Heavy	**5H**	0.0730316	Light
1F	0.0220807	Light	**6H**	0.02727	Light
2F	0.0227236	Light	**7H**	0.0789019	Light
3F	0.0218988	Light	**C1**	0.0007128	Light
4F	0.0234379	Light	**C2**	0.0007435	Light
Clean	0.0009199	Light	**C3**	0.0006861	Light
10BE	0.4460936	Very Heavy	**C4**	0.0008932	Light
7A	0.1866296	Medium	**C5**	0.0009242	Light
3DE	0.2893781	Heavy	**C6**	0.0007605	Light
2D	0.2961539	Heavy	**C7**	0.0007279	Light
4D	0.2765315	Heavy	**C8**	0.0008351	Light
1D	0.2735361	Heavy	**C9**	0.0009513	Light
1G	0.1066041	Medium	**C10**	0.0009336	Light
2G	0.1863462	Medium	**C11**	0.0007459	Light
3G	0.0206601	Light	**C12**	0.0008565	Light
4G	0.0217085	Light	**C13**	0.0009286	Light
5G	0.0759503	Light			

A careful look at the results shown in Tables 4.2 and 4.3, one can easily make a negative correlation between the level of contamination and the flashover voltage. For examples, in Table 4.2, it can be seen that the flashover voltage values for samples 12B and 14B are lower than the other samples. This can be attributed to the higher ESDD contamination levels of those samples as shown in Table 4.3. This leads to a conclusion that the higher the insulator contamination level the lower is the flashover voltage. Details results for ESDD measurements are provided in Appendix A.3.

4.5 Segmentation of Insulators Images

Image segmentation is the process of partitioning an image into meaningful regions (separating the objects from the background of an image) which have similar attributes. In this thesis, the surface of insulators was the important region in the image that needed to be examined and analyzed. Therefore, segmentation of the collected insulators images was done to exclude the background (sky) and the cap of insulator while retaining other parts in the image. Based on the analysis that will follow in Section 4.6, we found that the groups of images which have been taken from the fixed stand at morning are the more representative group to insulator surface. In addition this group clearly shows that there were differences between insulators images which have different pollution levels.

Many techniques of segmentation have been established in the literature such as intensity based segmentation, watershed, edge based segmentation, and Chan-Vese model. Intensity based segmentation has been tried and found to be simple in terms of its principle but it has a serious drawback which is basically the calculation of the appropriate threshold intensity value of non

trivial images. Watershed technique has been tested and found to be inefficient due to the loss of part of insulator surface. Edge based segmentation has been employed and found to be pretty efficient for extracting the whole insulator, and also less complex and less time consuming than the previous technique. Finally, although Chan-Vese model is time consuming due to solving partial differential equations, but it has been slightly used in excluding unnecessary parts of the insulator.

Segmentation of grayscale insulator images has been done in two stages using MATLAB™ software. In the first stage, the cap of insulator has been excluded from the image using Chan-Vese algorithm [60] as shown in Figure 4.5-a. By this model the edge between the cap and the insulator surface was found, meaning that the coordinate of the edge are known. Therefore, all the pixels values that are above this edge have been set to zero as shown in Figure 4.5-b.

The flow chart in Figure 4.6 illustrates the Chan-Vese algorithm that was used in stage 1 of segmentation. The stopping criteria of the Chan-Vese occurs when the solution is stationary (the energy is not changing or the contour is not moving) or when the maximum number of iterations is reached, which has been adopted in this thesis. The maximum number of iteration used was 200.

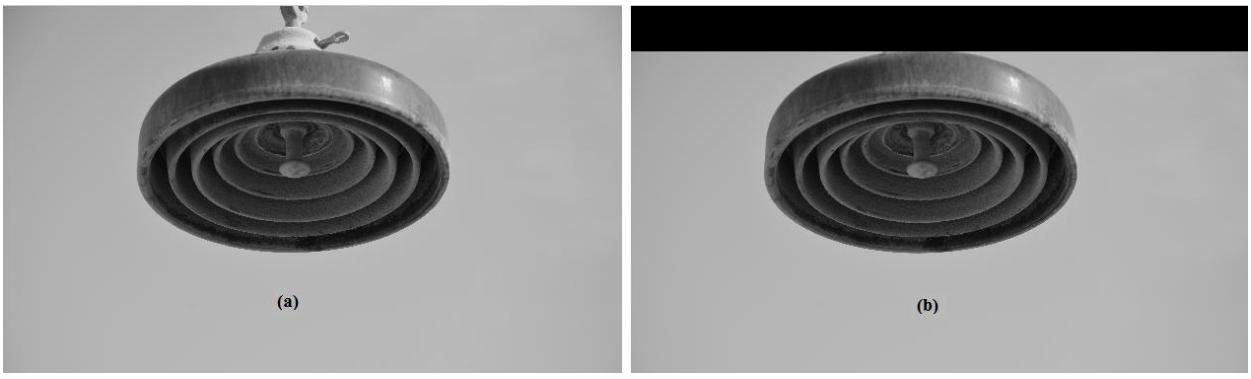

Figure 4.5 (a) Origin gray-scale image (b) First stage segmented image (exclude the insulator cap)

In the second stage of segmentation, edge-based segmentation method was used. The sobel edge detection algorithm was applied to the input image (result from first stage) to find its gradient. The pixels that have high gradients value (above a certain threshould value) represent the edges of the insulator surface area. After that, the resultant edges have been dilated and extended in order to connect the discontinuity between the edges, and the excess edges were eroded. The area inside the edges have been filled (this means that all the pixels inside the edges have value of 1(white)). Therefore, the insulator image at this step (final step in stage three) is binary where the excluded pixels are black and the white pixels representing insulator surface. Finally, the segmented image from stage two is multiplied by the RGB image (the one before applying segmentation) of insulator using matrix manipulation to have the final RGB segmented insulator image. The flow chart in Figure 4.7 shows the steps of segmentation in stage two and the result of each step, in addition to the final RGB segmented image.

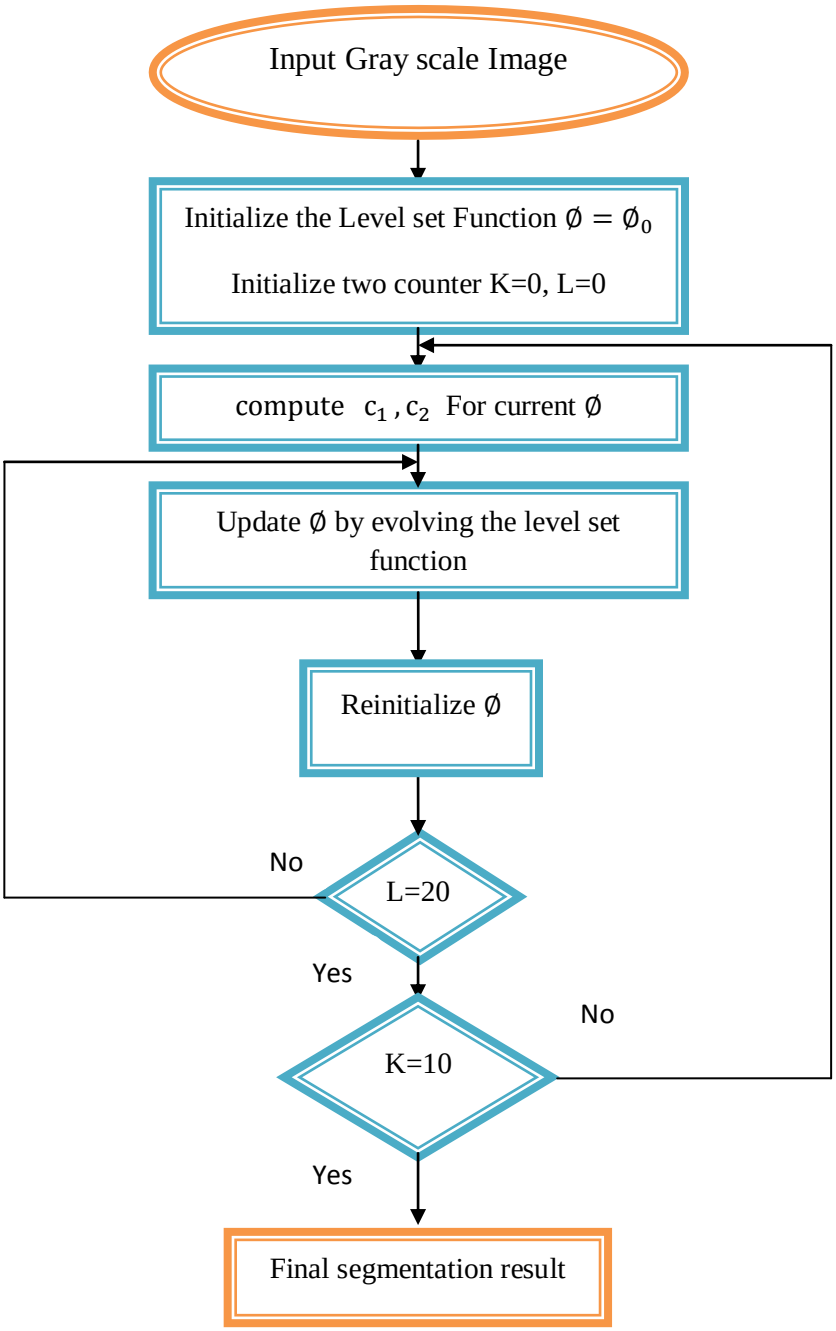

Figure 4.6 Chan-Vese segmentation algorithm [60]

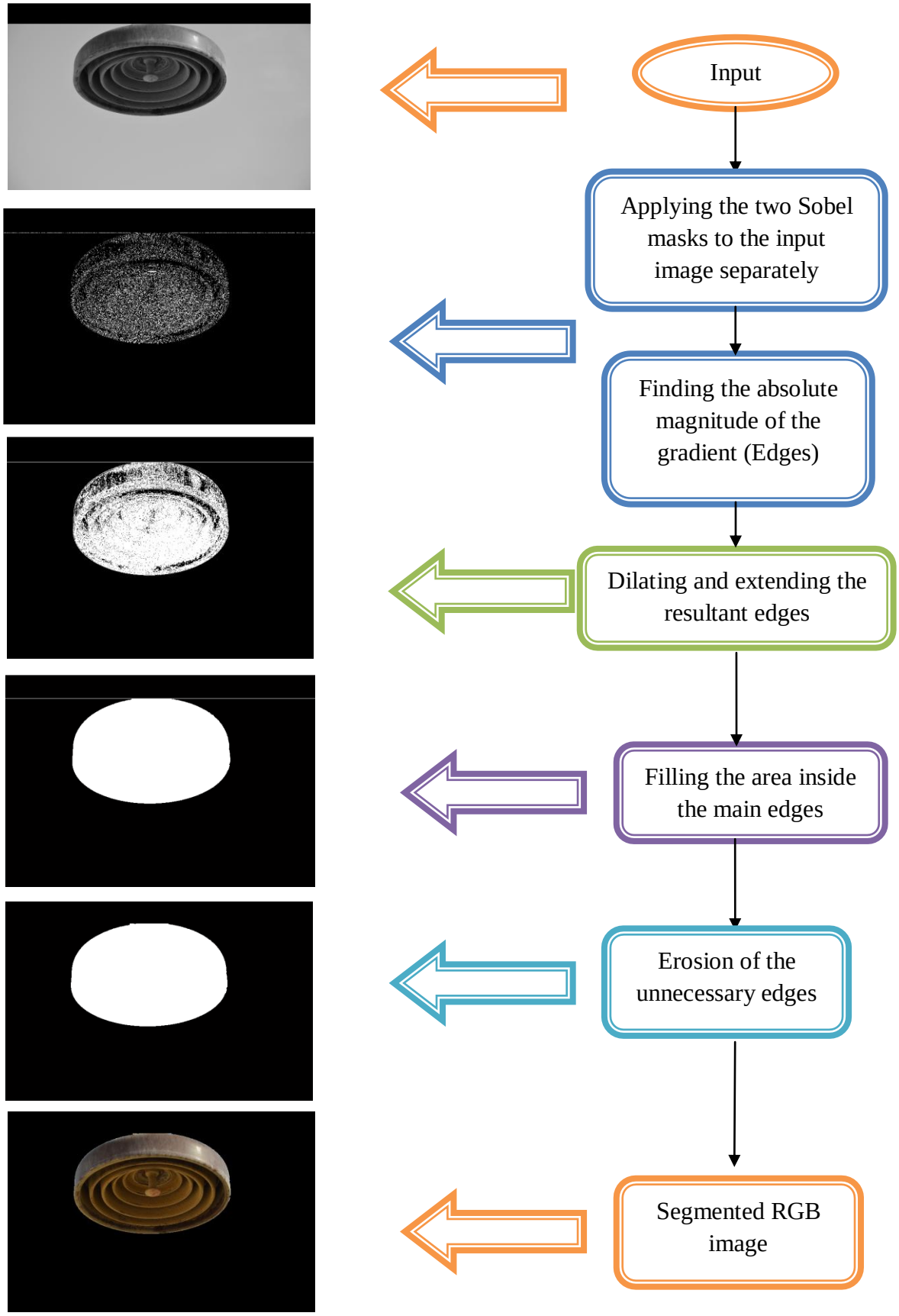

Figure 4.7 Flow chart of stage two of the segmentation process

4.6 Features Extraction

Image features is considered as a distinguishing primitive attributes or characteristic of an image. In this thesis, two groups of features were extracted from each insulator segmented image in order to represent the level of contamination on insulator surface. One of the groups was histogram-based statistical features while the other was SVD-based linear algebraic features.

Many color space models for feature extraction are available. RGB, Gray-scale and HSV are examples among others. In this thesis, RGB color space model and Gray-scale model have been tried for feature extraction. Unfortunately both were significantly affected by the illumination of the sun. On the other hand, HSV model has been shown to reduce the effect of uneven illumination on insulator surface as well as it aids in finding numerical differences between insulators of different pollution levels [70]. Therefore, in this thesis HSV color model has been used for feature extraction, especially the hue component. Accordingly, the RGB segmented insulator obtained in section 4.5 was transformed to HSV model. Based on the histogram of the hue image, all of the statistical features were extracted. These features are the mean, variance, skewness, kurtosis, energy, normalized histogram error and the percentage of the difference between the hue histograms of clean reference image and the collected ones. While the linear algebraic features are extracted by the decomposition of the hue image using the singular value decomposition theorem in order to find the singular values. In this thesis, the first 50 singular values $\sigma_1, \sigma_2, \sigma_3, \dots, \sigma_{50}$ are taken to be the linear algebraic features. Tables 4.4 and 4.5 show the statistical feature values and linear algebraic features (first 10 features) of different insulator samples, respectively as well as its corresponding ESDD values.

Table 4.4 Sample of statistical features and its corresponding ESDD values of different polluted insulators

Image code	C13	C9	1F	7A	9AE	12B	6DT	10BE
Difference	7.9534	8.7138	19.8588	27.1491	27.0451	57.1101	53.082	59.7362
Normalized error	0.2284	0.2422	1.1476	2.0792	1.8794	11.2469	9.0245	10.0607
Mean	19.116	19.041	20.6116	22.3834	23.01	23.5259	26.264	23.7964
Variance	896.83	818.05	570.818	701.83	748.312	273.236	896.72	312.24
Skewness	6.7184	6.9847	7.7834	5.9281	5.7977	9.4155	5.5034	9.1282
Kurtosis	47.672	52.149	66.0567	40.0282	38.3765	103.456	34.12	95.4254
Energy	0.0997	0.0975	0.0857	0.0643	0.061	0.1047	0.0816	0.0947
ESDD	0.000	0.0009	0.02208	0.18662	0.18173	0.41338	0.3023	0.44609

Table 4.5 Sample of linear algebraic features and its corresponding ESDD values of different polluted insulators

Image code	C13	C9	1F	7A	9AE	12B	6DT	10BE
σ_1	72.0788	68.0693	73.2658	84.1564	88.5965	79.6864	97.9153	78.8486
σ_2	41.68	38.6299	34.5704	41.8924	44.0381	19.7648	49.5979	26.2712
σ_3	33.8722	24.866	27.233	34.1485	37.2317	16.4573	37.064	18.9179
σ_4	28.1094	24.4085	18.9567	22.7163	23.7838	14.9891	24.388	17.8801
σ_5	25.6998	22.7834	16.76	20.5059	19.4633	14.6451	21.3667	16.7864
σ_6	21.3522	18.4643	14.9949	15.6106	15.3395	13.3997	18.3547	15.7582
σ_7	18.7574	17.0796	14.0339	13.9311	13.9087	12.6732	17.9563	15.0034
σ_8	17.8218	16.497	12.042	12.5835	12.2855	11.8095	15.5277	12.3665
σ_9	16.4155	15.4072	10.9992	12.0963	11.1721	11.1788	14.8168	11.6545
σ_{10}	15.263	15.2403	10.7853	11.6151	10.9325	10.7755	14.0275	11.0019
ESDD	0.00092	0.00095	0.02208	0.1866296	0.1817315	0.4133858	0.302393	0.4460936

4.7 Design, Training and Validation of the Artificial Neural Network

Multi-layer feed-forward neural network (MFNN) is considered as one of the most important commonly used method in regression and classification. In this thesis, this method was used to design a neural network which is capable of predicting the level of contamination (ESDD level) of polluted insulators. The input to the network is the extracted features of insulators images and the output is the pollution levels. The number of features patterns and their corresponding pollution levels which are used in training and testing of the neural network is shown in Table 4.6. Each feature pattern corresponds to a specific insulator image which consists of some statistical features and an appropriate number of linear algebraic features.

Table 4.6 Collected data

Pollution Level	Number of features patterns
Light level	29
Medium	9
Heavy	7
Very heavy	6

The design of the MFNN involves determining the number of inputs, outputs, hidden units as well as the number of hidden layers. In this thesis three different neural networks scenarios were developed. In the three developed scenarios, different numbers of hidden layers were employed in order to improve the performance of the networks. Results showed that using more than one hidden layer improved the training performance while the testing performance was almost the same. Accordingly, each developed neural network consists of one hidden layer. Therefore, the complexity and time consuming of the trained neural network will be reduced. In all scenarios,

the output is the same which is the pollution level as shown in Table 4.7, and the number of layers is also the same (input, hidden and output layers). The difference between the scenarios depends on the type and number of inputs features as well as the number of hidden units (neurons). The activation functions that have been used in the hidden layer and the output layer are the nonlinear (Tansig) and linear function (Purelin), respectively. In the first scenario, the input to the neural network was some statistical features only. In the second scenario, the input to the neural network was an appropriate number of linear algebraic features while in the last scenario the input to the neural network was a combination of statistical and linear algebraic features. To train and test these neural networks, the collected insulators have been divided into a training group and a testing one. Thirty six insulators with their features patterns and ESDD levels are used for training the neural networks. The other fifteen insulator samples with their features and ESDD values are used for testing the developed neural networks. In the three scenarios, training and testing data sets are the same in term of the number of features patterns but as mentioned before the size of the feature pattern vector are different in each scenario. The insulators groups with their code numbers and corresponding ESDD levels, selected for training and testing the networks, are given in Tables 4.8 and 4.9, respectively. The training of the three neural networks is accomplished using the most commonly used training algorithm (gradient back-propagation).

Table 4.7 Outputs of the neural network

Pollution Level	ESDD Range	Output
Light level	$\text{ESDD} < 0.1$	A
Medium	$(0.1 \leq \text{ESDD} < 0.2)$	B
Heavy	$(0.2 \leq ESDD < 0.3)$	C
Very heavy	$(0.3 \leq ESDD)$	D

Table 4.8 Training group of insulators

Insulator code	ESDD value mg/cm^2	Pollution level	Insulator code	ESDD value mg/cm^2	Pollution level
Clean	0.0009	Light	**7G**	0.1084	Medium
1F	0.0221	Light	**8G**	0.0907	Light
2F	0.0227	Light	**9G**	0.0882	Light
3F	0.0219	Light	**10G**	0.0357	Light
5AT	0.2107	Heavy	**2H**	0.1554	Medium
6AE	0.1701	Medium	**3H**	0.0314	Light
7A	0.1866	Medium	**4H**	0.1400	Medium
1D	0.2735	Heavy	**5H**	0.0730	Light
2D	0.2962	Heavy	**6H**	0.0273	Light
3DE	0.2894	Heavy	**C1**	0.0007	Light
5DE	0.2738	Heavy	**C2**	0.0007	Light
10BE	0.4461	Very Heavy	**C4**	0.0009	Light
11BE	0.4083	Very Heavy	**C5**	0.0009	Light
12B	0.4134	Very Heavy	**C6**	0.0008	Light
1G	0.1066	Medium	**C8**	0.0008	Light
3G	0.0207	Light	**C10**	0.0009	Light
5G	0.0760	Light	**C11**	0.0007	Light
6G	0.1659	Medium	**C12**	0.0009	Light

Table 4.9 Testing group of insulators

Insulator code	ESDD value mg/cm^2	Pollution level
4F	0.0234	Light
8A	0.2003	Heavy
C13	0.0009	Light
9AE	0.1817	Medium
4D	0.2765	Heavy
6DT	0.3024	Very Heavy
13BT	0.4468	Very Heavy
14B	0.4162	Very Heavy
2G	0.1863	Medium
4G	0.0217	Light
1H	0.0279	Light
7H	0.0789	Light
C3	0.0007	Light
C7	0.0007	Light
C9	0.0010	Light

4.7.1 Scenario I- Neural Network with Statistical Features

In this scenario, seven important statistical features are used as inputs to the neural network. These features are: difference, normalized histogram error (normalized error), mean, variance, skewness, kurtosis and energy. Therefore, the number of inputs of the developed neural network

is seven and the number of outputs is one as shown in Figure 4.8. A typical training input matrix looks as follows:

$$\begin{bmatrix} \text{Difference}_1 & \cdots & \text{Difference}_n \\ \text{Normalized error}_1 & \cdots & \text{Normalized error}_n \\ \text{Mean}_1 & \cdots & \text{Mean}_n \\ \text{Variance}_1 & \cdots & \text{Variance}_n \\ \text{Skewness}_1 & \cdots & \text{Skewness}_n \\ \text{Kurtosis}_1 & \cdots & \text{Kurtosis}_n \\ \text{Energy}_1 & \cdots & \text{Energy}_n \end{bmatrix} \tag{4.14}$$

where, *n* denotes the number of features patterns for training which equal to 36, each insulator image has one features pattern and the number of insulators used for training was 36. Samples of statistical feature values of some polluted insulators are given in Table 4.4. The outputs are assigned letters as in Table 4.7.

Different numbers of hidden units have been tried such that the performance of the network was optimized. The number of hidden neurons in the sub-optimized neural network was 7, where the mean square error (MSE) for training and testing was the minimum (MSE=0.0011) and (MSE=0.0024), respectively. The validation results of using the testing data given in Table 4.9 (for 15 insulators) indicated that the developed neural network was able to predicate correctly the level of contamination for 12 insulators, while for the other three the pollution level was wrongly estimated. Among those wrongly estimated pollution levels, one predicted ESDD level has been assigned to a category two levels away from the actual one (predicted level of pollution is A while the actual level is C) . Accordingly, the performance of the developed network is 80%. Further detail for validation results is given in Tables 4.10. The absolute error column in that Table represents the absolute difference between the measured and predicted ESDD value. Figure 4.9 shows a comparison between the measured (actual) and predicted ESDD values.

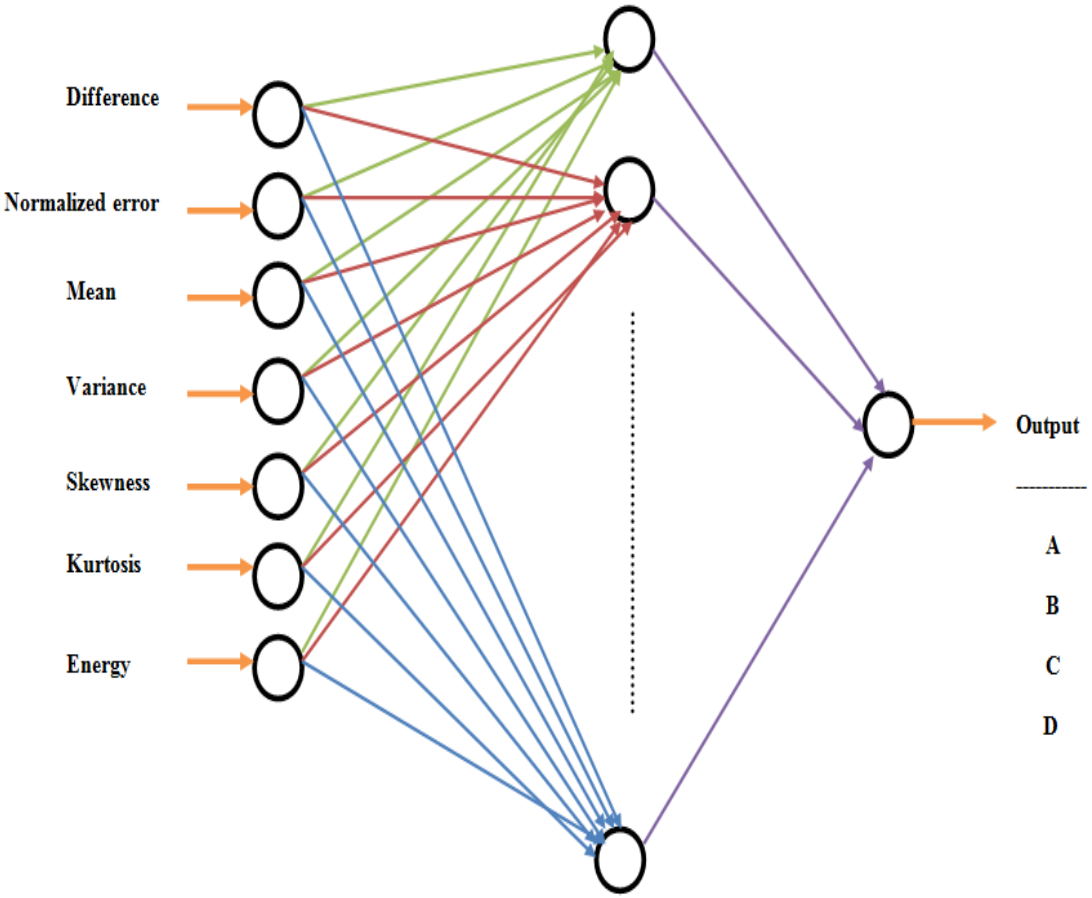

Figure 4.8 : Neural network structure – scenario I

Table 4.10 Validation result – scenario I

Insulator code	Measured ESDD value mg/cm^2	Actual Pollution level	Predicted ESDD value mg/cm^2	Predicted Pollution level	Absolute Error
4F	0.0234	A	0.0546	A	0.0312
8A	0.2003	C	0.073	A	0.1273
C13	0.0009	A	0.0129	A	0.012
9AE	0.1817	B	0.1435	B	0.0382
4D	0.2765	C	0.3317	D	0.0552
6DT	0.3024	D	0.2546	C	0.0478
13BT	0.4468	D	0.3804	D	0.0664
14B	0.4162	D	0.3992	D	0.017
2G	0.1863	B	0.1821	B	0.0042
4G	0.0217	A	0.0951	A	0.0734
1H	0.0279	A	0.0316	A	0.0037
7H	0.0789	A	0.0477	A	0.0312
C3	0.0007	A	0.0113	A	0.0106
C7	0.0007	A	0.0103	A	0.0096
C9	0.0010	A	0.0053	A	0.0043

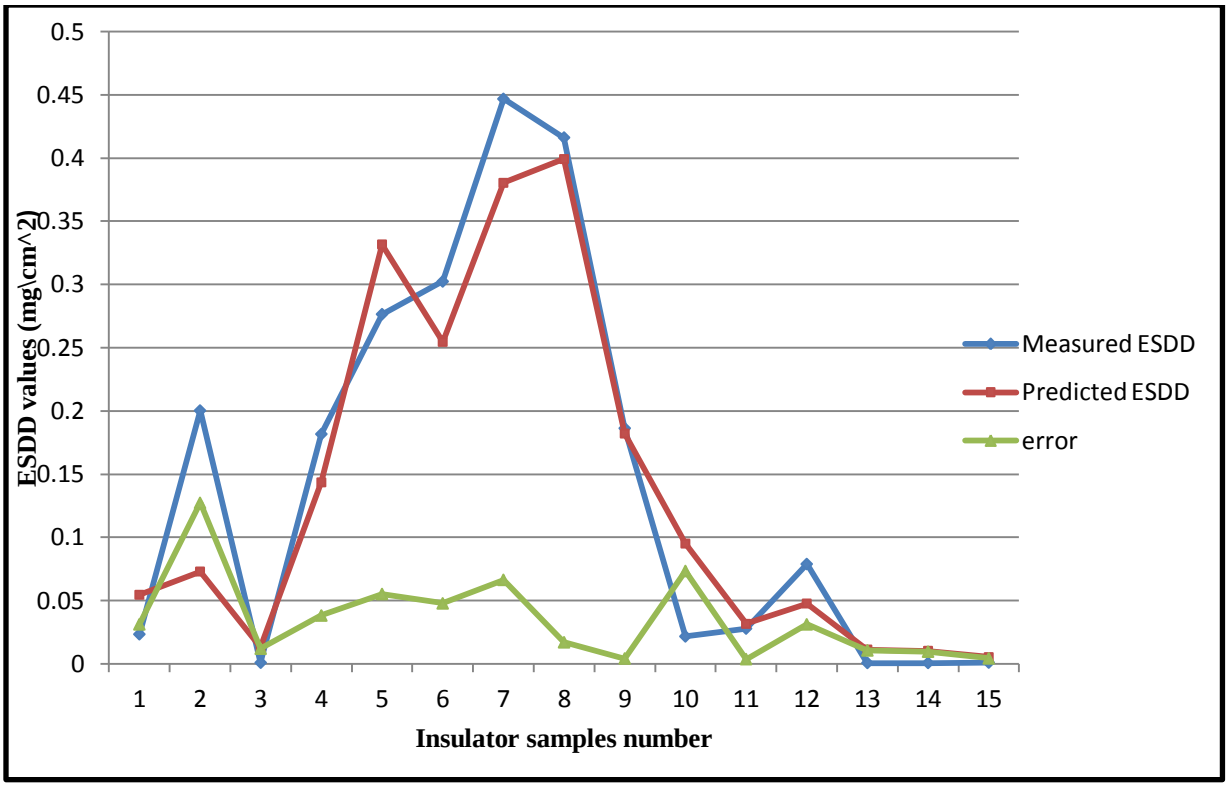

Figure 4.9 Comparison between the measured and predicted ESDD values – scenario I

4.7.2 Scenario II- Neural Network with Linear Algebraic Features

In this scenario linear algebraic features are used as inputs to the neural network. These features are the first *m* singular values of the hue image of insulator. Therefore, the number of inputs of the developed neural network is *m* and the number of outputs is one as shown in Figure 4.10. A typical training input matrix looks as follows:

$$\begin{bmatrix} \sigma_{1,1} & \cdots & \sigma_{1,n} \\ \sigma_{2,1} & \cdots & \sigma_{2,n} \\ \sigma_{3,1} & \cdots & \sigma_{3,n} \\ \sigma_{4,1} & \cdots & \sigma_{4,n} \\ \vdots & \cdots & \vdots \\ \sigma_{m-1,1} & \cdots & \sigma_{m-1,n} \\ \sigma_{m,1} & \cdots & \sigma_{m,n} \end{bmatrix} \quad (4.15)$$

Where, *n* denotes the number of features patterns for training which is equal to 36 and *m* is the number of singular values used as inputs. Samples of linear algebric feature values of some polluted insulators are given in Tables 4.5. The outputs are assigned letters as in Table 4.7.

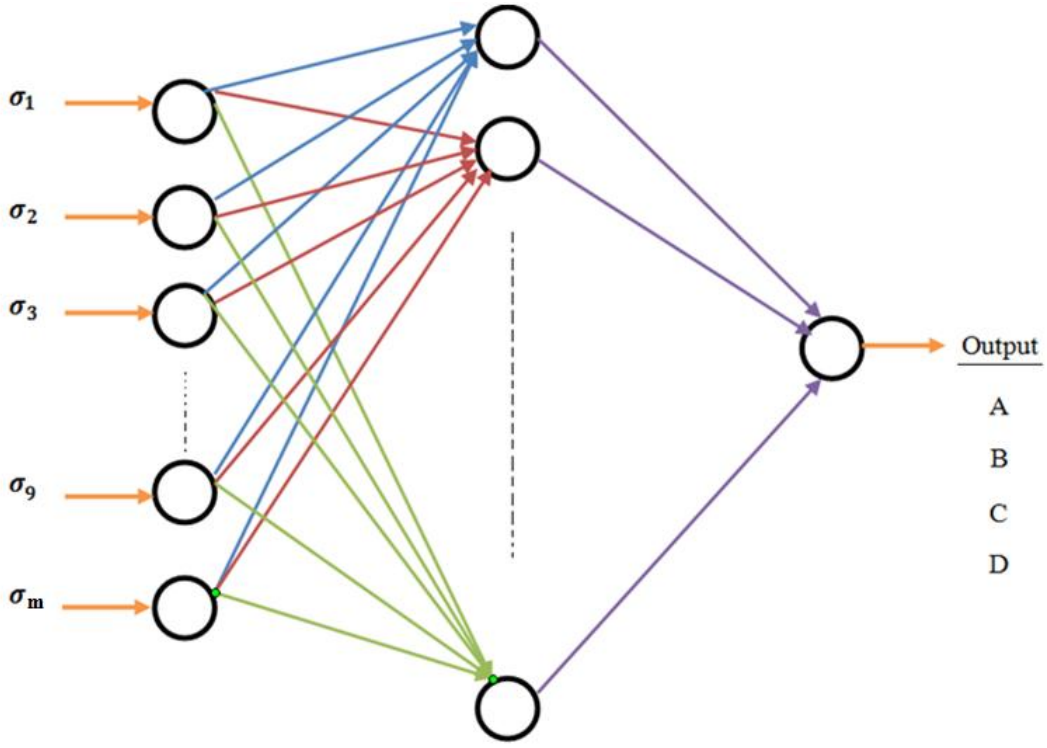

Figure 4.10 Neural network structure – scenario II

Different numbers of hidden neurons and singular values (*m*) have been tried such that the performance of the network is the best. For different cases, Table 4.11 shows the performance of the neural network for different combination of hidden neurons and singular values. It can be seen that although the testing performance of cases 2, 3, 4, 5, 6 and 7 are the same (80%), the MSE and maximum error for testing of case 2 are less than the other cases. In addition, case 2 is less complex in terms of number of inputs and hidden neurons. Accordingly, case2 is selected to be the sub-optimal configuration of the neural network where the number of hidden neurons is

nine and the mean square error (MSE) for training and testing are the minimum (MSE=0.0031 and MSE=0.0062, respectively). It is worth mentioning that the validation results of using the testing data given in Table 4.9 (for 15 insulators) indicated that the developed neural network was able to predicate correctly the level of contamination for twelve insulators, while for the other three insulators the pollution level was erroneously estimated. Among those erroneously estimated pollution levels, one predicted ESDD level has been assigned to a category two levels away from the actual one (predicted level of pollution is D while the actual level is B). Further details for validation result are given in Tables 4.12. Figure 4.11 shows a comparison between the measured (actual) and predicted ESDD values.

Table 4.11 Scenario II performance of neural network

Case number	Number of singular values	Performance of testing (%)	MSE of Testing	Maximum error of testing	Number of hidden neurons
1	5	73.33	0.0040	0.1900	3
2	10	80	0.0026	0.1920	9
3	15	80	0.0059	0.2125	9
4	20	80	0.0082	0.2906	11
5	25	80	0.0102	0.2586	15
6	30	80	0.0113	0.3655	15
7	50	80	0.0118	0.2840	13

Table 4.12 Validation result - scenario II

Insulator code	Measured ESDD value mg/cm^2	Actual Pollution level	Predicted ESDD value mg/cm^2	Predicted Pollution level	Absolute Error
4F	0.0234	A	0.0103	A	0.0131
8A	0.2003	C	0.2149	C	0.0146
C13	0.0009	A	0.0033	A	0.0024
9AE	0.1817	B	0.3481	D	0.1664
4D	0.2765	C	0.2592	C	0.0173
6DT	0.3024	D	0.2551	C	0.0473
13BT	0.4468	D	0.2548	C	0.192
14B	0.4162	D	0.4397	D	0.0235
2G	0.1863	B	0.1357	B	0.0506
4G	0.0217	A	0.0944	A	0.0727
1H	0.0279	A	0.0462	A	0.0183
7H	0.0789	A	0.0097	A	0.0692
C3	0.0007	A	0.0892	A	0.0885
C7	0.0007	A	0.0424	A	0.0417
C9	0.0010	A	0.0279	A	0.0269

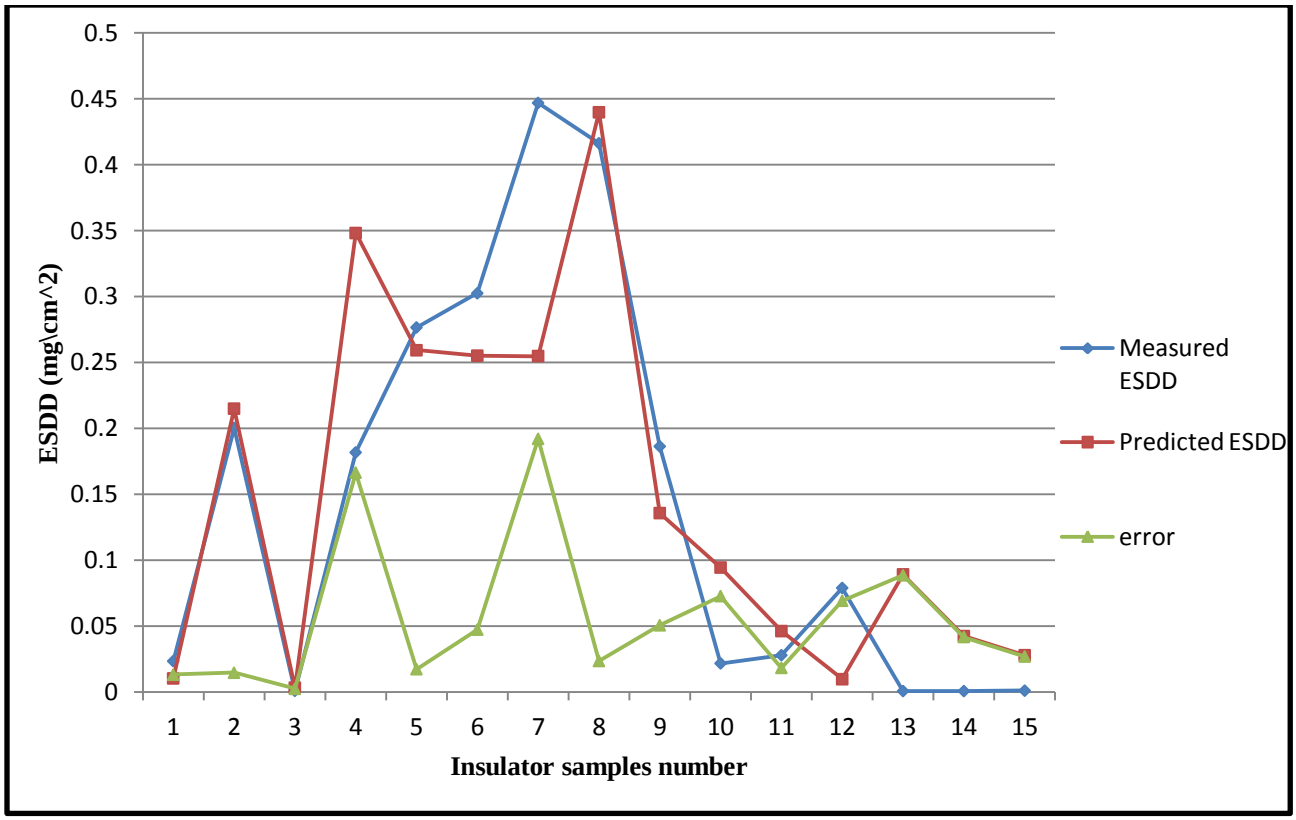

Figure 4.11 Comparison between the measured and predicted ESDD values – scenario II

4.7.3 Scenario III - Neural Network with combination of Linear Algebraic Features and statistical features

In this scenario, combination of statistical and liner algebraic features are used as inputs to the neural network. The feature vector was consisted of seven statistical features and ten linear algebraic features. Therefore, the number of inputs to the developed neural network is seventeen the number of outputs is one as shown in Figure 4.12. A typical training input matrix looks as follows:

$$\begin{bmatrix} \text{Difference}_1 & \cdots & \text{Difference}_n \\ \text{Normalized error}_1 & \cdots & \text{Normalized error}_n \\ \text{Mean}_1 & \cdots & \text{Mean}_n \\ \text{Variance}_1 & \cdots & \text{Variance}_n \\ \text{Skewness}_1 & \cdots & \text{Skewness}_n \\ \text{Kurtosis}_1 & \cdots & \text{Kurtosis}_n \\ \text{Energy}_1 & \cdots & \text{Energy}_n \\ \sigma_{1,1} & \cdots & \sigma_{1,n} \\ \sigma_{2,1} & \cdots & \sigma_{2,n} \\ \sigma_{3,1} & \cdots & \sigma_{3,n} \\ \vdots & \cdots & \vdots \\ \sigma_{9,1} & \cdots & \sigma_{9,n} \\ \sigma_{10,1} & \cdots & \sigma_{10,n} \end{bmatrix} \quad (4.15)$$

Where, n denotes the number of features patterns for training which equal thirty six. The outputs are assigned letters as in Table 4.7.

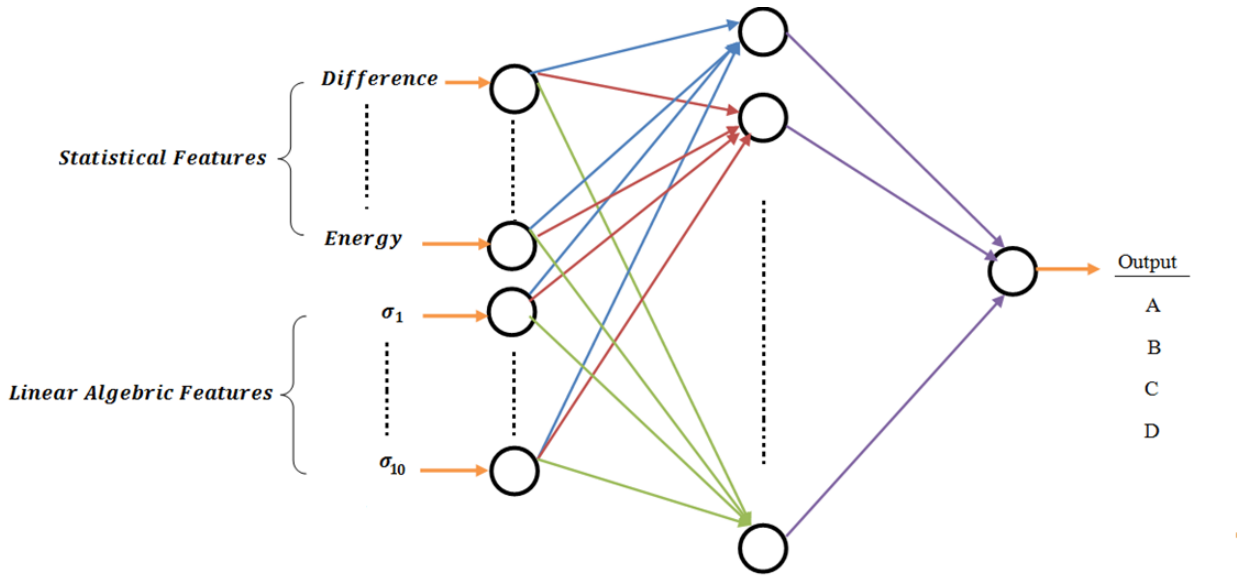

Figure 4.12 Neural network structure - scenario III

Different number of hidden units has been tried such that the performance of the network was optimized. The number of hidden neurons in the sub-optimized neural network was eleven, where the mean square error (MSE) for training and testing was the minimum (MSE=0.0001) and (MSE=0.0017), respectively. The validation results of using the testing data given in Table

4.9 (for fifteen insulators) indicated that the developed neural network was able to predicate correctly the level of contamination for thirteen insulators, while for the other two insulators the pollution level was wrongly estimated. According to that, the performance of the developed network is 86.67%. Further detail for validation result is given in Table 4.13. Figure 4.13 shows a comparison between the measured and predicted ESDD values.

Table 4.13 Validation result – scenario III

Insulator code	Measured ESDD value mg/cm^2	Actual Pollution level	Predicted ESDD value mg/cm^2	Predicted Pollution level	Absolute Error
4F	0.0234	A	0.0128	A	0.0106
8A	0.2003	C	0.1233	B	0.077
C13	0.0009	A	0.0011	A	0.0002
9AE	0.1817	B	0.2806	C	0.0989
4D	0.2765	C	0.2932	C	0.0167
6DT	0.3024	D	0.3028	D	0.0004
13BT	0.4468	D	0.3653	D	0.0815
14B	0.4162	D	0.4032	D	0.013
2G	0.1863	B	0.1911	B	0.0048
4G	0.0217	A	0.0257	A	0.004
1H	0.0279	A	0.0506	A	0.0227
7H	0.0789	A	0.0438	A	0.0351
C3	0.0007	A	00.006	A	0.0053
C7	0.0007	A	0.0062	A	0.0055
C9	0.0010	A	0.0119	A	0.0109

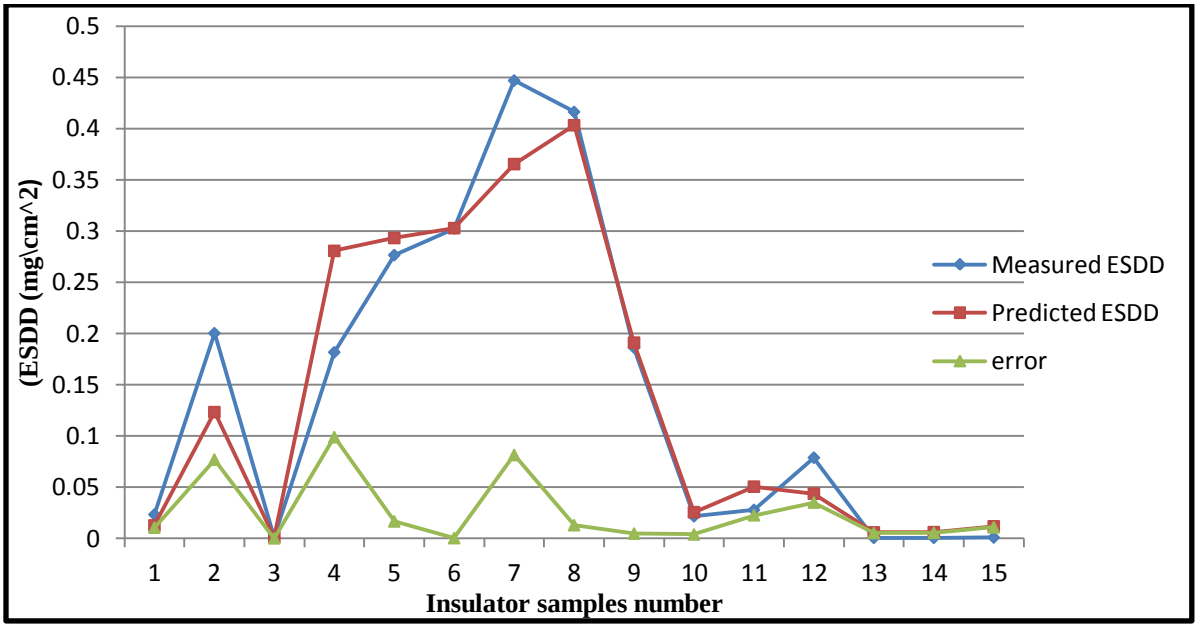

Figure 4.13 : Comparison between the measured and predicted ESDD values - scenario III

4.7.4 Comparison between the Three Developed Scenarios

Table 4.14 shows the performance of different scenarios in term of accuracy and complexity. Comparing scenarios I and II, It can be seen that both have the same testing performance (80%) with less values of MSE and maximum error of testing in scenario I. In addition, scenario I is less complex in terms of number of inputs and hidden neurons. On the other hand, it is quite clear that the performance of scenario III which is a combination of scenarios I and II outperforms the first two. The testing performance is 86.67% with an MSE of 0.0017 and maximum error of testing of 0.0989 as compared to a testing performance of 80% and an MSE of 0.0024 and maximum error of testing of 0.1273 in scenario I. this improvement in the performance is on the expense of more complex neural network configuration (17 inputs and 11 hidden neurons as compared to 7 inputs and 7 hidden neurons in scenario I). This complexity is

justified not only because it improves the testing performance but it also reduces the error in the number of category levels between the predicted and actual ESDD levels (for example the predicted level of pollution is B while the actual level is C).

Table 4.14 Comparison between the Three Developed Scenarios

	Scenario I	Scenario II	Scenario III
Number of inputs	7	10	17
Number of hidden neurons	7	9	11
Performance of testing	80%	80%	86.67%
MSE of testing	0.0024	0.0062	0.0017
Performance of training	88.89%	86.11%	97.2%
MSE of training	0.0011	0.0031	0.0001
Maximum error of testing	0.1273	0.1920	0.0989

4.7.5 Comparison between the Proposed and the Previously Reported Methods.

In order to demonstrate the effectiveness of the proposed monitoring method, Table 4.15 gives a detailed comparison between the present and previously reported techniques. It can be seen from the table that the present method gives a conclusive idea about the contamination level. The contamination level used cover the practical values (0-0.5) reported by different utilities [2] as opposed to all previous methods which used insulators with contamination levels which ranges from (0-0.3). This is an achievement when compared to all other methods. As such it can be concluded that the present method outperforms the previous methods. To be more specific, the technique of [32] depends on detecting the sound of partial discharge generated in the presence of contamination (ESDD from 0-0.123) which will have interference with other background

noise. Unfortunately, the reported results of [32] have been conducted in an indoor environment where it is easy to eliminate the background noise. As such, it is believed that its applicability to practical transmission lines is very limited. On the contrary, the proposed method which depends on a digital image has been taken outdoor (in the field) which represents a practical transmission line condition. The work of [22] demonstrated its performance using MAE. Although the MAE is low, the NN topology is more complex as it has 2 hidden layers, each with 11 neurons as compared to 1 hidden layer with 11 neurons in the present method. This is in addition to the very low range of insulator contamination levels tested (0-0.045) which will affect the reliability of the proposed method under sever contamination levels.

Table 4.15 Comparison between the proposed and the previously reported methods

Reference	**[22]**	**[32]**	**[35]**	**[71]**	**[28]**	**[41]**	**Proposed method**
Method	ESDD=F(metrological factors)	ESDD=F(ultrasonic signal)	ESDD=F(UV image)	ESDD=F(PD)	ESDD=F(LC)	ESDD=F(digital image)	ESDD=F(digital image)
Technique of data processing	ANN	ANN	Fuzzy logic	Statistical processing	Time and frequency domain analysis	Image Processing	ANN
Insulator pollution type	naturally	naturally	artificial	naturally	artificial	---	naturally
Number of sample for testing	10	120	---	---	35	--	15
ESDD range	0-0.045	0-0.123	0-0.3	0-0.25	0-0.3	---	0-0.5
Monitoring system	Online	Offline	Offline	Online	Offline	Offline	Offline
Performance (comments)	MAE=3.6%	Success Rate 96.6%	Not Reported	Not Reported	Not Reported	Only determine the size of contaminated area	Success Rate 86.6%

MAE: Mean Absolute Error

CHAPTER FIVE

CONCLUSIONS AND FUTER WORK

5.1 Conclusions

The purpose of this thesis was to develop a tool for monitoring the contamination level of high voltage insulators without the intervention of humans. The developed tool is based on a combination of image processing technique and artificial neural networks. The main achievements of this thesis can be summarized as follows:

- A comprehensive literature review has been accomplished for high voltage insulators contamination problem and the industry practices for mitigating its effects on power system performance.
- Fifty one samples of super fog porcelain insulators were collected; eleven samples from SEC (six from DAMMAM BSP - GHAZLAN POWER PLANT and five from QATIF BSP - RAS TANURA). The rest are from KFUPM Dhahran Electrical Insulator Research Station. All samples were manufactured by NJK Insulator LTD Company (Japan).
- Image data bank for the collected naturally contaminated insulators have been built using high resolution camera (Nikon D7000). Pictures capturing have been being done at scheduled intervals. Fixed stand for fixing the camera was designed and used to capture images for the insulators under testing. It has been found that many factors such as the

type and position of the camera, and picture capturing time have a significant effect on building representative image data sets for insulators.

- Six representative insulators samples were chosen to be tested to measure the flashover voltage (50% flashover voltage ($U_{50\%}$)) at the high voltage lab of the research institute at KFUPM. The procedure used to conduct the test is based on "Rapid Flashover Voltage Technique". In addition, the ESDD levels of the collected naturally contaminated insulators have been estimated at the same lab.
- The contamination levels (ESDD) of the collected insulators varies from 0 to 0.45. Accordingly, levels of contamination are classified into four ranges: light pollution level ($ESDD < 0.1$), medium pollution level($0.1 \leq ESDD < 0.2$), heavy pollution level ($0.2 \leq ESDD < 0.3$) and very heavy pollution level($0.3 \leq ESDD$). Results reveal that the higher the insulator contamination level (higher the ESDD value), the lower is the flashover voltage.

- In developing the estimation tool, it has been found that the surface of insulators is the important part in the image that needs to be examined and analyzed.
- Segmentation of insulator image has been done in two stages using MATLAB^{TM} software. In both stages, segmentation has been done for grayscale insulator image. In the first stage, the cap of insulator has been excluded from the image using Chan-Vese algorithm. In the second stage, edge based segmentation method was used to exclude the background.

- Image processing has been used to extract needed features form the captured images to assess the contamination level that would lead to a flashover. HSV (especially the hue

component) was the color model that has been used for extraction the features. This model aids in finding numerical differences between insulators of different pollution levels; moreover it helps in reducing the effect of uneven illumination on insulator surface.

- Two types of image features were considered. The first is “histogram based statistical feature” such as mean, variance, skewness, kurtosis, energy and normalized histogram error. The second feature is “singular value decomposition theorem linear algebraic feature” such as the singular values.
- Multi-layer Feed-forward Neural Network (MFNN) was used to design a neural network which is capable of predicting the level of contamination (ESDD level) of polluted insulators. The input to the network is the extracted features of insulators images and the output is the pollution levels.
- Three different neural networks scenarios were developed. In scenario I, the statistical features are used as inputs to the neural network. The performance of the developed network is 80%. In scenario II, the linear algebraic features are used as inputs to the neural network. The performance of the developed network is 80%. In scenario III, combination of statistical and liner algebraic features are used as inputs to the neural network. The performance of the developed network is 86.67%.
- The complexity of scenario III can be justified by its better performance in terms of ESDD estimation success rate.

- It is expected that the developed tool, if well implemented, will prevent catastrophic flashovers and reduces forced outage time by giving accurate information about the contamination level in advance without human intervention. Hence improving the overall

reliability of the electrical system. It will also enable efficient maintenance planning and reduce maintenance costs.

5.2 Future Work

In order to develop a general-purpose tool for monitoring the contamination level of high voltage insulators, a number of problems must be solved. These problems suggest a variety of research directions that need to be pursued to make such a system available. The following presents some suggestion of these research topics.

- Generalizing the developed tool to be able to detect the contamination levels of different types and shapes of insulators.
- Making the developed tool fully automated (online monitoring).
- Finding more representative features in order to improve the performance of the tool and decrease complexity and computational time.
- Selecting an optimal neural network configuration using other optimizing technique such as artificial intelligence algorithms.

REFERENCES

[1] R. S. Gorur, "Where is Insulator Technology Today:What has been Accomplished, What is still Missing?," in Insulator 2001 World Insulator Congress and Exhibition, Shanghai,China, 2011.

[2] I. AL-Hamoudi, "Preformance of Silicone Rubber Insulators in Eastern Region of Saudi Arabia," Ph.D.Thesis,American University of London, 2002.

[3] A.-S. H. Hamza, N. M. Abdelgawad and B. A. Arafa, "Effect of desert environmental conditions on the flashover voltage of insulators," Elsevier, Vols. Volume 43, Number 17, November 2002 , pp. 2437-2442(6), 2002.

[4] K. Siderakis, D. Pylarinos, E. Thalassinakis, I. and E. Pyrgiti, "Pollution Maintenance Techniques in Coastal High Voltage Installations," ETASR - Engineering, Technology & Applied Science Research, Vols. 1,No. 1, 2011, 1-7, 2011.

[5] The Research Institute of KFUPM, "high Voltage Insulator Preformance in the Kingdom of Saudi Arabia," Saudi Arabia ,report prepared for Electricity Corporatin KSA ,1990 pp. 9-127,821-840, 1990.

[6] R. S. Gorur, E. A. Cherney and J. T. Burnham, "Outdoor Insulators," pp.31,55-56,146,181-191,211, 1999.

[7] S. Venkataraman, R. S. Gorur and R. Olsen, "Prediction of Flashover Voltage of Insulators Using Low Voltage Surface Resistance Measurement," Power Systems Engineering Research Center, Arizona State University, November 2006.

[8] R. E. Kapal Sharma, Polymeric Insulators, Technical Article.

[9] J. B. Wardman, T. M. Wilson, B. S. Bodger, J. W. Cole and D. M. Johnston, "Investigating the electrical conductivity of volcanic ash and its effect on HV power systems," ELSEVIER, vol. 45–46, p. 128–145, 2012.

[10] M. T. Gencoglu and M. Cebeci, "The pollution flashover on high voltage insulators," Elsevier B.V., 2008.

[11] A. Ahmad, A. Saad and A. Shahnawaz, "Dimensional Analysis for Contamination Severity Assessment on High Voltage Insulators," in International Conference on Intelligent and Advanced Systems 2007, 2007.

[12] F. Amarh, "Electric Transmission Line Flashover Prediction System," Ph.D. Thesis and Final Report, Arizona State, 2001.

[13] M. A. Salam, Z. Nadir and N. EL-Fadil, "Characterization of Flashover Voltage of a Polluted Insulator Energized with DC Voltage," Ecti Transaction on Electrical Eng, Electroincs, and Communication Vol.4, No.1 February 2006.

[14] M. Abdus Salam, H. Goswami and Z. Nadir, "Determination of Equivalent Salt Deposit Density Using Wind Velocity for a Contaminated Insulator," Journal of Electrostatics,Elseiver, 2004.

[15] "IEC 60815: Guide for the selection and dimensioning of high-voltage insulators for polluted conditions".

[16] E. A. Cherney and R. S. Gorur, "RTV Silicone Rubber Coatings for Outdoor Insulators," Dielectrics and Electrical Insulation, Vols. 6 , Issue: 5, pp. 605- 611, Oct 1999.

[17] Suwarno and A. Basuki, "Mitigation of outdoor insulators failure using silicone coating," in Electrical Engineering and Informatics (ICEEI), Indonesia, 17-19 July 2011.

[18] T. Electronics, "High Voltage Creepage Extenders A remedy for Pollution Flashovers of Insulators," Tyco Electronics Raychem GmbH/Energy Division, Haidgraben 6, 85521 Ottobrunn/Munich, Germany.

[19] Y. Qing, S. Wenxia, D. Jiazhuo, Y. Tao and C. Lin, "New optimization method on electric field distribution of composite insulator," in Electrical Insulation and Dielectric Phenomena (CEIDP), Chongqing Univ., Chongqing, China, 2010.

[20] E. Akbari, M. Mirzaie, A. Rahimnejad and M. Asadpoor, "Finite Element Analysis of Disc Insulator Type and Corona Ring Effect on Electric Field Distribution over 230-kV Insulator Strings," International Journal of Engineering and Technology,, no. Science Publishing Corporation,Iran, 2012.

[21] G. G. Karady, M. Shah and R. Brown, "Flashover mechanism of silicone rubber insulators used for outdoor insulation-I," Power Delivery, IEEE Transactions , Vols. 10 , Issue: 4 , pp. 1965- 1971 , 1995.

[22] S. A. Ahmad, P. S. Ghosh, S. S. Ahmad and S. K. Aljunid, "Assessment of ESDD on High-Voltage Insulators Using Artificial Neural Network," Elsevier/Electric Power Systems Research, vol. 72, no. 2, pp. 131-136, 1 December 2004.

[23] M. A. Salam, S. M. Al-Alawi and A. A. Maqrashi, "Prediction of equivalent salt deposit

density of contaminated glass plates using artificial neural networks," Journal of Electrostatics, vol. 66, no. 9-10, pp. 526-530, September 2008.

[24] Y. Mizuno, H. Nakamura and K. Nmto, "Dynamic Simulation of Risk of Flashover of Contaminated Ceramic Insulators," IEEE Transactions on Power Delivery, vol. 12, no. 3, July 1997.

[25] T. Suda, "Frequency Characteristics of Leakage Current Waveforms of a String of Suspension Insulators," IEEE Transaction on Power Delivery, vol. 20, no. 1, January 2005.

[26] E. Fontana, J. F. Martins-Filho, S. C. Oliveira, F. J. Cavalcanti, R. A. Lima, G. O. Cavalcanti, T. L. Prata and R. B. Lima, "Sensor Network for Monitoring the State of Pollution of High-Voltage Insulators Via Satellite," IEEE Transactions on Power Delivery, vol. 27, no. 2, April 2012.

[27] C. N. Richard and J. D. Renowden, "Development of A Remote Insulator Contamination Monitoring System," IEEE Transactions on Power Delivery, vol. 12, no. 1, January 1997.

[28] J. Y. Li, C. X. Sun and S. A. Sebo, "Humidity and contamination severity impact on the leakage currents of porcelain insulators," Generation, Transmission & Distribution, IET, vol. 5, pp. 19- 28, Jan. 2011.

[29] D. C. Jolly, T. C. Cheng and D. M. Otten, "Dynamic Therory of Discharge Growth over Contaminated Insulator Surfaces," IEEE PES # C 74 068-3 Winter meeting in N. Y, pp. 1-9, February1-1974.

[30] C. M. Pei, N. Q. Shu, L. L. D, Z. P. Li and D. Wang, "An Acoustic Emission Method for On-line Monitoring the Contamination-causing Flashover of Insulator," in Electrical Machines and Systems, 2008. ICEMS 2008. , 17-20 Oct. 2008.

[31] C. M. Pei, N. Q. Shu, L. Li, Z. P. Li and H. Peng, "On-line Monitoring of Insulator Contamination causing Flashover Based on Acoustic Emission," DRPT2008 6-9 April 2008 Nanjing China.

[32] R. B. De Aquino, J. B. Bezerra, M. S. Lira, G. M. Santos, O. N. Neto and C. A. Lira, "Combining Artificial Neural Network for Diagnosing Polluted Insulators," in International Joint Conference on Neural Networks, Atlanta, Georgia, USA, June 14-19, 2009.

[33] J. M. De Barros Bezerra, A. M. Lima, G. S. Deep and E. G. da Costa, "An Evaluation of Alternative Techniques for Monitoring Insulator Pollution," IEEE Transactions on Power Delivery, vol. 24, 4, OCTOBER 2009.

[34] B. Li, X. Wang and L. Nian, "Remote Online Monitoring System for Suspension Insulator Strings," in 2006 IEEE International Symposium on Industrial Electronics, China, July 9-12, 2006.

[35] L. U. Fangcheng, W. Shenghui and L. Heming, "Insulator Pollution Grade Evaluation Based on Ultraviolet Imaging and Fuzzy Logic Inference," in Power and Energy Engineering Conference (APPEEC), 2010 Asia-Pacific, 28-31 March 2010.

[36] I. Girianttari, "Monitoring the insulator Condition by online Voltage Distrbution Measurement," in Condition Monitoring and Diagnosis, April 2008.

[37] N. Bashir and H. Ahmad, "Agning of Transmission Line Insulators," in IEEE Int.Power and Energy, Dec.2008.

[38] A. Bovik, Handbook of Image & Video Processing, Elsevier,2nd edition,2005.

[39] X. Jiang, J. Yuan, Z. Zhang, J. Hu and C. Sun, "Study n AC Artifical-Contaminated Flashover Preformance of Various Types of Insulators," in IEEE Transactions on Power Delivery, 2007.

[40] X. Mei, L. Tiecheng, W. Xiaoyun and Z. Bo, "Insulator surface Dirty Image Detection Technology Based on Improved Watershed Algorithm," in IEEE, 2012.

[41] Z. Xia, D. Hu, X. Hu, W. Xie, Z. Yuan and Q. Qin, "Application of an improved watershed algorithm in the insulator contamination monitoring," in IEEE, 2011.

[42] P. J. Lambeth and H. A. Ely, "Artificial-pollution test for high-voltage outdoor insulators," Proceedings of the Institution of Electrical Engineering, vol. 111, no. 5, pp. 991- 998, May 1964.

[43] S. PRAT, J. M. GEORGE and J. P. LOPEZ, "Performance Evaluation Method and Optimum Selection of Overhead Line Insulators for Contaminated Environments," in World Congress On Insulators, 2009.

[44] IEC 60507, International Electro Technical Commission (IEC) document.

[45] O. Marques, PracticalL Image and Video Processing Using MATLAB®, Wiely Press.

[46] T. Seemann, "Digital Image Processing using Local Segmentation," April 2002.

[47] J. Sachs, "Digital Image Basics," Copyright © 1996-1999 Digital Light & Color.

[48] A. Ford and A. Roberts, "Colour Space Conversions," August 11, 1998.

[49] MATLAB, "Image processing toolbox".

[50] T. Kumar and K. Verma, "A Theory Based on Conversion of RGB image to Gray image," International Journal of Computer Applications (0975 – 8887), Volume 7– No.2, September 2010.

[51] W. K. Pratt, Digital Image Processing: PIKS Inside, Third Edition., John Wiley & Sons, Inc.ISBNs: 0-471-37407-5 (Hardback); 0-471-22132-5 (Electronic), Copyright © 2001.

[52] O. Banimelhem and A. Yahya, "Multi-Thresholding Image Segmentation Using Genetic Algorithm," Jordan University of Science and Technology, Irbid, Jordan.

[53] S. B. Wesolkowski, "Color Image Edge Detection and Segmentation: A Comparison of the Vector Angle and the Euclidean Distance Color Similarity Measures," Waterloo, Ontario, Canada, 1999.

[54] S. Gupta and S. G. Mazumdar, "Sobel Edge Detection Algorithm," International Journal of Computer Science and Management Research, vol. Vol 2 , no. ISSN 2278-733X, Issue 2 February 2013.

[55] R. C. Gonzalez and R. E. Woods, Digital Image Processing Third Edition, Pearson Prentice Hall, © 2008 by Pearson Education, Inc.

[56] R. Muthukrishnan and M. Radha, "Edge Detection Techniques for Image Segmentation," International Journal of Computer Science & Information Technology (IJCSIT), vol. Vol 3, p. No 6, Dec 2011.

[57] M. Khelif, F. Derraz and M. Beladgahm, "Application of Active Contour Models in Medical Image Segmentation," Universite A Belkaid -Tlemcen, B.P 230, Tlemcen (13 000), Algerie.

[58] X. Feng Wanga, D. Shuang Huanga and H. Xua, "An efficient local Chan–Vese model for image segmentation," Pattern Recognition, no. 43(2010)603--618.

[59] M. Kass, A. Witkin and D. Terzopoulos, "Snakes:activecontourmodels," Int.J.Comput.Vision, no. 1(4)(1987)321–331..

[60] T. F. Chan and L. A. Vese, "Active Contours Without Edges," IEEE Transactions on Image Processing, Vol. 10, NO. 2, February 2001.

[61] D. MUMFORD and J. SHAH, "Optimal Approximations by Piecewise Smooth Functions

and Associated Variational Problems," Communications on Pure and Applied Mathematics, Vol. XLII 577-685 (1989).

[62] K. Zhang, L. Zhang, K. Man Lam and D. Zhang, "A Locally Statistical Active Contour Model for Image Segmentation with Intensity Inhomogeneity," The Hong Kong Polytechnic University.

[63] C. L. Phillips, "The Level-Set Method," MIT Undergraduate Journal of Mathematics.

[64] T. Chan and L. Vese, "An Active Contour Model without Edges," Vols. M. Nielsen et al. (Eds.): Scale-Space'99, LNCS 1682, pp. 141{151, 1999., no. Springer-Verlag Berlin Heidelberg 1999.

[65] L. Cao, "Singular Value Decomposition Applied To Digital Image Processing," Arizona State University Polytechnic Campus, Mesa, Arizona 85212.

[66] M. V. Malakooti, Z. FerdosPanah and S. M. Hashemi, "Image Recognition Method based on Discrete Wavelet Transform (DWT) and Singular Value Decomposition (SVD)," ISBN: 978-0-9853483-3-5 ©2013 SDIWC.

[67] J. K. Basu, D. Bhattacharyy and T. Kim, "Use of Artificial Neural Network in Pattern Recognition," International Journal of Software Engineering and Its Applications,Vol. 4, No. 2, April 2010.

[68] P. Andries and P. Engelbrecht, Computational Intelligence: An Introduction, 2nd Edition, WILEY.

[69] J. C. Principe, N. R. Euliano and W. C. Lefebvre, Neural and Adaptive Systems: Fundamentals through Simulations, WILEY.

[70] P. Sebastian, Y. Voon and R. Comley, "Colour Space Effect on Tracking in Video Surveillance," International Journal on Electrical Engineering and Informatics, Volume 2, Number 4, 2010.

[71] A. Levinzon, D. Kottick, R. Knijnik and L. Frenkel, "On-Line Wireless PD Monitoring System for Contamination Detection on High Voltage Overhead Transmission Lines Insulators," CIGRE 2012.

APPENDIX

A.1 Insulators Image Data Bank.

Figure A.1 (a) - insulator 1D (b) - 1F (c) - insulator 1G (d) – insulator 1H (e) – insulator 2D (f) insulator 2F

Figure A.2 (a) - insulator 2G (b) – 2H (c) - insulator 3DE (d) – insulator 3F (e) – insulator 3G (f) insulator 3H

Figure A.3 (a) - insulator 4D(b) – 4F (c) - insulator 4G (d) – insulator 4H (e) – insulator 5AT (f) insulator 5DE

Figure A.4 (a) - insulator 5G (b) insulator– 5H (c) - insulator 6AE (d) – insulator 6DT (e) – insulator 6G (f) insulator 6H

Figure A.5 (a) - insulator 7A (b) insulator– 7G (c) - insulator 7H (d) – insulator 8A (e) – insulator 8G (f) insulator 9AE

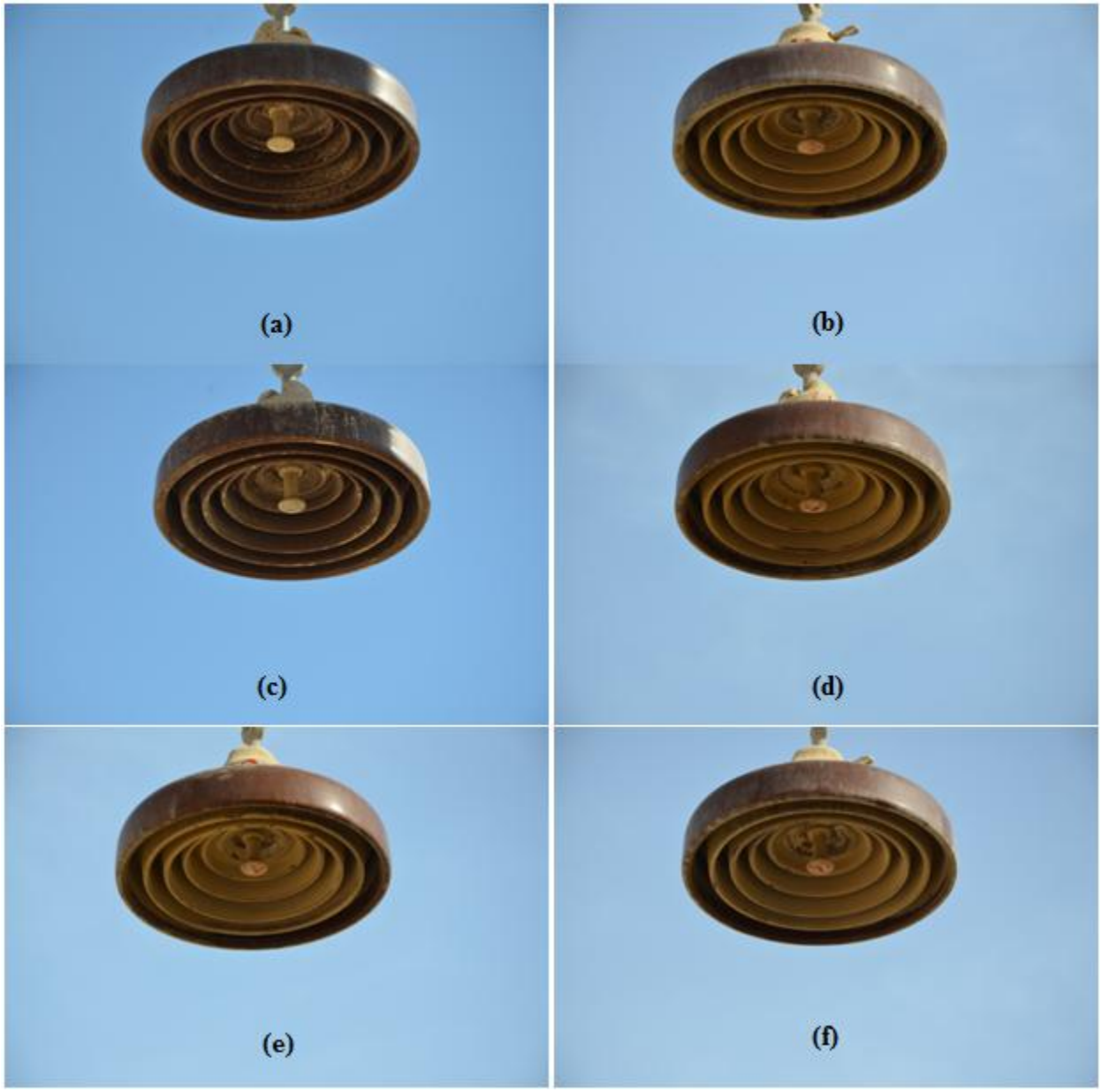

Figure A.6 (a) - insulator 9G (b) insulator– 10BE (c) - insulator 10G (d) – insulator 11BE (e) – insulator 12B (f) insulator 13bt

Figure A.7 (a) – insulator 14b (b) insulator– C1 (c) - insulator C2 (d) – insulator C3 (e) – insulator C4 (f) insulator C5

Figure A.8 (a) – insulator C6 (b) insulator– C7 (c) - insulator C8 (d) – insulator C9 (e) – insulator C10 (f) insulator C11

Figure A.9 (a) – insulator C12 (b) insulator– C13 (c) – insulator Clean

A.2 Flashover Voltage Tests Results

The results of the flashover voltage for the six tested insulators 12B, 14B, 2D, 6DT, 5AT and 6AE are listed in Tables A.1, A.3, A.5, A.7, A.9 and A.11, respectively. Moreover, the relation between flashover voltage time and the magnitude for these insulators are listed in Tables A.2, A.4, A.6, A.8, A.10 and A.12, respectively.

Table A.1 Flashover test results for insulator 12B

Rapid Flashover Test				Date : 26-3-2013		
Insulator type : Super Fog				Insulator code: 12B		
#	Test voltage (KV)	Time		Flashover voltage (KV)	Flashover voltage time(minute)	Remarks
		Start (H:M:S)	Stop (H:M:S)			
1	50	9:43:00	10:03:18	50	20.3	Flashover
2	44	10:03:18	10:06:18	---	3	Withstand
3	46	10:06:18	10:09:18	---	3	Withstand
4	48	10:09:18	10:10:42	48	1.4	Flashover
5	42	10:10:42	10:13:42	---	3	Withstand
6	44	10:13:42	10:15:42	44	2	Flashover
7	39	10:15:42	10:18:42	---	3	Withstand
8	40.7	10:18:42	10:21:42	---	3	Withstand
9	42.4	10:21:42	10:21:51	42.4	0.16	Flashover
10	37	10:21:51	10:24:51	---	3	Withstand
11	38.7	10:24:51	10:27:51	---	3	Withstand
12	40.4	10:27:51	10:30:51	---	3	Withstand
13	42	10:30:51	10:31:00	42	0.15	Flashover
14	37	10:31:00	10:31:00	---	3	Withstand
15	38.7	10:31:00	10:32:27	40.1	1.45	Flashover
16	34	10:32:27	10:35:27	---	3	Withstand
17	35.5	10:35:27	10:38:27	---	3	Withstand
18	31.2	10:38:27	10:41:27	35.5	3	Flashover
19	32.4	10:41:27	10:44:27	---	3	Withstand

Table A.1 Flashover test results for insulator 12B (continued)						
#	Test voltage (KV)	Time		Flashover voltage (KV)	Flashover voltage time(minute)	Remarks
		Start (H:M:S)	Stop (H:M:S)			
20	33.6	10:44:27	10:47:27	---	3	Withstand
21	29.5	10:47:27	10:48:27	33.6	1	Flashover
22	30.8	10:48:27	10:51:27	---	3	Withstand
23	31.1	10:51:27	10:54:27	---	3	Withstand
24	33.4	10:54:27	10:57:27	---	3	Withstand
25	34.7	10:57:27	10:59:09	34.7	1.6	Flashover
26	30.5	10:59:09	11:05:09	---	3	Withstand
27	31.9	11:05:09	11:08:09	---	3	Withstand
28	33.3	11:08:09	11:11:09	---	3	Withstand
29	34.7	11:11:09	11:11:27	34.7	0.3	Flashover
30	30.5	11:11:27	11:14:27	---	3	Withstand
31	31.9	11:14:27	11:17:27	---	3	Withstand
32	33.3	11:17:27	11:20:27	---	3	Withstand
33	34.7	11:20:27	11:20:45	34.7	0.3	Flashover
34	30.5	11:20:45	11:23:45	---	3	Withstand
35	31.9	11:20:45	11:20:45	---	3	Withstand
36	33.3	11:23:45	11:26:45	---	3	Withstand
37	34.7	11:26:45	11:29:45	---	3	Withstand
38	36.1	11:29:45	11:32:45	---	3	Withstand
39	37.5	11:32:45	11:35:45	---	3	Withstand
40	38.9	11:35:45	11:38:45	---	3	Withstand
41	40.3	11:38:45	11:41:45	---	3	Withstand

Table A.1 Flashover test results for insulator 12B (continued)						
#	Test voltage (KV)	Time		Flashover voltage (KV)	Flashover voltage time(minute)	Remarks
		Start (H:M:S)	Stop (H:M:S)			
42	41.7	11:41:45	11:44:45	---	3	Withstand
43	43.1	11:44:45	11:47:45	---	3	Withstand
44	44.5	11:47:45	11:50:45	---	3	Withstand
45	45.9	11:50:45	11:53:45	---	3	Withstand
46	47.3	11:53:45	11:56:45	---	3	Withstand
47	48.7	11:56:45	11:59:45	---	3	Withstand
48	50.3	11:59:45	12:02:45	---	3	Withstand
49	51.7	12:02:45	12:05:21	51.7	2.6	Flashover

Table A.2 The Relation between flashover voltage time and magnitude (Insulator 12B)

N	Time (minute)	Flashover (KV)
1	20.18	50
2	28.55	48
3	34.2	44
4	40.8	42.4
5	50.6	42
6	55.7	40.1
7	62	35.5
8	68.85	33.6
9	82.7	34.7
10	92.2	34.7

Table A.3 Flashover test results for insulator 14B

Rapid Flashover Test				Date : 31/3/2013		
Insulator type : Super Fog				Insulator code: 14B		
#	Test voltage (KV)	Time		Flashover voltage (KV)	Flashover voltage time	Remarks
		Start (H:M:S)	Stop (H:M:S)			
1	45	9:46:00	10:11:00	---	25	Withstand
2	47	10:11:00	10:12:00	---	1	Withstand
3	49	10:12:00	10:12:06	49	0.1	Flashover
4	43	10:12:06	10:15:06	---	3	Withstand
5	45	10:15:06	10:14:52	45	2.77	Flashover
6	40	10:14:52	10:17:52	---	3	Withstand
7	41.8	10:17:52	10:20:52	---	3	Withstand
8	43.6	10:20:52	10:23:52	43.6	3	Flashover
9	39.6	10:23:52	10:26:52	---	3	Withstand
10	41.4	10:26:52	10:29:52	41.4	3	Flashover
11	36.4	10:29:52	10:32:52	---	3	Withstand
12	37.9	10:32:52	10:33:04	37.9	0.2	Flashover
13	33.3	10:33:04	10:36:04	---	3	Withstand
14	34.6	10:36:04	10:39:04	---	3	Withstand
15	35.9	10:39:04	10:41:04	---	3	Withstand
16	37.2	10:41:04	10:42:10	37.2	1.1	Flashover
17	32.8	10:42:10	10:45:10	---	3	Withstand
18	34.3	10:45:10	10:48:10	---	3	Withstand
19	35.8	10:48:10	10:50:04	35.8	1.9	Flashover

Table A.3 Flashover test results for insulator 14B (continued)						
#	Test voltage (KV)	Time		Flashover voltage (KV)	Flashover voltage time	Remarks
		Start (H:M:S)	Stop (H:M:S)			
20	31.5	10:50:04	10:53:04	---	3	Withstand
21	32.9	10:53:04	10:56:04	---	3	Withstand
22	34.3	10:56:04	10:56:04	34.3	0	Flashover
23	30	10:56:04	10:59:04	---	3	Withstand
24	31.3	10:59:04	11:02:04	---	3	Withstand
25	32.6	11:02:04	11:05:04	---	3	Withstand
26	33.8	11:05:04	11:05:20	33.8	0.27	Flashover
27	30	11:05:20	11:08:20	---	3	Withstand
28	31.4	11:08:20	11:11:20	---	3	Withstand
29	32.8	11:11:20	11:14:20	---	3	Withstand
30	34	11:14:20	11:17:20	---	3	Withstand
31	35	11:17:20	11:17:39	35	0.32	Flashover
32	31	11:17:39	11:20:39	---	3	Withstand
33	32.4	11:20:39	11:23:39	---	3	Withstand
34	33.8	11:23:39	11:26:39	---	3	Withstand
35	35.2	11:26:39	11:29:39	---	3	Withstand
36	36.6	11:29:39	11:29:55	36.6	0.27	Flashover
37	32.2	11:29:55	11:32:55	---	3	Withstand
38	33.7	11:32:55	11:35:55	---	3	Withstand
39	35.2	11:35:55	11:38:55	---	3	Withstand
40	36.7	11:38:55	11:41:55	---	3	Withstand
41	38.2	11:41:55	11:33:03	38.2	0.14	Flashover

Table A.4 The relation between flashover voltage time and magnitude (Insulator 14B)

N	Time (minute)	Flashover voltage (KV)
1	26.3	49
2	32	45
3	42	43.6
4	45.2	41.4
5	48.6	37.9
6	59.2	37.2
7	67.6	35.8
8	74.6	34.3
9	86.7	33.8
10	99.2	35
11	112.3	36.6
12	124.6	38.2

Table A.5 Flashover test results for insulator 2D

Rapid Flashover Test				Date : 27/4/2013		
Insulator type : Super Fog				Insulator code: 2D		
#	Test voltage (KV)	Time		Flashover voltage (KV)	Flashover voltage time	Remarks
		Start (H:M:S)	Stop (H:M:S)			
1	62	9:55:00	10:16:08	62	21.14	Flashover
2	54.5	10:16:08	10:19:08	---	3	Withstand
3	57	10:19:08	10:22:08	---	3	Withstand
4	59.5	10:22:08	10:22:42	59.5	0.57	Flashover

Table A.5 Flashover test results for insulator 2D (continued)						
#	Test voltage (KV)	Time		Flashover voltage (KV)	Flashover voltage time	Remarks
		Start (H:M:S)	Stop (H:M:S)			
5	52.3	10:22:42	10:25:42	---	3	Withstand
6	54.7	10:25:42	10:28:42	---	3	Withstand
7	27.1	10:28:42	10:29:54	57.1	1.2	Flashover
8	50.2	10:29:54	10:31:54	---	3	Withstand
9	52.5	10:31:54	10:34:54	---	3	Withstand
10	54.8	10:34:54	10:35:28	54.8	0.57	Flashover
11	48.2	10:35:28	10:38:28	---	3	Withstand
12	50.4	10:38:28	10:41:28	---	3	Withstand
13	52.6	10:41:28	10:41:48	52.6	0.34	Flashover
14	46.3	10:41:48	10:44:48	---	3	Withstand
15	48.4	10:44:48	10:47:44	48.4	2.93	Flashover
16	42.5	10:47:44	10:50:44	---	3	Withstand
17	44.5	10:50:44	10:53:44	---	3	Withstand
18	46.5	10:53:44	10:56:44	---	3	Withstand
19	48.5	10:56:44	10:56:54	48.5	0.17	Flashover
20	42.5	10:56:54	10:59:54	---	3	Withstand
21	44.5	10:59:54	11:01:27	44.5	1.56	Flashover
22	39.1	11:01:27	11:04:27	---	3	Withstand
23	41	11:04:27	11:07:27	---	3	Withstand
24	42.8	11:07:27	11:10:27	---	3	Withstand
25	44.6	11:10:27	11:13:27	---	3	Withstand

Table A.5 Flashover test results for insulator 2D (continued)						
#	Test voltage (KV)	Time		Flashover voltage (KV)	Flashover voltage time	Remarks
		Start (H:M:S)	Stop (H:M:S)			
26	46.4	11:13:27	11:16:27	---	3	Withstand
27	48.2	11:16:27	11:19:27	---	3	Withstand
28	50.9	11:19:27	11:19:41	50.9	0.23	Flashover
29	44.7	11:19:41	11:22:41	---	3	Withstand
30	46.7	11:22:41	11:25:41	---	3	Withstand
31	48.7	11:25:41	11:28:41	---	3	Withstand
32	50.7	11:28:41	11:28:57	50.7	0.27	Flashover

Table A.6 The relation between flashover voltage time and magnitude (Insulator 2D)

N	Time (minute)	Flashover voltage (KV)
1	21.1	62
2	27.8	59.5
3	35.3	57.1
4	41.9	54.8
5	48.4	52.6
6	54.4	48.4
7	63.7	48.5
8	69.2	44.5
9	87.6	50.9
10	97	50.7

Table A.7 Flashover test results for insulator 6DT

Rapid Flashover Test				Date : 13/4/2013		
Insulator type : super fog				Insulator code: 6DT		
#	Test voltage (KV)	Time		Flashover voltage (KV)	Flashover voltage time	Remarks
		Start (H:M:S)	Stop (H:M:S)			
1	55	10:08:00	10:33:00	---	25	Withstand
2	57.8	10:33:00	10:34:00	---	1	Withstand
3	60.7	10:34:00	10:35:00	---	1	Withstand
4	63.7	10:35:00	10:35:25	63.7	0.42	Flashover
5	56	10:35:25	10:38:25	---	3	Withstand
6	58.6	10:38:25	10:37:42	58.6	2.29	Flashover
7	51.5	10:37:42	10:40:42	---	3	Withstand
8	53.8	10:40:42	10:43:42	---	3	Withstand
9	56.1	10:43:42	10:44:02	56.1	0.34	Flashover
10	49.3	10:44:02	10:47:02	---	3	Withstand
11	51.5	10:47:02	10:50:02	---	3	Withstand
12	53.7	10:50:02	10:50:07	53.7	0.09	Flashover
13	47.2	10:50:07	10:53:07	---	3	Withstand
14	49.3	10:53:07	10:56:07	---	3	Withstand
15	51.4	10:56:07	10:59:07	---	3	Withstand
16	53.5	10:59:07	10:59:15	53.5	0.14	Flashover
17	47	10:59:15	11:02:15	---	3	Withstand
18	49	11:02:15	11:05:15	---	3	Withstand
19	51.2	11:05:15	11:08:15	---	3	Withstand

Table A.7 Flashover Test Results for insulator 6DT (continued)						
#	Test voltage (KV)	Time		Flashover voltage (KV)	Flashover voltage time	Remarks
		Start (H:M:S)	Stop (H:M:S)			
20	51.9	11:08:15	11:08:33	51.9	0.3	Flashover
21	45.7	11:08:33	11:11:33	---	3	Withstand
22	47.7	11:11:33	11:14:33	---	3	Withstand
23	49.7	11:14:33	11:17:33	---	3	Withstand
24	51.7	11:17:33	11:17:59	51.7	0.43	Flashover
25	45.5	11:17:59	11:20:59	---	3	Withstand
26	47.5	11:20:59	11:23:59	---	3	Withstand
27	49.5	11:23:59	11:26:59	---	3	Withstand
28	51.5	11:26:59	11:27:15	51.5	0.27	Flashover
29	45.3	11:27:15	11:30:15	---	3	Withstand
30	47.3	11:30:15	11:33:15	---	3	Withstand
31	49.3	11:33:15	11:36:15	---	3	Withstand
32	51.3	11:36:15	11:36:36	51.3	0.35	Flashover
33	45.1	11:36:36	11:39:36	---	3	Withstand
34	47.1	11:39:36	11:42:36	---	3	Withstand
35	49.1	11:42:36	11:45:36	---	3	Withstand
36	51.1	11:45:36	11:47:36	51.1	2	Flashover
37	45	11:47:36	11:50:36	---	3	Withstand
38	47	11:50:36	11:53:36	---	3	Withstand
39	49	11:53:36	11:56:36	---	3	Withstand
40	51	11:56:36	11:58:12	51	1.6	Flashover

Table A.7 Flashover test results for insulator 6DT (continued)

#	Test voltage (KV)	Time		Flashover voltage (KV)	Flashover voltage time	Remarks
		Start (H:M:S)	Stop (H:M:S)			
41	44.8	11:58:12	12:01:12	---	3	Withstand
42	46.8	12:01:12	12:04:12	---	3	Withstand
43	48.8	12:04:12	12:07:12	---	3	Withstand
44	50.8	12:07:12	12:08:00	50.8	.83	Flashover
45	44.7	12:08:00	12:11:00	---	3	Withstand
46	46.7	12:11:00	12:14:00	---	3	Withstand
47	48.7	12:14:00	12:17:00	---	3	Withstand
48	50.7	12:17:00	12:17:29	50.7	0.48	Flashover
49	44.6	12:17:29	12:20:29	---	3	Withstand
50	46.6	12:20:29	12:23:29	---	3	Withstand
51	48.5	12:23:29	12:23:50	48.5	0.36	Flashover
52	42.7	12:23:50	12:26:50	---	3	Withstand
53	44.7	12:26:50	12:29:50	---	3	Withstand
54	46.7	12:29:50	12:32:50	---	3	Withstand
55	48.7	12:32:50	12:34:32	48.7	1.7	Flashover
56	42.8	12:34:32	12:37:32	---	3	Withstand
57	44.8	12:37:32	12:40:32	---	3	Withstand
58	46.8	12:40:32	12:43:32	---	3	Withstand
59	48.8	12:43:32	12:46:32	---	3	Withstand
60	50.8	12:46:32	12:46:47	50.8	0.25	Flashover

Table A.7 Flashover test results for insulator 6DT (continued)						
#	Test voltage (KV)	Time		Flashover voltage (KV)	Flashover voltage time	Remarks
		Start (H:M:S)	Stop (H:M:S)			
61	44.7	12:46:47	12:49:47	---	3	Withstand
62	46.7	12:49:47	12:52:47	---	3	Withstand
63	48.7	12:52:47	12:54:55	48.7	2.13	Flashover
64	42.8	12:54:55	12:57:55	---	3	Withstand
65	44.8	12:57:55	01:00:55	---	3	Withstand
66	46.8	01:00:55	01:03:55	---	3	Withstand
67	48.8	01:03:55	01:04:55	48.8	1	Flashover
68	43	01:04:55	01:07:55	---	3	Withstand
69	45	01:07:55	01:10:55	---	3	Withstand
70	47	01:10:55	01:13:55	---	3	Withstand
71	49.6	01:13:55	01:14:57	49.6	1.03	Flashover
72	43.6	01:14:57	01:17:57	---	3	Withstand
73	45.6	01:17:57	01:20:57	---	3	Withstand
74	47.6	01:20:57	01:23:57	---	3	Withstand
75	50	01:23:57	01:25:26	50	1.48	Flashover
76	43.9	01:25:26	01:28:26	---	3	Withstand
77	46	01:28:26	01:31:26	---	3	Withstand
78	48	01:31:26	01:34:26	---	3	Withstand
79	50	01:34:26	01:36:26	50	2	Flashover
80	44	01:36:26	01:39:26	---	3	Withstand
81	46	01:42:26	01:45:26	---	3	Withstand

Table A.8 The relation between flashover voltage time and magnitude (Insulator 6DT)

N	Time (minute)	Flashover voltage (KV)
1	27.2	63.7
2	33	58.6
3	40	56.1
4	47.5	53.7
5	57.2	53.5
6	67.15	51.9
7	77.3	51.7
8	87.7	51.5
9	98.9	51.3
10	110.6	51.1
11	122	51
12	132.5	50.8
13	142.7	50.7
14	149.3	48.5
15	159.6	48.7
16	172.4	50.8
17	180.7	48.7
18	191	48.8
19	201.5	49.6
20	213.8	50
21	225.6	50

Table A.9 Flashover test results for insulator 5AT

Rapid Flashover Test				Date : 11/4/2013		
Insulator type : Super Fog				Insulator code: 5AT		
#	Test voltage (KV)	Time		Flashover voltage (KV)	Flashover voltage time	Remarks
		Start (H:M:S)	Stop (H:M:S)			
1	55	10:00:00	10:25:00	---	25	Withstand
2	57.6	10:25:00	10:26:00	---	1	Withstand
3	60.5	10:26:00	10:27:00	---	1	Withstand
4	63.2	10:27:00	10:27:33	63.2	0.55	Flashover
5	55.6	10:27:33	10:30:33	---	3	Withstand
6	58.1	10:30:33	10:31:16	58.1	0.72	Flashover
7	51	10:31:16	10:34:16	---	3	Withstand
8	53.3	10:34:16	10:37:16	---	3	Withstand
9	55.6	10:37:16	10:37:26	55.6	0.18	Flashover
10	49	10:37:26	10:40:26	---	3	Withstand
11	51.2	10:40:26	10:42:44	51.2	2.3	Flashover
12	45	10:42:44	10:45:44	---	3	Withstand
13	47	10:45:44	10:48:44	---	3	Withstand
14	49	10:48:44	10:49:17	49	0.54	Flashover
15	43	10:49:17	10:52:17	---	3	Withstand
16	45	10:52:17	10:55:17	---	3	Withstand
17	47	10:55:17	10:55:23	47	0.11	Flashover
18	41.4	10:55:23	10:58:23	---	3	Withstand
19	43.3	10:58:23	11:00:32	43.3	2.15	Flashover

Table A.9 Flashover test results for insulator 5AT (continued)						
#	Test voltage (KV)	Time		Flashover voltage (KV)	Flashover voltage time	Remarks
		Start (H:M:S)	Stop (H:M:S)			
20	38	11:00:32	11:03:32	---	3	Withstand
21	39.7	11:03:32	11:06:32	---	3	Withstand
22	41.4	11:06:32	11:09:32	---	3	Withstand
23	43	11:09:32	11:12:32	---	3	Withstand
24	44.7	11:12:32	11:15:32	---	3	Withstand
25	46.4	11:15:32	11:15:45	46.4	0.22	Flashover
26	40.8	11:15:45	11:18:45	---	3	Withstand
27	42.7	11:18:45	11:21:45	---	3	Withstand
28	44.6	11:21:45	11:22:34	44.6	0.81	Flashover
29	39	11:22:34	11:25:34	---	3	Withstand
30	40.8	11:25:34	11:28:34	---	3	Withstand
31	42.6	11:28:34	11:31:34	---	3	Withstand
32	44.4	11:31:34	11:34:34	---	3	Withstand
33	46	11:34:34	11:37:34	---	3	Withstand
34	47.8	11:37:34	11:38:25	47.8	0.85	Flashover
35	42	11:38:25	11:41:25	---	3	Withstand
36	44	11:41:25	11:44:25	---	3	Withstand
37	46	11:44:25	11:47:25	---	3	Withstand
38	48	11:47:25	11:47:34	48	0.15	Flashover
39	42.2	11:47:34	11:50:34	---	3	Withstand
40	44.2	11:50:34	11:53:34	---	3	Withstand

Table A.10 The relation between flashover voltage time and magnitude (Insulator 5AT)

N	Time (minute)	Flashover voltage (KV)
1	27.5	63.2
2	32	58.1
3	38.8	55.6
4	44.6	51.2
5	51.4	49
6	59.4	47
7	64.2	43.3
8	80.4	46.4
9	87.7	44.6
10	104.2	47.8
11	114.2	48

Table A.11 Flashover test results for insulator 6AE

Rapid Flashover Test				Date : 9/4/2013		
Insulator type : super fog				Insulator code: 6AE		
#	Test voltage (KV)	Time		Flashover voltage (KV)	Flashover voltage time	Remarks
		Start (H:M:S)	Stop (H:M:S)			
1	60	09:00:00	09:16:00	60	16	Flashover
2	53	09:16:00	09:19:00	---	3	Withstand

Table A.11 Flashover test results for insulator 6AE (continued)						
#	Test voltage (KV)	Time		Flashover voltage (KV)	Flashover voltage time	Remarks
		Start (H:M:S)	Stop (H:M:S)			
3	55.4	09:19:00	09:22:00	---	3	Withstand
4	57.8	09:22:00	09:22:18	57.8	0.3	Flashover
5	51	09:22:18	09:25:18	---	3	Withstand
6	53.3	09:25:18	09:28:18	---	3	Withstand
7	55.6	09:28:18	09:29:11	55.6	0.89	Flashover
8	49	09:29:11	09:32:11	---	3	Withstand
9	51.2	09:32:11	09:32:29	51.2	.3	Flashover
10	45	09:32:29	09:35:29	---	3	Withstand
11	47	09:35:29	09:38:29	---	3	Withstand
12	49	09:38:29	09:41:29	---	3	Withstand
13	51	09:41:29	09:41:42	51	0.22	Flashover
14	44.8	09:41:42	09:44:42	---	3	Withstand
15	46.8	09:44:42	09:47:42	---	3	Withstand
16	48.8	09:47:42	09:47:52	48.8	0.16	Flashover
17	43	09:47:52	09:50:52	---	3	Withstand
18	45	09:50:52	09:51:48	45	0.93	Flashover
19	39.6	09:51:48	09:54:48	---	3	Withstand
20	41.4	09:54:48	09:57:48	---	3	Withstand
21	43.2	09:57:48	10:00:48	---	3	Withstand
22	45	10:00:48	10:01:16	45	0.47	Flashover
23	39.6	10:01:16	10:04:16	---	3	Withstand

Table A.11 Flashover test results for insulator 6AE (continued)

#	Test voltage (KV)	Time		Flashover voltage (KV)	Flashover voltage time	Remarks
		Start (H:M:S)	Stop (H:M:S)			
24	41.4	10:04:16	10:07:16	---	3	Withstand
25	43.2	10:07:16	10:07:40	43.2	0.4	Flashover
26	38	10:07:40	10:10:40	---	3	Withstand
27	39.7	10:10:40	10:13:40	---	3	Withstand
28	41.4	10:13:40	10:16:40	---	3	Withstand
29	43.1	10:16:40	10:19:40	---	3	Withstand
30	44.8	10:19:40	10:20:16	44.8	0.6	Flashover
31	39.4	10:20:16	10:23:16	---	3	Withstand
32	41.2	10:23:16	10:26:16	---	3	Withstand
33	43	10:26:16	10:26:34	43	0.3	Flashover
34	37.8	10:26:34	10:29:34	---	3	Withstand
35	39.5	10:29:34	10:32:34	---	3	Withstand
36	41.2	10:32:34	10:35:34	---	3	Withstand
37	43	10:35:34	10:38:34	---	3	Withstand
38	44.7	10:38:34	10:38:40	44.7	0.1	Flashover
39	39.3	10:38:40	10:41:40	---	3	Withstand
40	41	10:41:40	10:43:40	---	3	Withstand
41	42.8	10:43:40	10:46:40	---	3	Withstand
42	44.6	10:46:40	10:48:12	44.6	1.54	Flashover
43	39.2	10:48:12	10:51:12	---	3	Withstand
44	41	10:51:12	10:53:12	---	3	Withstand

Table A.11 Flashover test results for insulator 6AE (continued)						
#	Test voltage (KV)	Time		Flashover voltage (KV)	Flashover voltage time	Remarks
		Start (H:M:S)	Stop (H:M:S)			
45	42.8	10:53:12	10:56:12	---	3	Withstand
46	44.6	10:56:12	10:59:12	---	3	Withstand
47	46.4	10:59:12	11:00:12	---	3	Withstand
48	48.2	11:00:12	11:00:34	48.2	0.37	Flashover
49	42.4	11:00:34	11:03:34	---	3	Withstand
50	44.4	11:03:34	11:06:34	---	3	Withstand
51	46.4	11:06:34	11:07:52	46.4	1.3	Flashover
52	40.8	11:07:52	11:10:52	---	3	Withstand
53	42.7	11:10:52	11:13:52	---	3	Withstand
54	44.6	11:13:52	11:16:52	---	3	Withstand
55	46.5	11:16:52	11:19:52	---	3	Withstand
56	48.4	11:19:52	11:22:52	---	3	Withstand
57	50.3	11:22:52	11:25:52	---	3	Withstand
58	52.2	11:25:52	11:28:52	---	3	Withstand

Table A.12 The relation between flashover voltage time and magnitude (Insulator 6AE)

N	Time (minute)	Flashover voltage (KV)
1	17	60
2	24.2	57.8
3	31.6	55.6
4	35.4	51.2
5	44.6	51
6	51.5	48.8
7	56	45
8	66.4	45
9	73.5	43.2
10	83.6	44.8
11	90.2	43
12	102.4	44.7
13	113.4	44.6
14	129.4	48.2
15	136.6	46.4
16	161.8	56

A.3 ESDD Measurement Results

The results of the ESDD measurement tests for the collected insulators are listed in Tables A.13 and A.14.

Table A.13 ESDD test results part I

ESDD Measurement (IEC Standard) **Insulator type: Super Fog**					**Date: 27-3-2013**				
Distilled water conductivity (us/cm): 2.7					**Distilled water temperature: 22**				
Top surface area (cm^2) : 1315		**Bottom surface area(cm^2): 2810**			**Total surface area (cm^2): 4125**		**Creepage distance(mm) : 640**		
Insulator code	**Volume Distilled water(ml) Top**	**Conductivity (us/cm) Top**	**Temperature (c) Top**	**ESDD (mg\cm^2) Top**	**Volume Distilled water(ml) bottom**	**Conductivity (us/cm) Bottom**	**Temperature (c) Bottom**	**ESDD (mg\cm^2) bottom**	**Total ESDD value**
5DE	**600**	**257.5**	**22.7**	**0.05874838**	**600**	**3232**	**22.9**	**0.37437559**	**0.2737574**
8A	**600**	**72.61**	**22.7**	**0.015498509**	**600**	**2479**	**22.6**	**0.2867492**	**0.2002777**
11BE	**600**	**1572**	**22.9**	**0.380430779**	**600**	**3585**	**22.4**	**0.42136061**	**0.4083126**
12B	**600**	**2088**	**25.6**	**0.480172052**	**600**	**3465**	**25.2**	**0.38213715**	**0.4133858**

Table A.14 ESDD test results part II

ESDD Measurement (IEC Standard) **Insulator type: Super Fog**					**Date: 8-4-2013**				
Distilled water conductivity (us/cm): 1.66					**Distilled water temperature: 25**				
Top surface area (cm^2) : 1315		**Bottom surface area(cm^2): 2810**			**Total surface area (cm^2): 4125**		**Creepage distance(mm) : 640**		
Insulator code	**Volume Distilled water(ml) Top**	**Conductivity (us/cm) Top**	**Temperature (c) Top**	**ESDD (mg\cm^2) Top**	**Volume Distilled water(ml) bottom**	**Conductivity (us/cm) Bottom**	**Temperature (c) Bottom**	**ESDD (mg\cm^2) bottom**	**Total ESDD value**
5DE	**600**	**257.5**	**22.7**	**0.05874838**	**600**	**3232**	**22.9**	**0.37437559**	**0.2737574**
8A	**600**	**72.61**	**22.7**	**0.015498509**	**600**	**2479**	**22.6**	**0.2867492**	**0.2002777**
11BE	**600**	**1572**	**22.9**	**0.380430779**	**600**	**3585**	**22.4**	**0.42136061**	**0.4083126**
12B	**600**	**2088**	**25.6**	**0.480172052**	**600**	**3465**	**25.2**	**0.38213715**	**0.4133858**
14B	**600**	**2028**	**25.1**	**0.471347589**	**600**	**3522**	**25**	**0.39046378**	**0.4162485**
13BT	**600**	**2351**	**25.1**	**0.548911033**	**600**	**3605**	**25.1**	**0.3990743**	**0.4468404**
5AT	**600**	**64.88**	**25**	**0.013281872**	**600**	**2755**	**25**	**0.30314768**	**0.2107419**
9AE	**600**	**99.85**	**26.5**	**0.020225112**	**600**	**2425**	**26.5**	**0.25731191**	**0.1817315**
6AE	**600**	**96**	**28.1**	**0.018757925**	**600**	**2275**	**26.5**	**0.24092218**	**0.1700989**
6DT	**600**	**330.3**	**25**	**0.073513959**	**600**	**3665**	**24.7**	**0.40950191**	**0.3023930**
1F	**600**	**183.5**	**23.9**	**0.040413063**	**600**	**131.6**	**23.5**	**0.01350181**	**0.0220807**
2F	**600**	**138.5**	**23.7**	**0.030292643**	**600**	**183.2**	**23.2**	**0.01918162**	**0.0227236**
3F	**600**	**181.4**	**23.7**	**0.040113086**	**600**	**130.7**	**23.6**	**0.01337511**	**0.0218988**
4F	**600**	**196.5**	**23.6**	**0.043686055**	**600**	**136.2**	**23.6**	**0.01396244**	**0.0234379**
Clean	**600**	**7.55**	**23.3**	**0.001209279**	**600**	**9.75**	**23.2**	**0.00078462**	**0.0009199**
10BE	**600**	**2160**	**22.2**	**0.536782696**	**600**	**3430**	**22.3**	**0.40365492**	**0.4460936**
7A	**600**	**58.7**	**22.2**	**0.012742906**	**600**	**2300**	**22.2**	**0.26799701**	**0.1866296**
3DE	**600**	**212.8**	**24.1**	**0.046922975**	**600**	**3584**	**24.4**	**0.40284024**	**0.2893781**
2D	**600**	**184.2**	**24.3**	**0.040210602**	**600**	**3689**	**24.3**	**0.41592814**	**0.2961539**
4D	**600**	**191**	**24.2**	**0.04184769**	**600**	**3449**	**24.5**	**0.38635684**	**0.2765315**
1D	**600**	**267.6**	**24.3**	**0.059244766**	**600**	**3326**	**24.3**	**0.37381839**	**0.2735361**
1G	**600**	**121**	**26.7**	**0.024621947**	**600**	**1390**	**26.5**	**0.14496949**	**0.1066041**
2G	**600**	**596.6**	**27**	**0.128044032**	**600**	**2058**	**27.3**	**0.21362875**	**0.1863462**
3G	**600**	**124.2**	**27.2**	**0.025033511**	**600**	**193**	**27**	**0.01862169**	**0.0206601**
4G	**600**	**94**	**26.3**	**0.019067121**	**600**	**232**	**26.2**	**0.02293318**	**0.0217085**

Table A.14 ESDD test results part II (continued)									
Insulator code	Volume Distilled water(ml) Top	Conductivity (us/cm) Top	Temperature (c) Top	ESDD (mg\cm^2) Top	Volume Distilled water(ml) bottom	Conductivity (us/cm) Bottom	Temperature (c) Bottom	ESDD (mg\cm^2) bottom	Total ESDD value
5G	600	447	28	0.093047962	600	687.7	28	0.06795965	0.0759503
6G	600	713.8	28.8	0.148470092	600	1731	28.6	0.17399663	0.1658598
7G	600	172	26.6	0.035603064	600	1378	26.9	0.1424642	0.1083919
8G	600	272.2	26.8	0.057099423	600	1039	26.9	0.10646575	0.0907294
9G	600	101.7	26.7	0.020529017	600	1170	27.1	0.11983365	0.0881737
10G	600	263.5	27	0.054974508	600	198.5	26.7	0.02671053	0.0357207
1H	600	230	31.4	0.043705215	600	230.1	31.2	0.02053944	0.0279298
2H	600	347.3	31.2	0.067260623	600	2048	31.2	0.19667038	0.1554117
3H	600	222.6	31.2	0.042405444	600	291.3	31.2	0.02623357	0.0313867
4H	600	501	33.2	0.09475539	600	1731	32.6	0.16116877	0.1399967
5H	600	598.9	31.7	0.117077346	600	569.7	31.3	0.0524206	0.0730316
6H	600	204.9	31.3	0.038833641	600	249.7	31.4	0.02227438	0.02727
7H	600	378.5	31.4	0.073250227	600	873.9	31.3	0.08154671	0.0789019
C1	600	7.55	33.3	0.000927956	600	9.75	33.2	0.00061217	0.0007128
C2	600	7.8	33.1	0.000975164	600	10	33	0.00063513	0.0007435
C3	600	7.55	29	0.001033212	600	8.2	30.2	0.00052372	0.0006861
C4	600	8.3	29	0.001172314	600	11	30.2	0.00076272	0.0008932
C5	600	9.35	29.2	0.001361092	600	10.5	30.2	0.00071986	0.0009242
C6	600	7.06	28.3	0.000960688	600	9.9	30.3	0.00066693	0.0007605
C7	600	7.22	29.3	0.000964434	600	9.23	29.8	0.00061732	0.0007279
C8	600	8.14	28.7	0.001151491	600	10.06	29.9	0.00068709	0.0008351
C9	600	9.12	28.9	0.001328271	600	11.1	30	0.00077490	0.0009513
C10	600	9.45	28	0.001421704	600	10.33	30.2	0.00070530	0.0009336
C11	600	7.23	28.5	0.00098719	600	9.43	29.9	0.00063296	0.0007459
C12	600	8.52	29.3	0.001204017	600	10.12	29.8	0.00069391	0.0008565
C13	600	8.7	92.1	0.001243556	600	11.09	29.6	0.00078135	0.0009286

VITA

- Luqman Sulyman Faez Maraaba
- Born in Tulkarm City of Palestine in 1987
- Received Bachelor's degree in Science of Electrical Engineering from Palestine, An-Najah National University, Nablus-Palestine in June 2010.
- I am Research Assistant in the Research Institute, Center of Engineering Research, King Fahd University of Petroleum and Minerals, Since September of 2011 till now.
- I was Research Assistant in Electrical Engineering Department of An-Najah National University, form September of 2010 to July of 2011.
- E-mails: luqman.sulyman@gmail.com , lmaraaba@kfupm.edu.sa .
- Skype Name ''luqman265''
- Mobile # +966537611270, #+970597143146